The distribution and enrichment of scandium in garnets from the Tørdal pegmatites, and its economic implications

Georg Steffenssen

Master Thesis in Geosciences
Study programme: Geology
60 credits

Department of Geosciences
Faculty of Mathematics and Natural Sciences

University of Oslo

01/06/2018

Supervisors: Prof. Axel Müller (Natural History Museum, University of Oslo)
Associate prof. Henrik Friis (Natural History Museum, University of Oslo)

This work is published digitally through DUO – Digitale Utgivelser ved UiO
http://www.duo.uio.no
It is also catalogued in BIBSYS (http://www.bibsys.no/english)

Glossary

REEs – Rare Earth Elements (Lanthanides: La-Lu)

HREEs – Heavy Rare Earth Elements (Gd – Lu)

LREEs – Light Rare Earth Elements (La - Eu)

ppm - parts per million

GPS - Global Positioning System

PPL – Plane Polarized Light

XPL – Cross Polarized Light

MORB - Mid Ocean Ridge Basalt

Q-ICP-MS - Quadrupole Inductively Coupled Plasma Mass Spectrometry

S-ICP-MS - Solution Inductively Coupled Plasma Mass Spectrometry

IBMA – Ion Beam Micro Analysis

XRF – X-Ray Fluorescence

LCT – Lithium-Cesium-Tantalum

NYF – Niobium-Yttrium-Fluorine

Acknowledgments

I sincerely appreciate the help and support of my supervisors Axel Müller and Henrik Friis during this master thesis. Many thanks to Nanna Rosing-Schow for her assistance and collaboration during the fieldwork in Tørdal and for sharing insights on granitic pegmatites particularly from the Tørdal pegmatite field. My gratitude to the friendly people of Tørdal and especially to Lars Tveit for allowing us to visit the Høydalen pegmatites as well as other pegmatite locations in Tørdal.

I thank Muriel Erambert for her assistance throughout electron microprobe analysis, and Siri Simonsen and Nèlia Castro for their assistance in using the scanning electron microscope. My additional gratitude for the assistance from Magnus Kristoffersen during laser ablation inductively coupled plasma mass spectrometry and Frans Munnik during ion beam microanalysis. Lastly, I would like to thank Salahalldin Akhavan for preparing both thick and thin section samples.

ACME Labs (Bureau Veritas Commodities Canada Ltd.) in Vancouver, Canada executed whole rock geochemical analysis of host rock samples.

Abstract

The Tørdal pegmatite field, located in the county of Telemark in southern Norway, is known for its enrichment in Sc as well as other rare metals. During the last decade, the interest for Sc has increased, due to its important uses in e.g. the aircraft, automotive and space industries. In light of its economic importance, mineable resources of Sc are of great interest. Garnet, which is a common accessory mineral in the Tørdal pegmatites, naturally incorporates Sc in the B-site of its structure. Besides mica, garnet is a major host for Sc in pegmatites. In addition, various and very rare Sc minerals have been described from the Tørdal pegmatites (bazzite, cascandite, heftetjernite, kristiansenite, oftedalite, scandiobabingtonite, and thortveitite). Therefore, mapping and sampling of garnet-bearing Tørdal pegmatites and their host rocks was performed, with the intent for chemical analysis.

The regional distribution of Sc in the garnets from 16 Tørdal pegmatites was determined by electron microprobe analysis (EPMA) and laser ablation inductively coupled plasma mass spectrometry (LA-ICP-MS). The chemical data indicate a general Sc increase from the SW (Butvatnet-Grønliheii areas) to the NE (Heftetjern-Høydalen area) in the studied area. Energy Dispersive X-ray Spectroscopy (EDS) demonstrates that only wall zone garnets from the Sc abundant pegmatite locations (Upper Høydalen and Svåheii 2) contain Sc-rich (thortveitite) micro inclusions. The Sc-enrichment is accompanied by an increase in the spessartine component from 30 up to 60 mol.% (up to 0.29 Sc_2O_3 wt.% and 2197 ppm Sc). However, garnets from both Sc-rich SW (Svåheii 2 location: ~47 mol.% spess) and Sc-poor NE corners (Bratterud and Sjauset locations: ~54 mol.% and ~76 mol.%, respectively) do not apply to the general systematic increase of Sc. Through internal fractionation in the most evolved NYF pegmatites of Høydalen, Sc drops from both the Sc- and almandine-rich wall zone spessartines (max. 1538 ppm Sc and ~50 mol.% spess) to the nearly Sc-absent “cleavelandite”-zone garnets (81-93 mol.% spess). The Sc-rich wall zone garnets from the Heftetjern, Upper Høydalen, and Svåheii 2 locations show a general decrease from the core to the crystal margin (max. 688 ppm Sc difference). In particular, this decrease of the Sc contents in the Heftetjern garnets is correlated with decreasing Mn/(Mn+Fe) ratios and Y and HREE contents as seen from BSE-imaging. Similarly, IBMA-imaging shows Sc-rich cores where Sc may slightly decrease towards the rim of the investigated Sc-rich garnets from the Heftetjern and Svåheii 2 locations. The rest of the analyzed and relatively Sc-poorer garnets from the Tørdal do not exhibit any clear correlation for intracrystalline Sc nor with any other trace elements such as e.g. Y and HREEs.

It has long been believed that the Tørdal pegmatites are formed by fractionated melt derived from the Tørdal granite pluton, located in the south of the Tørdal pegmatite field. Scandium was, according to this theory, leached from the mafic supracrustals of the Nissedal outlier into the pegmatitic melts, when the melts moved from the pluton to their final destination of emplacement. This theory was verified by geochemical whole rock analysis, which demonstrates that Sc is much more abundant in amphibolitic host rocks of the outlier (29-30 ppm) than in the Tørdal granite (2 ppm). However, fieldwork evidence proves that the pegmatites were generated by direct and local anatexis by these host rocks. This anatectic origin is supported by recent dating of the pegmatites and the Tørdal granite, which indicate that the Sc-enriched pegmatites Tørdal cannot originate from the ~40 Ma older Tørdal granite. Plausibly, through SW-NE migration of the increasingly fractionated and continuously Sc-enriched anatectic pegmatite melt, Sc was mobilized and transported by ScF ligands, while mostly ending up in the Sc-rich pegmatites of the Heftetjern-Høydalen area. Scandium was in these pegmatites mostly incorporated into late hydrothermal wall zone micas and garnets. Most importantly, the main outcome of this study clearly demonstrates that the Heftetjern-Høydalen area, being most Sc-enriched, proves to be the best potential for future exploitation of Sc. Scandium contents in the garnets were found to be consistent within each pegmatite. Therefore, garnet is a very useful and reliable pathfinder mineral for exploration of Sc mineralization in granitic pegmatite fields. However, during Sc exploration, it is of utmost importance to bear in mind, especially for the most evolved NYF pegmatites, which zone the garnets originate from since Sc decreases drastically through internal fractionation.

Table of Contents

1. Introduction

The pegmatites of the Tørdal area in the county of Telemark have for a long time been known to be enriched in Sc, Li and Sn, as well as other rare metals (e.g. Bergstøl and Juve, 1988; Kristiansen, 1998; Raade and Kristiansen, 2000; Kolitsch et al., 2010). These granitic pegmatites are part of the Nissedal pegmatite district, which belongs to the Sveconorwegian pegmatite province of the Sveconorwegian orogeny in Southern Norway (Müller et al., 2017). Garnets, which are a group of silicate minerals, occur as a common accessory mineral in the Tørdal pegmatites. The garnets found in the Tørdal pegmatites are spessartine-almandine garnets with the general formula - $Mn_3Al_2(SiO_4)_3$-$Fe_3Al_2(SiO_4)_3$. These garnets have previously shown to be enriched in Sc in some of the Tørdal pegmatites to sub-economic levels (Raade and Kristiansen, 2000, 2003). The industrial demand for Sc has been steadily increasing in the past decade due to its crucial technical applications in various industries. For that reason, the Tørdal pegmatites were the target of several Sc exploration campaigns during the last decades.

Garnet is, besides mica, the major carrier of Sc in granitic pegmatites. However, the Sc content in mica is more variable within individual pegmatite bodies (Rosing-Schow et al., 2018). In contrast, the Sc contents in garnets from one pegmatite seem to be much more consistent. For that reason, garnet has been utilized by mineral exploration companies and in this study as the major pathfinder mineral for Sc mineralization related to granitic pegmatites. Scandium is abundant in the Earth's crust, but due to its trivalent oxidation state, crystal chemical behavior and ionic size it is readily incorporated into minerals. These minerals are typically ferromagnesian minerals, where Sc in particular, will substitute for Al, Fe, Mg, and also other elements (e.g. Shchekina and Gramenitskii, 2008). In the garnets Sc enters the B-site (ideal formula: $A_3B_2(SiO_4)_3$; A = Mn, Fe, Mg, Ca; B = Al, Fe, Mn, Ti, Cr, Zr, V), making garnet a useful prospecting tool for Sc exploration. However, limited data exist on the Sc contents and its intracrystalline distribution in garnets from granitic pegmatites, and the origin of Sc in pegmatite melts in general. Thus, the origin of Sc enrichment in the Tørdal pegmatites and elsewhere is still strongly debated. Therefore, a better understanding of the enrichment of Sc in the Tørdal pegmatites will certainly contribute to improving the exploration success of Sc mineralizations in general. These considerations lead to the four aims of this master thesis: (1) determination of the regional distribution of Sc in garnet-bearing granitic pegmatites of the Tørdal pegmatite field, (2) investigation of the intracrystalline distribution of Sc within the garnet crystals, (3) establishment of potential sources of the Sc enrichment in the Tørdal pegmatites, and (4) economic implications of the findings made in this study for the exploration of Sc mineralization in the Tørdal area.

1.1 Granitic pegmatites

1.1.1 Genesis, classification, and industrial importance

Pegmatites are holocrystalline igneous intrusive rocks, which exhibit several specific rock texture traits. These traits include the coarse grain size (>3 cm), very heterogeneous distribution of the grain sizes, distinctly zoned mineral assemblages, and the occurrence of skeletal crystal shapes (including the characteristic graphic intergrowths) (London, 2008). In general, pegmatites are probably the least understood rocks in terms of genesis. No conclusive explanation or satisfactory hypothesis on the origins of pegmatites was developed until Jahns (1953a), who concluded that pegmatites have a magmatic origin with or without the assistance of hydrothermal fluids. Jahns and Burnham (1969a), who concluded that the presence of a vapor phase distinguishes pegmatites from granites, further developed this model. According to this model, granites were considered as the crystalline product of a magma, which is initially undersaturated in H_2O. The H_2O saturation is observable at the textural transition between the granite and pegmatite, where the typical pegmatitic textures are the indication of when the aqueous vapor phase in the melt reaches its saturation. Furthermore, the model proposed that crystal fractionation was an essential factor in the formation of granitic pegmatites, wherein the pegmatites are derivatives of relatively large batches of granitic plutons (London, 1996). Nowadays, the general consensus is that pegmatites may either be formed as late-stage segregations of relatively large granite intrusions, i.e. plutons (London, 2008) or by direct anatexis of the country rock (Müller et al., 2017). Evidently, most pegmatites crystallize from eutectic granitic melts (in the system $NaAlSi_3O_8$-$KAlSi_3O_8$), in which they are either slightly peralkaline or peraluminous (Černý et al., 2012). This chemistry is reflected in the major mineralogy of granitic pegmatites, in which the main constituents are quartz, feldspars (sodic plagioclase and K-feldspar) and micas.

During the 20th century, scientists tried to classify pegmatites, in order to distinguish pegmatites with potential economic mineralization and barren (non-mineralized) pegmatites. The earliest attempts of classification were based largely on field-based subdivisions, which include: internal structure, paragenetic relationships, bulk chemical composition, petrogenetic aspects, nature of parent medium, geochemical signatures, etc. The first generally recognized pegmatite classification was established by the Russian mineralogist and petrologist Fersman in 1930 (1930, 1931). Fersman's classification emphasized the thermal evolution of pegmatitic melts or, in other words, the crystallization temperature (Fersman, 1930 and 1931). Later on, Ginsburg & Rodionov (1960) distinguished four pegmatite classes based on crustal environment (depth of intrusion), and relationship to metamorphism and relationships to granitic plutons. Ginsburg et al. (1979) developed this further into new classes: the abyssal, muscovite, rare-element and miarolitic classes. The Ginsburg classification is also referred to as the "depth-zone" classification, since it utilizes the intrusion depth of pegmatites as classification criteria. Černý (1990, 1991a) revised the latter classification (improving the petrological, paragenetic and geochemical criteria) and introduced the three new petrogenetic pegmatite families; the Lithium-Cesium-Tantalum (LCT), the Niobium-Yttrium-Fluorine

(NYF) and mixed LCT+NYF family. The LCT family of pegmatites is peraluminous to hyperalumionous, which is genetically related to sedimentary (S-type) and igneous (I-type) magmatism. This family of pegmatites is enriched in elements such as Li, Rb, Cs, Be, Sn, Ta, and Nb, whereby the Nb content is generally lower than the Ta content. In addition, this enrichment also includes B, P, and F as the fractionation of the pegmatite melt progresses. On the other hand, pegmatites of the NYF family are subaluminous to metaluminous, which shows an affinity to granitic anorogenic (A-type) and igneous (I-type) magmatism. Elements enriched in this family include Ti, Y, Sc, REE, Zr, U, Th, F, Nb and Ta, in which concentrations of Nb are generally higher than the Ta content. (Černý and Ercit, 2005) revised the depth-zone classification of Ginsburg & Rodionov (1960) by improving the petrological, paragenetic and geochemical criteria. Consequently, this lead to a division of the five major pegmatite classes: abyssal, muscovite, muscovite-rare element, rare-element, and miarolitic pegmatites. These classes were subdivided into the ten subclasses (HREE, LREE, U, Li), which reflect both differences in geochemistry and geological features. Further subdivision gave rise to types and subtypes, which display even slighter variations in traits of trace element geochemistry and crystallization environments, expressed through the various accessory mineral assemblages. Today, both the class-classification by (Černý and Ercit, 2005) and the family-classification by Černý (1990, 1991a) of pegmatites are the most applied classifications (Figure 1.1).

Class	Subclass	Type	Subtype	Family
Abyssal	HREE			NYF
	LREE			
	U			NYF
	BBe			LCT
Muscovite				
Muscovite–rare element	REE			NYF
	Li			LCT
Rare element	REE	allanite–monazite		NYF
		euxenite		
		gadolinite		
	Li	beryl	beryl–columbite	LCT
			beryl–columbite–phosphate	
		complex	spodumene	
			petalite	
			lepidolite	
			elbaite	
			amblygonite	
		albite–spodumene		
		albite		
Miarolitic	REE	topaz–beryl		NYF
		gadolinite–fergusonite		
	Li	beryl–topaz		LCT
		spodumene		
		petalite		
		lepidolite		

Figure 1.1: Displayed geochemical distinctions of pegmatites taken from (Černý et al., 2012) modify-cation of (Černý and Ercit, 2005)), which divides them into different classes and petrogenetic families.

Granitic pegmatites are the hosts of a vast assemblage of industrial minerals and rare metals. Important industrial minerals with a long tradition of several industrial applications, include mostly feldspars and kaolinite (major source for porcelain and other ceramics), quartz (important constituent for e.g. processors, solar cells, and glasses), and micas (major appliances in e.g. cosmetics and industrial lubricants) (Glover *et* al., 2012). These minerals are foremost found in great abundances in abyssal, also called "barren" or "ceramic", pegmatites, where gemstones and rare metals are absent (Glover *et* al., 2012). Chemically more evolved rare element pegmatites contain rare metals such e.g. Li, Be, Cs, Ta, and REEs (London, 2008), which are of crucial importance for the modern society. These metals yields several technical applications, in which some of these include Li-based rechargeable batteries, medicines, glass-making and ceramics, incorporation of Be in various alloys, cesium providing several appliances within the oil and gas industry, tantalum applied in capacitors in computers and smartphones, and REEs applied in super magnets (Linnen et al., 2012; U.S. Geological Survey, 2016).

1.2 Scandium

1.2.1 Natural occurrence and economic significance

The chemical element, scandium, was first discovered in the two minerals euxenite and gadolinite by the Swedish chemist Lars Fredrik Nilson in 1879 (Raade and Segalstad, 2002). Scandium is a lithophile element (typically trivalent) and has a relatively small ionic radius, which makes its geochemical behavior akin to the ferromagnesian elements Fe, V, Cr, Co, and Ni (Voncken, 2016). Both Sc and the similar element Y, are often grouped together with the lanthanides (La-Lu) as REE, due to their similar geochemical behavior and valence states (Voncken, 2016). Trivalent Sc forms solid solutions with trivalent Y and the heavy REE (Er-Yb), and additionally tetravalent Ti, Sn, Zr, and trivalent Al (Shchekina and Gramenitskii, 2008).

Scandium is a widely dispersed element in Earth's crust with an average of 22 ppm (Raade and Segalstad, 2002). Rudnick and Gao's (2003) estimated that Sc is most abundant in the deep crust and in mafic rocks (Table 1.1). This is again reflected in ferromagnesian minerals such as pyroxenes, amphiboles, micas, garnets, and epidote-group minerals are minerals where Sc appears as a trace element (Raade, 2003) (Table 1.2). In these minerals, Sc typically substitutes Al and trivalent Fe (Raade, 2003). This substitution mechanism is possible because Sc's ionic radii and coordination number (6 [2,6]) are both akin to the generally widely dispersed ferromagnesian minerals (Shannon, 1976). In chemically evolved magmatic rocks such as NYF pegmatites, where incompatible trace elements are enriched and ferromagnesian elements are depleted, Sc occasionally can be enriched. However, the reasons for both the source and enrichment of Sc is still a matter of discussion.

Only a few minerals, in which Sc is the main constituent, are known to science. These 18 Sc-minerals are displayed in Table 1.3. All these Sc minerals were described from pegmatites (except allendite and davisite). However, in pegmatites, Sc is predominantly bound in garnets and micas as trace element with relatively high concentrations in comparison with other pegmatite-forming minerals (Table 1.2). High abundances in garnet have recently also been discovered. Previous data by (Raade and Kristiansen, (2000, 2003) of spessartine from the Heftetjern pegmatite of Tørdal have shown Sc_2O_3 concentrations of 0.3 wt.% to ~ 0.5 wt.%. Ti-Zr-rich garnets, situated in Russian aposkarn rocks, show even higher abundances of scandium containing up to ~ 6 wt.% Sc_2O_3 and ~ 0.45 *apfu* (Galuskina *et al.*, 2005).

Table 1.1 Bulk Average Scandium Abundances

Authors	**Upper Crust** ***(µg/g)***	**Deep crust (Middle and Lower Crust)** ***(µg/g)***	**Average crust** ***(ppm)***	**Ultramafic rocks** ***(ppm)***	**Mafic rocks (Basalts)** ***(ppm)***	**Intermediate rocks (Syenite, T. and W., Diorite, V.)** ***(ppm)***	**Felsic rocks (Ca-rich and Ca-poor, T. and W., Granite etc., V.)** ***(ppm)***
Shaw et al. (1967,1976)	7	-	-	-	-	-	-
Shaw et al. (1994)	-	5.4	-	-	-	-	-
Rudnick and Fountain (1995)	-	22	-	-	-	-	-
Eade and Fahrig (1973)	12	-	-	-	-	-	
Condie (1993)	13.4	-		-	-	-	-
Gao et al. (1998a)	15	15	-	-	-	-	-
Taylor and McLennan (1985,1995)	13.6[c]	-	-	-	--	-	-
Wedepohl (1995a)	[7]	-	-	-	-	-	-
Rudnick and Gao (2003)	14.0	19					
Turekian & Wedepohl, 1961	-	-	-	15	30	3	14 & 7,resp.
Vinogradov, 1962	-	-	-	5	24	2.5	3
Raade, 2003	-	-	22	-	-	-	-

Table 1.1: Bulk average scandium abundances of the different layers of the crust, as well as ultramafic-felsic igneous rocks taken from (Rudnick and Gao, 2003 and sources therein).

Table 1.2 Scandium in rock-forming minerals

Minerals	***Bulk concentration, ppm***	***Authors***
Hornblende	**34.2 ± 0.4**	(Higuchi and Nagasawa, 1969)
Amphibole, augite, hypersthene	**5 – 85**	(Das *et al.*, 1971)
Feldspars (Kfsp & plagioclases)	**0.1 – 8**	(Das *et al.*, 1971)
Chlorites	**0.6 – 20**	(Das *et al.*, 1971)
Micas	**2 – 23**	(Das *et al.*, 1971)
Garnet (Pyrope)	**114 ± 3**	(Fedorowich et al., 1995)

Table 1.2: Scandium bulk concentrations (ppm) in common rock-forming minerals.

Table 1.3 Scandium-rich minerals

Mineral name	*Ideal formula*	*Reference*
Allendeite	Sc_4Zr_3O12	(Ma and Beckett, 2009)
Bazzite	$Be_3(Sc,Al)_2Si_6O_{18}$	(Demartin *et al.*, 2000)
Cascandite	$Ca(Sc,Fe^{2+})Si_3O_8(OH)$	(Mellini and Merlino, 1982)
Davisite	$CaScAlSiO_6$	(Ma and Rossman, 2009)
Eringaite	$Ca_3Sc_2(SiO_4)_3$	(Galuskina *et al.*, 2010)
Heftetjernite	$ScTaO_4$	(Kolitsch *et al.*, 2010)
Jervisite	$NaScSi_2O_6$	(Mellini *et al.*, 1982)
Juonniite	$CaMgSc(PO_4)_2(OH)\cdot 4H_2O$	(Jambor *et* al., 1998)
Kampelite	$Ba_6Mg_3Sc_8(PO_4)_{12}(OH)_6\cdot 7H_2O$	(Hålenius *et al.*, 2017)
Kangite	$(Sc,Ti,Al,Zr,Mg,Ca,\square)_2O_3$	(Ma *et al.*, 2013)
Kolbeckite	$Sc(PO_4)\cdot 2H_2O$	(Yang *et al.*, 2007)
Kristiansenite	$Ca_2ScSn(Si_2O_7)(Si_2O_6OH)$	(Raade *et al.*, 2002)
Oftedalite	$KSc_2\square_2Be_3Si_{12}O_{30}$	(Cooper *et al.*, 2006)
Panguite	$(Ti,Al,Sc,Mg,Zr,Ca)_{1.8}O_3$	(Ma *et al.*, 2012)
Pretulite	$Sc(PO_4)$	(Bernhard *et al.*, 1998)
Scandiobabingtonite	$(Ca,Na)_2(Fe^{2+},Mn)(Sc,Fe^{3+})Si_5O_{14}(OH)$	(Orlandi *et* al., 1998)
Thortveitite	$Sc_2Si_2O_7$	(Bianchi *et al.*, 1988)
Warkite	$Ca_2Sc_6Al_6O_{20}$	(Williams *et al.*, 2014)

Table 1.3: List of recognized minerals with Sc as one of their main constituents. Fifteen of the Sc-minerals are terrestrial, while three of them (allendeite, davisite, and warkite) are extra-terrestrial and only found in meteorites.

The notion of Sc's scarcity in nature and limited supply makes it a valuable commodity because of its special properties, being a light metal making strong alloys with other metals. The reason for this is simply that, its natural valence state Sc^{3+}, is not commonly compatible with anions common in ore mineralization (Hedrick, 2002; U.S. Geological Survey, 2016). Compared to other metals, Sc production nowadays is very limited with only 10-15 metric tons per year, with most Sc being produced from thortveitite and uranium operations as byproduct leachant in the US (U.S. Geological Survey, 2016). Although the interest and demand for Sc are generally increasing, low success for large-scale distribution and supply up to this date is still the case. The price of 99.99% pure Sc has varied during the past decade from US$ 4000/kg to US$ 20.000/kg, making it one of the most expensive naturally occurring elements (Strategic Metal Investments Ltd., 2018). Scandium, in various industries, is mainly used as additions in aluminum alloys (Voncken, 2016), and in e.g. "SOFCs" (solid oxide fuel cells) (Scandium International Mining Corp., 2018a). For industries such as the aircraft, space, and automotive industries, Sc has proven most crucial. Relatively small additions of Sc makes a considerable impact, in terms of enhancing overall strength and decreasing weight of Al alloys (Raade, 2003). In "SOFCs" Sc as a performance enhancer, which greatly improves conductivity and the mediation of heat in these batteries (Scandium International Mining Corp., 2018a).

According to (U.S. Geological Survey, 2016) the most prominent and sizeable Sc resources are all nowadays located in Australia (Table 1.4). One of these resources (Syerston project) is the Syerston-Flemington lateritic deposit in New South Wales. The laterites, which originate from relatively Sc-rich clinopyroxenes (~80 ppm), in a complex of ultramafic-mafic intrusives, reside in relatively stable tectonic settings (Chassé *et al.*, 2017, and sources therein). Through long-term weathering of the clinopyroxenes forming the lateritic soil, wherein Sc-rich waters circulate and enrich Sc in goethite and partly in hematite by replacing Fe^{3+} by Sc^{3+} (Chassé *et al.*, 2017). Other notable productions of Sc as a byproduct from other metals are located in Quebec, Canada (extracted Sc and Al from red mud, fly ash, and mine tailings), Japan (recovered from TiO_2), Philippines (from a nickel laterite leachant), and Russia (extraction from red mud) (U.S. Geological Survey, 2016).

Table 1.4 Expected prominent scandium mining-grade productions

Scandium projects	Total Sc abundance, tons	Mining-grade, ppm	Sc_2O_3, tons/year
Nyngan	3100	100	36
Syerston	1200	600	*a*
SCONI	2700	100	50

Table 1.4: The table display the most prominent scandium projects, with expected potential for production of scandium oxide (U.S. Geological Survey, 2016). *a: Not reported.*

1.3 Geological background

The Sveconorwegian pegmatites of the Tørdal area are located in the county of Telemark, Southern Norway, which is a part of the Nissedal pegmatite district (Fig. 1.2) (Ihlen and Müller, 2009b; Müller et al., 2017). The granitic pegmatites throughout Tørdal occur as hundreds of relatively small and large bodies/intrusions, which are situated on top of the Nissedal volcanosedimentary outlier (1300-1200 Ma), and the underlying gneissic basement (<1500 Ma) (e.g. Segalstad and Eggleston, 1993; Raade and Kristiansen, 2000). The supracrustal rocks of the Nissedal outlier consist mainly of amphibolite with occurrences of volcano-sedimentary rocks, various gneissic basement rocks, and also mafic to felsic intrusives (Bergstøl and Juve, 1988). Suggested by several authors (e.g. Segalstad and Eggleston, 1993; Raade and Kristiansen, 2000) the pegmatite-forming melts originate from the anorogenic (A-type) Tørdal granite in the south (960-850 Ma), which has intruded the relative older supracrustal rocks and basement. Both the Tørdal granite and its closely adjacent pegmatites were formed at 8-10 km depth, at ~600ºC and 2.4 ± 0.4 kbar (Segalstad and Eggleston, 1993).

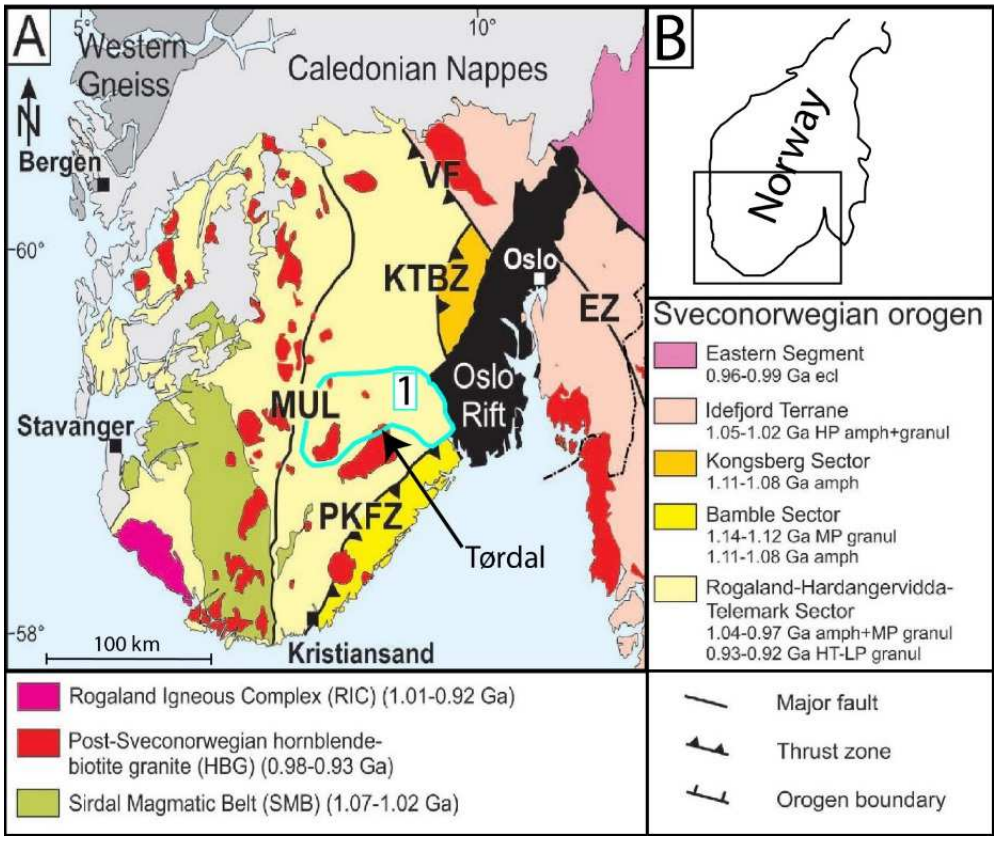

Figure 1.2: (A) - Regional map of Southern Norway, and Sveconorwegian Orogeny, modified from (Müller et al., 2017). Displayed shear and trust zones are presented as: EZ – Elverum Shear Zone, KTBZ – Kongsberg-Telemark Boundary Zone, MUL – Mandal-Ustaoset shear zone, PKFZ – Porsgrunn-Kristiansand Fault Zone, SFDZ – Sveconorwegian Frontal Deformation Zone, and VF – Vardefjell shear zone. Metamorphic grades in the orogeny: amph – amphibolite facies, ecl – eclogite facies, granul – granulite facies. The Tørdal area is situated in a Post-Sveconorwegian hornblende-biotite granite field (marked with a black arrow in the image), located within the Nissedal pegmatite district (1; marked in turquoise). (B) – Map of southern Norway.

Geochemically, the pegmatites of the Tørdal area are geochemically distinct, wherein the elements Sn, Sc, Y, Be, and Li are enriched compared to other Sveconorwegian pegmatite fields (Bergstøl and Juve, 1988). The Tørdal area host both chemical complex and simple pegmatites (Segalstad and Eggleston, 1993), which in general exhibit NYF affinity with accessory monazite-(Ce), allanite-(Ce), and gadolinite-(Y). Some chemically evolved pegmatites, e.g. Upper and Lower Høydalen, exhibit “cleavelandite” replacement zones with “lepidolite”. Because these replacement zones have a chemical LCT signatures, these pegmatites were previously described as mixed NYF-LCT pegmatites (Bergstøl and Juve, 1988; Ihlen and Müller, 2009a) but should be considered as evolved NYF pegmatites. Previous mapping by (Segalstad and Eggleston, 1993) was focused on the area in the proximity of the lake of Kleppsvatn. The authors divide the pegmatites in this area into different regional zones based on K-feldspar colors: the “amazonite”, white K-feldspar, and pink K-feldspar zones (Fig. 1.3). In this map, complex type pegmatites comprise of the Skardsfjell, Heftetjern, and Upper and Lower Høydalen pegmatites, residing in the “amazonite” zone. Pegmatites from the Kleppe and Storemyr locations are situated in the pink dominated K-feldspar zone.

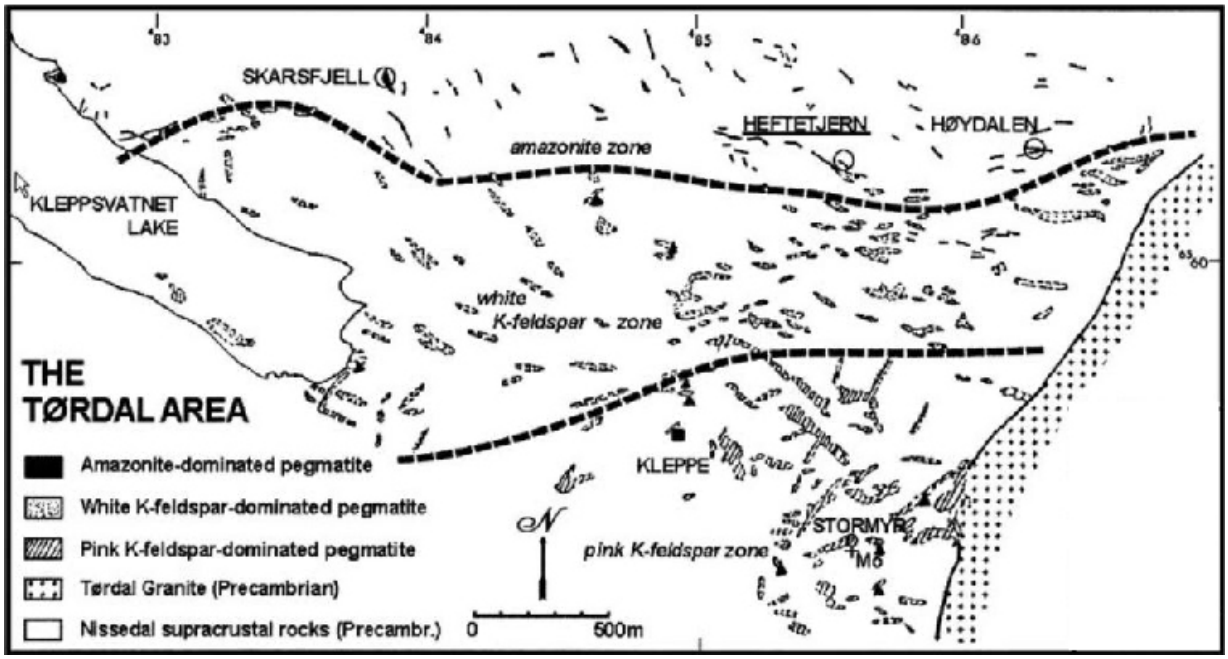

Figure 1.3: Modified regional map of the northern part of Tørdal by (Raade and Kristiansen, 2003) reproduced from (Segalstad and Eggleston, 1993). Pegmatites residing in the amazonite-zone include the evolved NYF pegmatites from the Skardsfjell, Heftetjern, and Upper and Lower Høydalen locations. The area mapped in the study lies southwest of this map.

2. Methods

Fieldwork

The mountainous Tørdal area yields both deep valleys and high peaks. The general terrain is a mixture of dense forest and bog, which made sampling challenging. Yet, some pegmatite outcrops were situated by the main road, while smaller trails in the terrain made it possible to reach otherwise unreachable pegmatite locations. During the 14-days field trip, several of the pegmatites in Tørdal were mapped within an area of approximately 8.6 km^2 (8°41'45"-46'0"E, 59°8'50"-9'50"N: Fig. 3.4) using GPS, and later on by satellite photos. Samples of 17 garnet-bearing granitic pegmatites and 3 host rocks, were collected and labeled throughout the Tørdal area (~50 km^2: 8°39'20"-50'10"E, 59°8'50"-12'10"N: Fig. 3.35) for later analyses in Oslo. The own collected sample set (Grønliheii, Kleppe quarry (amphibolite), Kleppe quarry (granite outcrop), Lislegrønlia, Mjeltedalen 2a, Mjeltedalen 2b (amphibolite), Sjauset, Storemyr 3 and Upper Høydalen 12) were complemented with samples collected during previous field trips to Tørdal (Bratterud, Butvatnet, Heftetjern 1-2, Kleppe quarry, Lower Høydalen, Storemyr 1-2, Svåheii 2-3 and Upper Høydalen 1 samples) (Appendix 7.1)

Sample preparation

Samples of garnet and host rock were cut and prepared for thick/thin section preparation, and chemical bulk rock analysis at the Natural History Museum (NHM). The host rocks, comprising the two amphibolite and granite samples, were sent to ACME Laboratories in Vancouver, Canada, for bulk rock analysis. Standard thin section (35 µm thick) and thick sections for optical microscopy, EPMA, SEM/EDS, LA-ICP-MS and IBMA analyses (300

µm thick) were prepared at the thin section laboratory the Department of Geosciences, University of Oslo. A total of 17 thick sections of garnet-bearing granitic pegmatite samples (Appendix 7.1-3), and 3 thin sections of host rocks (Appendix 7.1 and 7.4) were made. The thick sections were carbon coated using Cressington 208C before further analysis.

Optical Microscopy

A Leica DMLP optical microscope equipped with a Leia digital camera MC170HD, at the Natural History Museum of Oslo, was used for both studying and imaging 32 garnet grains in x thin sections and the petrography of 3 host rock samples. The garnets in the pegmatite samples were imaged in plane polar light (PPL). Images of the host rock petrography were obtained in both PPL and XPL (cross-polar light). Mineral abbreviations for rock-forming minerals for the host-rock mineral assemblages by (Whitney and Evans, 2010) were applied.

Scanning electron microscopy

Energy Dispersive X-ray Spectroscopy (EDS) was conducted both at the Department of Geosciences, University of Oslo and at the Natural History Museum of Oslo. The instruments used were a Hitachi SU5000 Scanning Electron Microscope, equipped with a Bruker XFlash 6|30 detector (at the Department of Geosciences), and a Hitachi S-3600N Scanning Electron Microscope equipped with Dual Bruker XFlash30 EDS system. Both instruments were used for identifying the mineral inclusions in garnet, situated in the different pegmatite samples. Backscatter electron (BSE) imaging of the garnet grains was done with the EMPA instrument described below (Appendix 7.5), while micro inclusions images were obtained using both the SEM at the NHM at Økern and EMPA instrument at Blindern. The website Mindat.org was utilized for both the mineral identification (on the base of EDS spectra/data), and to get an overview over known minerals reported from the Tørdal pegmatites (Appendix 7.9).

Electron probe microanalysis

Compositions of major and trace element compositions were determined by Electron Probe Micro Analysis (EPMA) on a Cameca SX100 equipped with five wavelength dispersive spectrometers (WDS), housed at the Department of Geosciences, University of Oslo. Chemical analysis of 32 garnet grains in different 17 pegmatite samples (prepared as thick sections) was performed (Appendix 7.6). Parameters set for analyzed major elements (Si, Al, Mg, Mn, Fe, and Ca) were 15kV and 20nA, and for analyzed trace elements (Y, Yb, Sc, Na, and Sn) 20kV and 100nA. The applied calibration standards and X-ray lines were: Wollastonite (Si Kα, Ca Kα), Al_2O_3 (Al Kα), MgO (Mg Kα), pyrophanite (Ti Kα, Mn Kα), Fe metal (Fe Kα), albite (Na Kα), SnO_2 (Sn Lα), and synthetic orthophosphates (Y Lα, Sc Kα, and Yb Lα, by Jarosewich and Boatner (1991). The Cameca PAP procedure, by Pouchou and Pichoir (1984), was applied for matrix effects, while a detailed WDS scan showed no elemental overlaps. All concentrations below the detection limit were corrected by the latter procedure. The electron beam was focused with a beam size of 1 µm. Peak count times for Si, Al, Mn, Fe, Ca, and Ti were 10s, 20s for Na and Mg, 40s for Y, and 60s for Sc and Yb. An Excel spreadsheet by (Locock, 2008) was applied for the calculation of garnet endmembers proportions (Appendix 7.6)

Laser ablation inductively coupled plasma mass spectrometry (LA-ICP-MS)

Eighteen garnet grains from eight pegmatite samples were analyzed for trace elements at the Department of Geosciences, University of Oslo. The instrument used was a Bruker Aurora Elite (QICPMS) equipped with a Cetac LSX-213 G2+ laser. A total of 88 data points were acquired to explore core to rim compositional variations. The isotope of trace elements include: ^{23}Na, ^{45}Sc, ^{49}Ti, ^{89}Y, ^{93}Nb, ^{118}Sn, ^{139}La, ^{140}Ce, ^{141}Pr, ^{143}Nd, ^{152}Sm, ^{151}Eu, ^{158}Gd, ^{159}Tb, ^{163}Dy, ^{165}Ho, ^{166}Er, ^{169}Tm, ^{171}Yb, ^{175}Lu, ^{179}Hf, ^{181}Ta, and ^{232}Th. For isotope data calculations, the software Glitter was applied. Silicon from EPMA was used as internal standard, while external standards NIST610, BCR2G, and GJ were used to set up and monitor instrument drift. All trace element data were normalized accordingly to the measured value ^{29}Si. Chondrite data by (Anders and Grevesse, 1989) was applied for chondrite normalized plots of the lanthanide concentration in the various garnets (Appendix 7.7).

The bulk compositions of pegmatite wall rocks, two amphibolite, and one Tørdal granite samples were determined with ICP-MS at ACME laboratories in Vancouver, Canada (ACME Labs, 2018). The applied analytical codes for analyses were PRP70-250 (crushing and pulverizing of 250 g), LF202 (major and minor element analysis by ICP-ES and trace elements by solution ICP-MS using Lithium Borate Fusion), PF370 (Peroxide Fusion ICP-ES for Li analysis) and GC841 (X-ray fluorescence analysis for S and F determination). The lithium borate fusion provides an exceptional breakdown of even the most resistant mineral phases and makes an extraordinary determination of the total element compositions during both ICP-ES/MS analysis. Excluded elements (below the detection limit) were As, Cd, Sb, Bi, Ag, Au, Hg, Se, and W. Based on the lowest mean detection for each element, the two programs LF200 and AQ200 were applied. LF200 was used for all major oxides. For the trace elements, LF200 was used with the exception of the elements Ni, Mo, Cu, Pb, Zn, and Ti, in which the AQ200 was applied. The programs PF370 and GC841 was only used for S and F, respectively (Appendix 7.8)

Ion beam microanalysis (IBMA)

Three garnet grains from three different pegmatite samples (Svåheii 2, Heftetjern 1, and Heftetjern 2 locations) were selected for determination of the distribution of the elements Mn, Fe, Ca, Sc, Y, Yb, and Ti within crystals. The instruments used were Particle Induced X-ray Emission (PIXE) and Rutherford Backscattering Spectrometry (RBS) at the Helmholtz-Zentrum Dresden-Rossendorf (HZDR) in Germany. The applied ion beam was a 3 MeV H^+ beam focused to 5-8 μm in diameter. At first, a quick and large scan of an area (2 x 2mm^2) of the sample was initiated, in order to find the smaller areas of particular interest. After the grain of interest was targeted, a higher resolution scan with a step size of 8 μm was applied in order to image the whole grain. X-rays emitted from the samples were detected with a Ketek Silicon drift detector, which was collimated to 80 mm^2. This detector, positioned outside the sample chamber, is equipped with a 1 μm silicon-nitride window, a 6 mm air layer and a 25 μm Be window. The contamination of light elements was reduced using a 110 μm Mylar absorber. A collimated strip detector was used to detect backscattered photons at a scattering

angle of 173°. The acquired data was gathered in a “Fastcom MPA3 – PC data acquisition” format. Measurements obtained from RBS were for affirming major element compositions, while the application CSIRO Dynamic Analysis method in the software GeoPIXE was used in analyzing the X-ray data. The latter method in GeoPIXE selected the elements of interest and created a dynamic analysis, which finally emerges as spatial element images. The detection limits are based on the lowest peak size for an X-ray line, which is discriminated from the background (including overlaps from X-ray lines of other elements).

Software data programs

Both ArcGIS and Adobe Illustrator CS6 were used to create a regional map displaying the regional Sc distribution of the investigated pegmatite bodies. Additionally, Adobe Illustrator was used in accentuating studied garnet grains in the different pegmatite samples. The contrast and brightness of BSE-images were adjusted to improve picture quality by the use of Adobe Photoshop CS6, which was also used to modifying PPL-images of both analyzed garnet grains and mineral assemblages of host rocks.

3. Results

3.1 Field description of Tørdal pegmatites

During the fieldwork in Tørdal the Grønliheii, Kleppe quarry, Lislegrønlia, Mjeltedalen, Sjauset, Storemyr (3), and Upper Høydalen garnet-bearing pegmatites were visited and sampled. Additionally, garnet samples from the Bratterud, Butvatnet, Heftetjern (1-2), Svåheii (2-3), Storemyr (1-2), Upper Høydalen (1), and Lower Høydalen were supplemented by previous field trips in Tørdal. All of these garnet samples are listed in Appendix 7.1 (all from the wall zone except two “cleavelandite”-zone garnets, comprising the Upper Høydalen 12 and Lower Høydalen samples), and viewed in both a smaller mapped area and a larger regional map of Tørdal (Fig. 3.4 and 3.35, respectively). The closely studied pegmatites comprise the Upper Høydalen, Kleppe quarry and Mjeltedalen locations because the outcrops at these locations were more accessible. The main minerals observed in the Tørdal pegmatites are pink, white and green K-feldspar, white albite, quartz, and mica (Juve and Bergstøl, 1997). “Amazonite”, the green color variety of K-feldspar, is abundant but occurs in certain areas only, in particular in the northern part of the Tørdal pegmatite field. Molybdenite is a common and characteristic accessory mineral of the Tørdal pegmatites, which is found predominantly in the southeastern part of the pegmatite field. The chemical evolved pegmatites at Lower and Upper Høydalen, being Li- and Sn-enriched, contain in addition cassiterite (tin-rich) (Oftedal, 1942; Segalstad and Eggleston, 1993). During the fieldwork accessory magnetite was observed in pegmatites close to the Tørdal granite in the southern part of the pegmatite field. Other common accessory minerals of the Tørdal pegmatites include e.g. beryl, ixiolite, topaz, fluorite, zinnwaldite, spessartine, tantalite etc. (e.g. Oftedal, 1942; Juve and Bergstøl, 1997).

Previous field descriptions by (e.g. Oftedal, 1942; Segalstad and Eggleston, 1993; Kristiansen, 1998; Segalstad and Raade, 2003 and own field observations), including Upper and Lower Høydalen, Heftetjern, and Skardsfjell, revealed that the chemical evolved Tørdal pegmatites exhibit complex internal zoning. This zoning, from the margin to the core, comprise: **1)** a 2-5 cm wide border zone with medium-grained granitic texture containing biotite, **2)** a wall zone characterized by coarse quartz-plagioclase intergrowths (graphic granite) **3)** a megacrystic intermediate zone with an increasing proportion of K-feldspar compared to plagioclase, and bent and/or curved white micas ("ballpen mica") **4)** and a massive quartz core. The pegmatite contacts with the wall rock are sharp. At the border between the intermediate zone and the core and within the core zone discordant "cleavelandite" zones with coarse pink mica ("lepidolite") are developed. Less evolved Tørdal NYF pegmatites do not have "cleavelandite" zones and primitive abyssal pegmatites do not show any particular zoning at all, e.g. pegmatites exposed in the Kleppe quarry. Figure 3.5 shows the schematic zoning of the Upper Høydalen pegmatite.

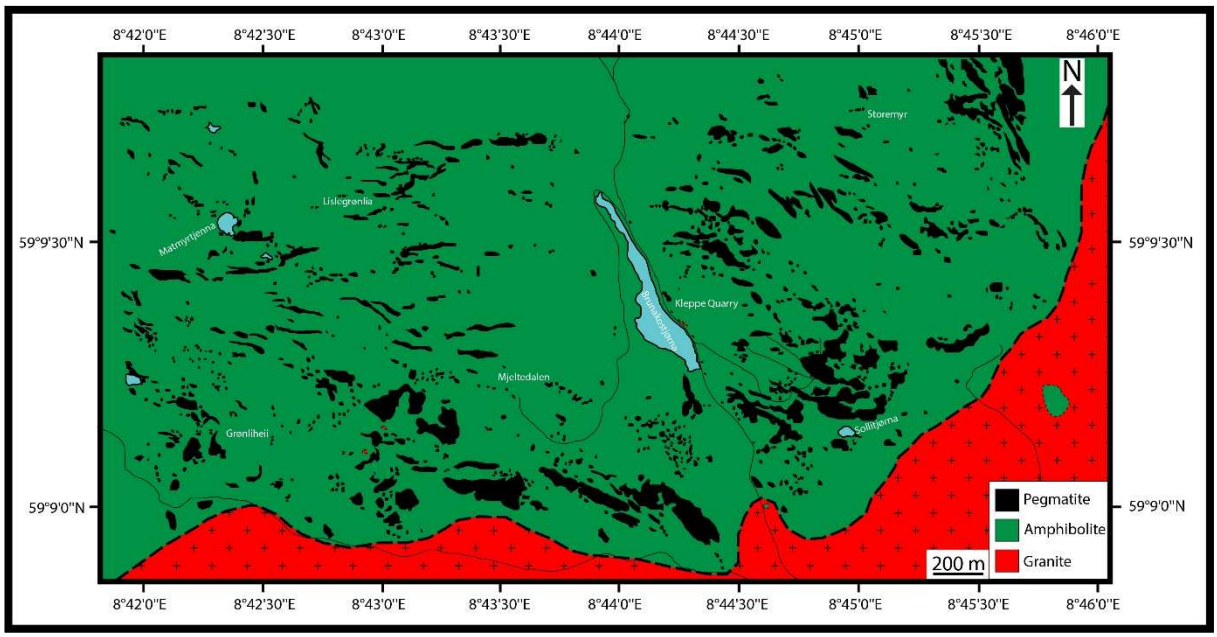

Figure 3.4: Geological map of the mapping area showing the distribution of mapped pegmatite bodies. Many of the pegmatites were both mapped in the field, and additionally identified through satellite photos (Kartverket, 2017). Some xenoliths of amphibolite (green) are present in the midst of the Tørdal pluton red).

Figure 3.6 shows examples of typical textures of the different zones (mentioned above) of the Upper Høydalen pegmatite. In Fig. 3.6 A and B) the contact between wall rock and pegmatite can be seen. At the contact, the 2 to 5 cm thick pegmatite border zone 2 exhibits a medium-grained texture with intergrown quartz, white K-feldspar and plagioclase and a few biotite crystals. The wall zone is characterized by the occurrence of large (up to 1 m in diameter) spherical plagioclase megacrysts, which are graphically intergrown with quartz. On the periphery of the plagioclase megacrysts concentric lines of coarse and dark brown almandine-spessartine garnet and "ballpen mica" are developed (Fig. 3.6 C). The intermediate or blocky zone is dominated by large (0.5-2 m) "amazonite" megacrysts, which are embedded in quartz

and framed by muscovite booklets (Fig. 3.6 D). The pegmatite core consists of massive quartz. Characteristically for the Upper Høydalen pegmatite is the occurrence of "cleavelandite" replacement zones with paragenetic megacrystic "lepidolite" (with sheets up to 30 cm in size), topaz and moganite (pink variety of beryl) (Fig. 3.6 E-F). Accessory minerals were observed in the "cleavelandite" zone include tantalite, fluorite, orange spessartine, and cassiterite. So far no minerals with Sc as its main constituent have been reported from the Upper Høydalen pegmatite (Segalstad and Raade, 2003), although relatively Sc-rich ixiolite or wodginite micro inclusions (1.28 wt.% Sc_2O_3) in cassiterite have been reported by Raade and Brastad (1993). No data of the Sc content of garnets neither from the wall zone, intermediate zone nor from the "cleavelandite" replacements zones have been reported from the Upper Høydalen pegmatite so far.

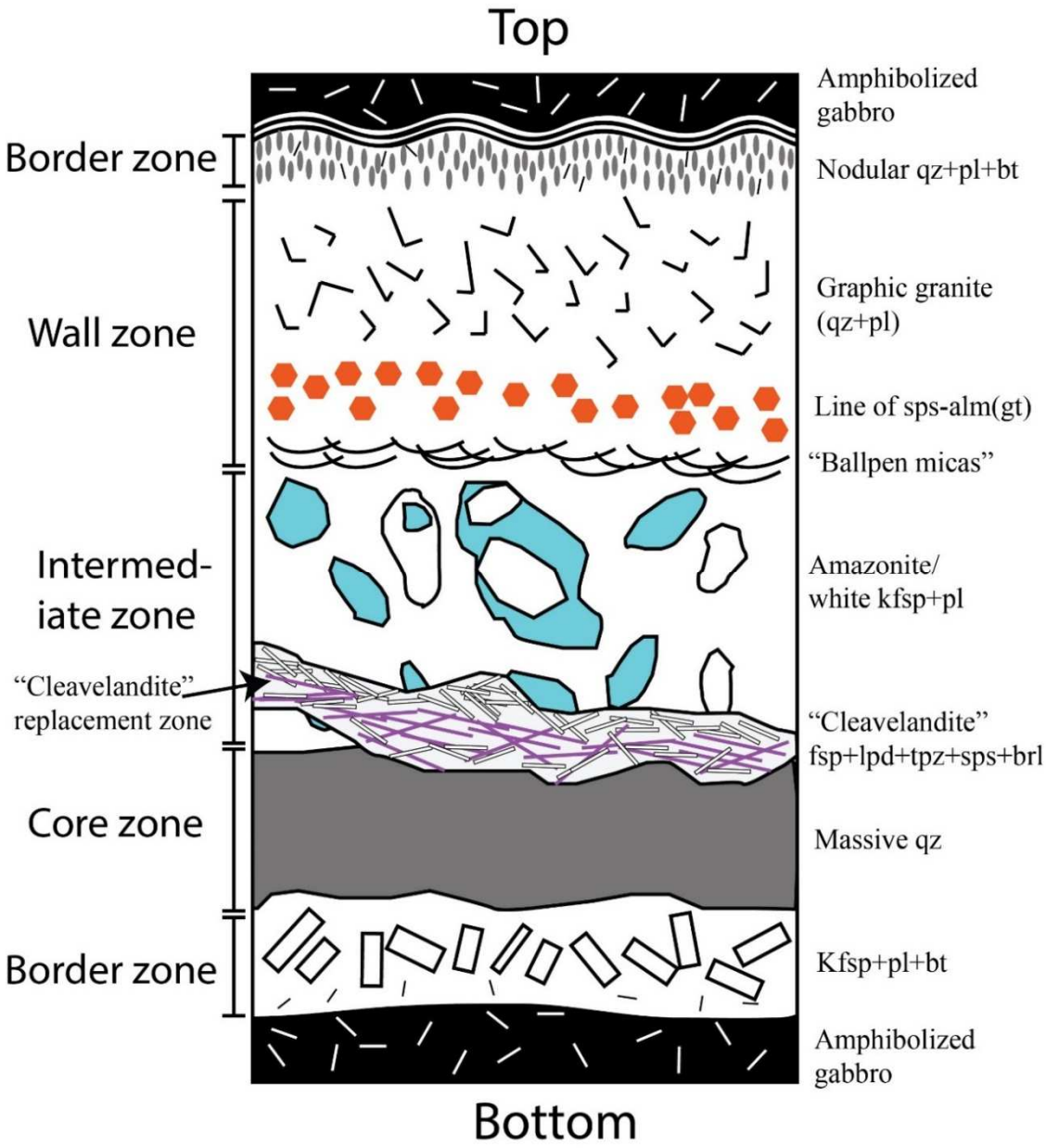

Figure 3.5: A simplified bottom-top sketch of the Upper Høydalen pegmatite. Layer thickness and crystal sizes are not up to scale. Mineral abbreviations: qz = quartz, pl = plagioclase, gt = garnet, sps = spessartine, alm = almandine, bt = biotite, Kfsp = K-feldspar, fsp = feldspar, lpd =lepidolite, tpz = topaz, brl =beryl.

Figure 3.6: Pegmatite textures from the Upper Høydalen pegmatite. Both top pictures (A-B): are displaying the contact/border between the host rock (amphibolized gabbro), and the pegmatite. At this contact, paleosomes and leucosomes are present, with the additional presence of "nodular" quartz, plagioclase, and biotite. Middle left (C): The presence of the line of garnets (spessartine-almandine), and «ballpen» micas residing in the wall zone of the Upper Høydalen pegmatite. Middle right (D): A relatively large spherical crystal of partly amazonite/white K-feldspar, which is situated in the intermediate zone of the pegmatite (~60 cm yardstick for scale). Both bottom pictures: Both pictures display the 'cleavelandite' replacement zone, which partly penetrates the intermediate and core zones, in which 'cleavelandite' feldspar, sheets of lepidolite, topaz, moganite (pink beryl), and spessartine garnet are present.

The pegmatites of the Heftetjern area have the highest abundance and variety of Sc-bearing minerals, which include bazzite, cascandite, heftetjernite, kristiansenite, oftedalite, scandiobabingtonite, "scandian ixiolite", and thortveitite (Kristiansen, 2009). The pegmatites exhibit a similar internal zoning as the Upper Høydalen pegmatite but lacks the "cleavelandite" replacement zones. Analyses of garnets by Raade and Kristiansen (2000, 2003), from Heftetjern yield relatively high Sc concentrations from ~ 0.3 wt.% to ~ 0.5 wt.%. Dark brown almandine-spessartine garnet occurs commonly in the wall zones (sampled for this study). Raade et al. (2002) state that these garnets Sc-rich garnets are not primary, but part of the late hydrothermal phase, which may explain the high Sc content as the Sc-minerals at Heftetjern are typically hydrothermal in origin. In addition, Chukanov et al. (2017) described the occurrence of spessartine in small cavities of the "cleavelandite" zone.

In the following, some of the less evolved pegmatites are described more in detail. The relatively large and abyssal pegmatites at the Kleppe Quarry form a network of large pegmatite lenses partially interconnected with pegmatite veinlets (Fig. 3.7 A-B). Some of the larger pegmatite lenses comprise pegmatitic layers alternating with aplitic layers. The main minerals in these pegmatites are smoky quartz, plagioclase, pink and white K-feldspar, with accessory garnet and molybdenite (Fig. 3.7 C-D). The garnet crystals are present both in the coarser pegmatitic layers (crystal size: 2 mm – 1cm), and in the fine-grained aplite layers (crystal sizes: 0.1 – 1 mm). Other minerals reported from this location include blue alkali- and Mg-rich beryl (Juve and Bergstøl, 1997). In addition to the "real" pegmatites, both thin layers of paleosomes and leucosomes were interpreted as evidence in situ partial melting of amphibolites, which were situated next to the pegmatites (Fig. 3.7 E). Some of the large leucosomes form foliation-parallel pegmatitic veins (in the amphibolites), which are partially boudinaged due to shearing during crystallization (Fig. 3.7 E). This observation may be evident that the pegmatite melts emplaced when the host rock was ductile, which implies that the pegmatite veins are syn-intrusive/kinematic in regards to the host rock deformation. This may further suggest that the pegmatite melts were probably formed by local anatexis of the amphibolites and that the anatectic pegmatite-forming melts did not move far from their origin.

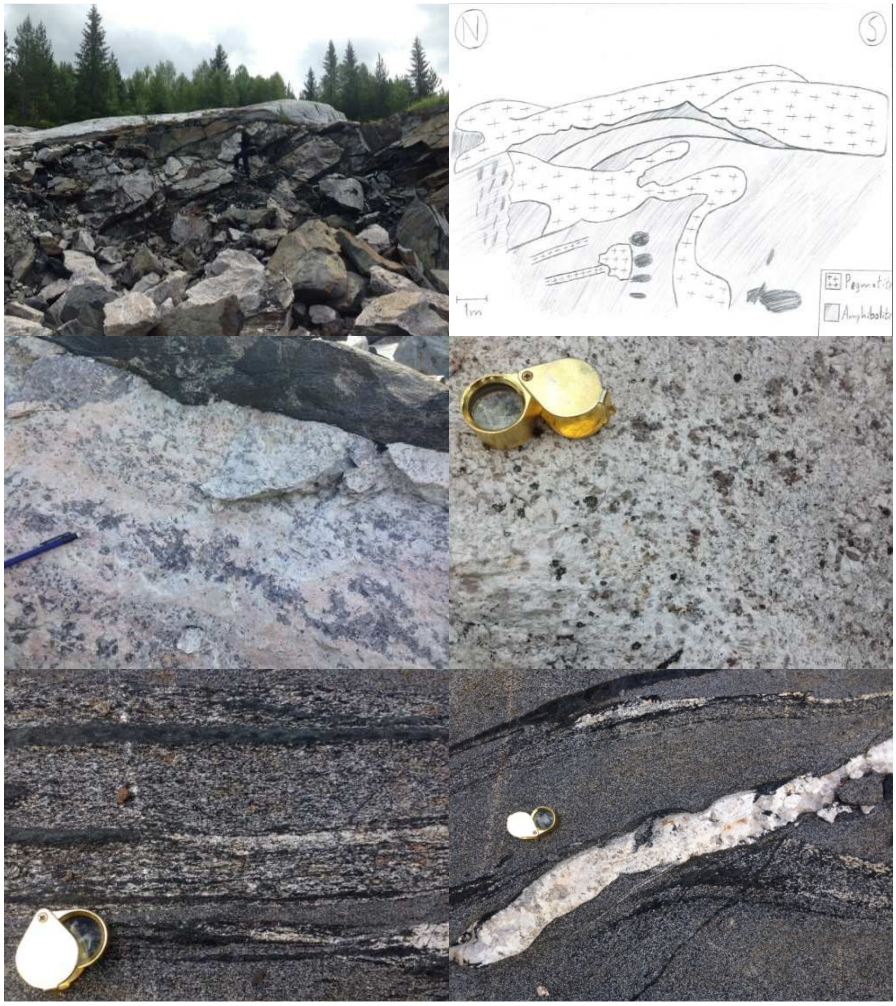

Figure 3.7: Both top pictures (A-B): Image of the pegmatite dykes and bodies exposed in the Kleppe Quarry, with a corresponding sketch (B) of the photograph shown in (A). Middle left (C): A contact between the pegmatite and amphibolite.

The pegmatite contains both pegmatitic and aplitic layers. Occasionally molybdenite appears as an accessory mineral. Middle right (D): Garnets (black dots) residing in an aplite layer. Lower left (E): Display both paleosome and leucosome layers within the amphibolitic host rock. Lower right (F): Relatively large pegmatitic, boudinaged leucosome consisting of quartz, feldspar and biotite.

As seen for many other pegmatites in Tørdal, the Mjeltedalen pegmatite forms a large boudinaged (max. thickness of ~ 1.5 m) intrusion in the amphibolitic host rock. The pegmatite shows distinct two-type texture: pegmatite blobs surrounded by fine-grained aplite (Fig. 3.8 A). The main minerals of this pegmatite comprise pink K-feldspar, plagioclase, quartz (partly smoky), and biotite. Garnet occurs as accessory mineral both in the pegmatitic and aplitic layers (Fig. 3.8 B). Similarly, other sampled pegmatites with the same mineral assemblages and interlayering comprise the Lislegrønlia, Grønliheii (gadolinite present), and Storemyr locations. Accessory molybdenite has been reported from the Storemyr area (Juve and Bergstøl, 1997). The Sjauset pegmatite contains "amazonite" and muscovite, with accessory yellow beryl and garnet.

Figures 3.8: Left (A): The Mjeltedalen pegmatite appears as a boudinaged pegmatitic sill, which emplaced in foliated amphibolite. The internal zoning of this pegmatite shows distinct layering (top-bottom): Aplite, coarse pegmatite, finer aplite with occurring pegmatitic layer above and blobs below (marked in red), and aplite. Right (B): The sampled garnet crystals occur in the lower aplite layer.

3.2 Petrography of garnets in the Tørdal pegmatites

3.2.1 Optical Microscopy

Under the optical microscope, the Tørdal garnets are commonly euhedral to subhedral exhibiting six- or eight-sided cross-sections, due to their three dimensional dodecahedral {110} or trapezohedral {112} habit, respectively (Nesse, 2013). Some grains appear amoeboid to skeletal due to the high abundance of quartz inclusions, which are commonly concentrically arranged around the crystal cores. Crystal sizes of garnets in Tørdal commonly range: 0.1 – 4.0 mm for smaller grains, larger grains of 6.0 – 7.0 mm, and 1.2 – 2 cm for the largest crystals. The characteristics of the garnet samples observed with optical microscopy are summarized in Appendix 7.2 and imaged in Fig. 3.9:

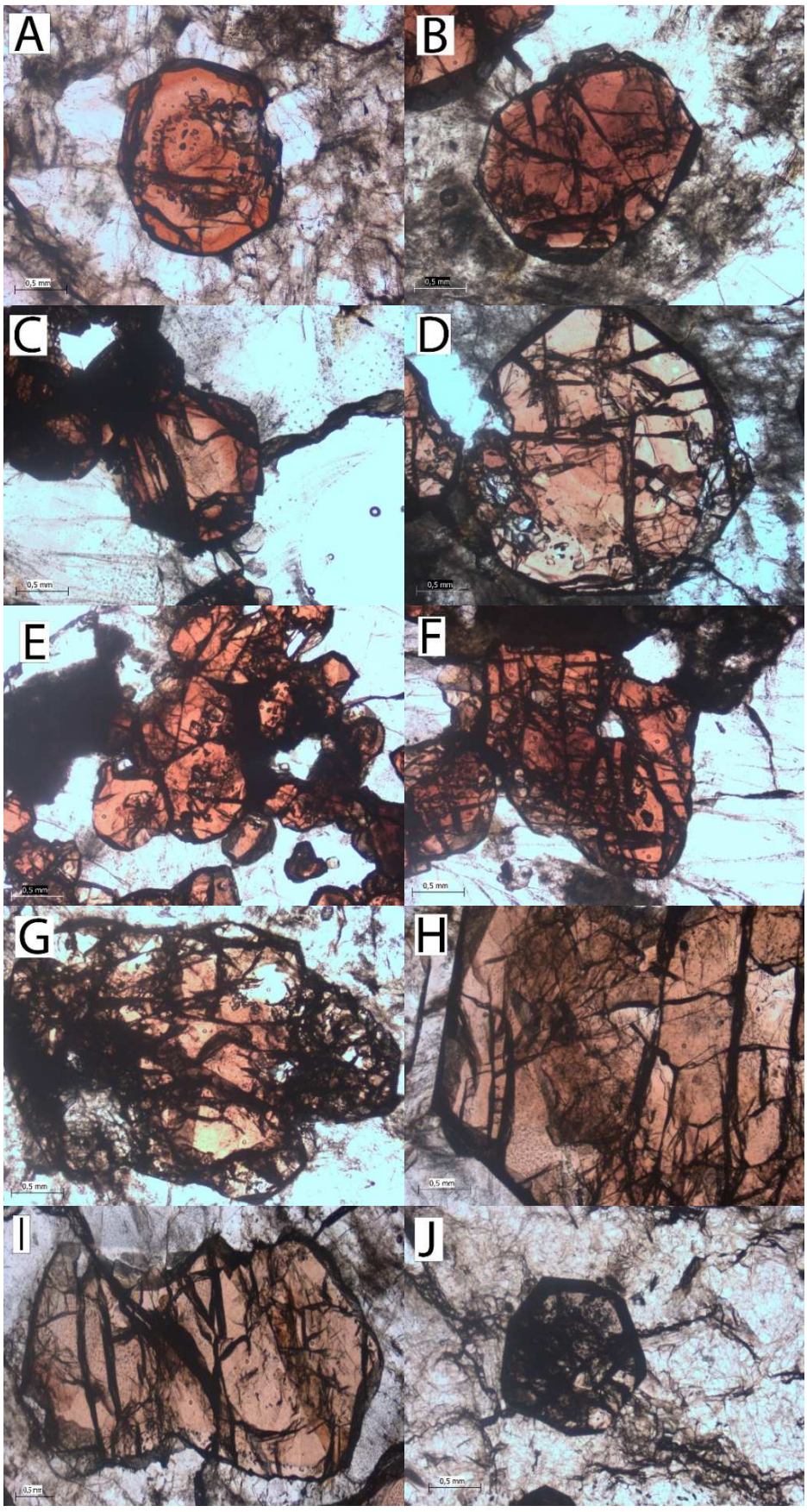
A
B
C
D
E
F
G
H
I
J

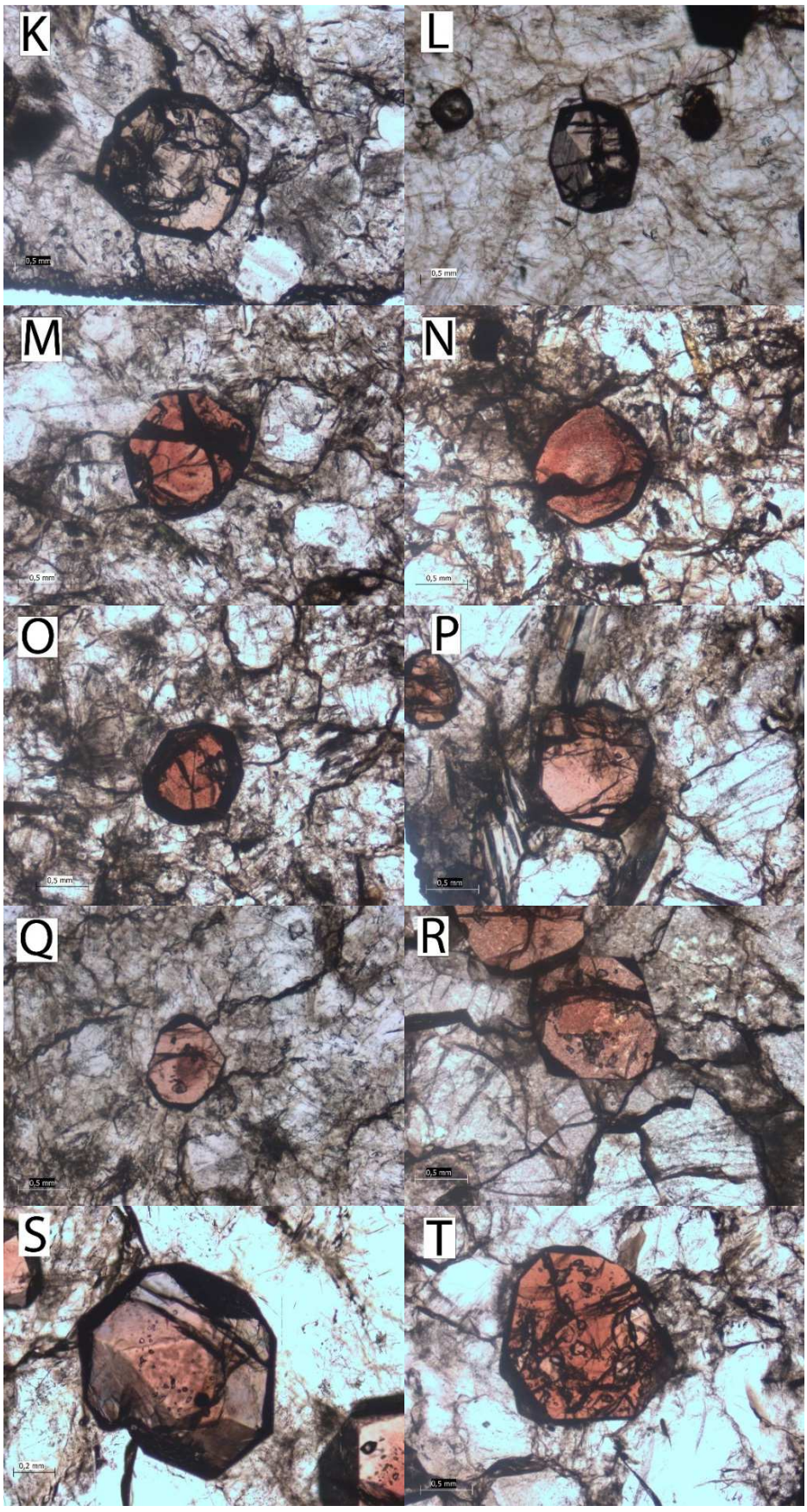
K
L
M
N
O
P
Q
R
S
T

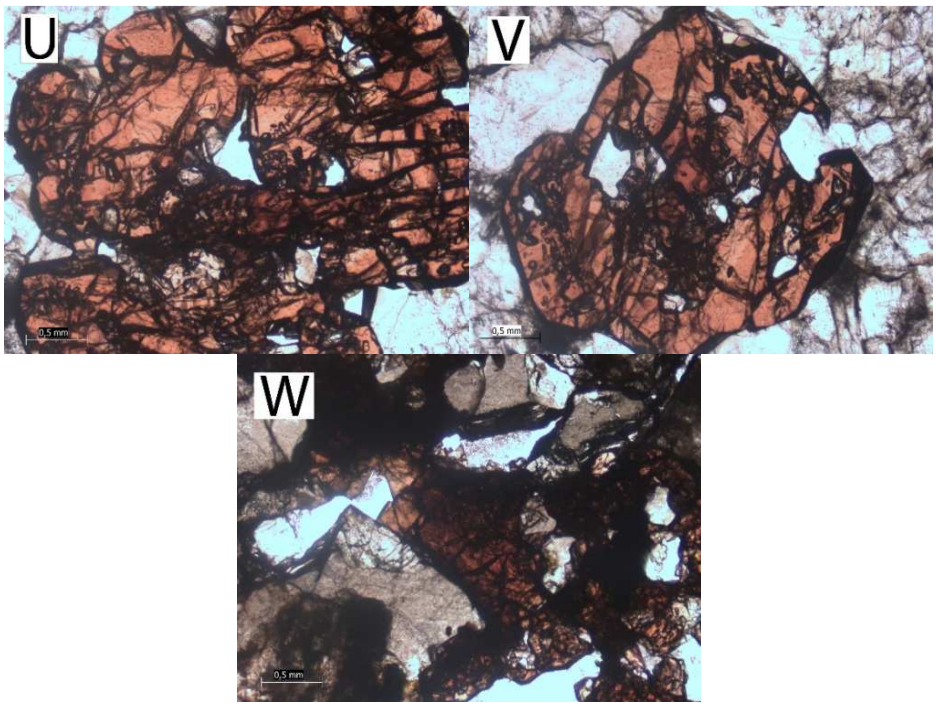

Figure 3.9: Representative PPL-images of garnet grains from analyzed pegmatite samples: A - Svåheii 2 (grain 1), B – Butvatnet (grain 1) C - Storemyr 2 (grain 1), D - Storemyr (grain 1), E - Kleppe (grain 1), F - Kleppe (grain 2), G - Bratterud (grain 1), H – Heftetjern 1 (grain 1), I – Heftetjern 2 (section of grain 1), J - Sjauset (grain 1), K - Sjauset (grain 2), L - Sjauset (grain 3), M – Lislegrønlia (grain 1), N - Lislegrønlia (grain 2), O - Lislegrønlia (grain 3), P – Grønliheii (grain 1), Q - Grønliheii (grain 2), R - Grønliheii (grain 3), S - Grønliheii (grain 4), T- Mjeltedalen 2a (grain 1), U - Mjeltedalen 2a (section of grain 3), V - Mjeltedalen 2a (grain 4), W – Storemyr 3 (grain 1)

3.2.2 BSE imaging

Growth zones within garnet crystals are commonly explored by BSE imaging. In magmatic almandine-spessartine garnets, zonations are mainly caused by fluctuations in the Y and HREE contents (Müller et al., 2012). The growth zoning provides insight into the crystallization history of garnets and, thus, the magmatic evolution of the pegmatites. In the studied garnets, the zoning primarily comprises concentric oscillatory growth zoning (e.g. Fig. 3.13 A), step zoning (e.g. Fig. 3.14 A) and resorption surfaces (e.g. Fig. 3.12 A).

The formation of fine-scale (1- 20 µm) *oscillatory growth zoning* with relative low contrast between the growth zones is generally explained by self-organizing growth (“intrinsic” according to Shore and Fowler, 1996), which is a diffusion-controlled mechanism on the crystal-melt boundary layer (Sibley et al., 1976; Haase et al., 1980; Allègre et al., 1981; Loomis, 1982; Simakin,1984; Pearce, 1993). Oscillatory growth zones form very slowly, at low degrees of undercooling and oversaturation under near-equilibrium conditions. This is possible only when the crystallizing system on the solid-liquid interface is not disturbed, i.e. thus the melt should not convect (Allègre et al., 1981). The observed oscillatory zonation can be explained by the following model (e.g. Allègre et al., 1981): Saturation of Si, Al, Fe, and Mn in the reaction zone increase the garnet growth rate. The increasing growth rate results in the decrease of Fe, Mn, Y and HREE concentrations near the surface of the growing crystal, if the growth rate exceeds the diffusion rate of these elements (results in the formation of a

relatively depleted zone of those elements). The high growth rate favors the incorporation of impurities such as Y and HREE due to the change of planar to the cellular interfaces with rather high specific free energy. The growth rate will slow down when garnet growth is so fast that Fe and/or Mn becomes depleted in the reaction zone and boundary layer. Consequently, the diffusion rate becomes the dominant crystal growth controlling process. The growth rate starts to rise again as soon as the silica in the reaction zone has been recovered. Physical or chemical changes in the bulk magma are not required to develop oscillation zones.

However, wider growth zones (>20 µm) with strong contrasts (sharp boundaries in BSE imaging) may reflect physicochemical changes of the garnet-forming melt ("extrinsic" according to Shore and Fowler, 1996) such as temperature, pressure and magma composition (Bottinga et al., 1966; Allègre et al., 1981). Bottinga et al. (1966) called the non-periodic zones compositional zoning whereas Allègre et al. (1981) referred to them as stepped zoning, which is a term that will be used throughout this thesis. Depending on the type of the physicochemical change (degassing, magma mixing or ascent), the trace element concentrations show an abrupt change, mostly represented by variations of Y and HREE, and sometimes of Fe and Mn. The described oscillatory and step zoning can be disrupted by resorption events, which are visualized as surfaces truncating the previous growth zones (Müller et al., 2010). These abrupt events are suggested to be consequences of sudden changes in temperature, pressure and/or chemistry of the pegmatite-forming melt, which resulted in the partial dissolution (resorption) of the crystal (Müller et al., 2010). Figures 3.10-14 show BSE images of representative garnet crystals 400 to 3000 µm in size. Occasionally larger grains were examined but the images are not provided here. Seven groups of garnets (A, B, C, D, E, F, and G) are distinguished based on the observed structural features:

Group A:

Garnets of this group, include samples from the Svåheii 2 and 3, and Lislegrønlia pegmatites, show contrast-rich oscillatory step zoning (40-290 µm wide) with sub-ordinate fine-scale oscillatory zoning (<20 µm µm wide). The core of the garnets is relatively either light (Fig. 3.10 A-B) or dark (Fig. 3.10 C-D). In all crystals, the core is overgrown by one or two bright step zones (40-120 µm wide). The outer bright step zone displays in some cases a wavy surface accompanied with numerous quartz inclusions, which partially truncate darker growth zones (Fig. 3.10 A). The outmost step zone (140-240 µm wide) with sub-ordinate low-contrast oscillatory zoning appears dull and relatively homogenous in the BSE images.

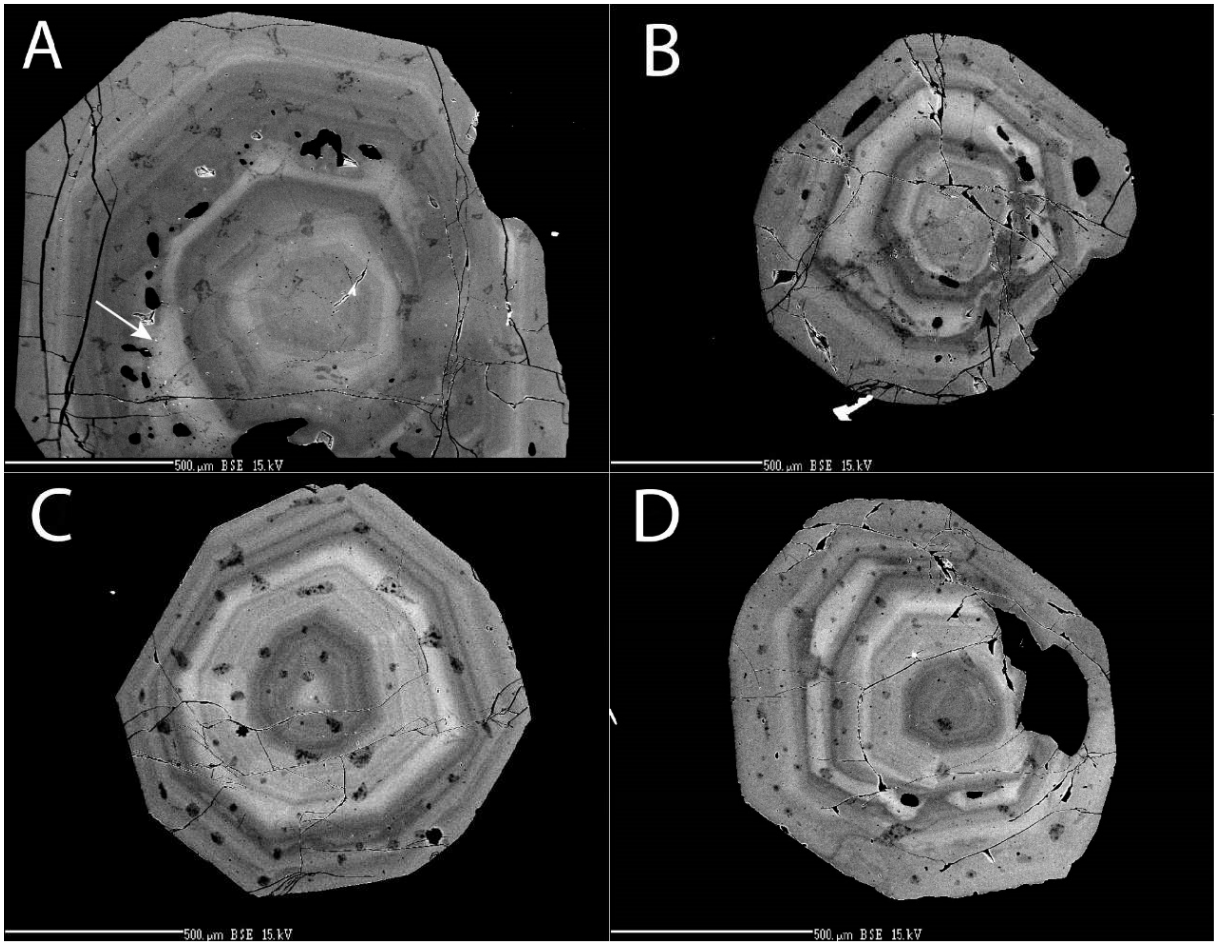

Figure 3.10: BSE images of group A garnets. A - Svåheii 2 (grain 1): displaying the truncating bright wavy surface accompanied with numerous quartz inclusions (white arrow), B - Lislegrønlia (grain 1), C - Lislegrønlia (grain 2), D - Lislegrønlia (grain 3). The Svåheii 3 crystal is not included due to it being too large for whole crystal imaging.

Group B:

Group B garnets are characterized by high abundance of quartz inclusions (30 – 330 µm in size; Fig. 3.11 A), which have disturbed crystal growth and resulted in amoeboid to skeletal crystal habits in some cases (Fig. 3.11 B-D). The crystals commonly contain a bright core, which in most of the cases is partially resorbed. The outer margin (step zone) of the crystals is relatively homogenous exhibiting fine-scale oscillatory growth zoning of low contrast.

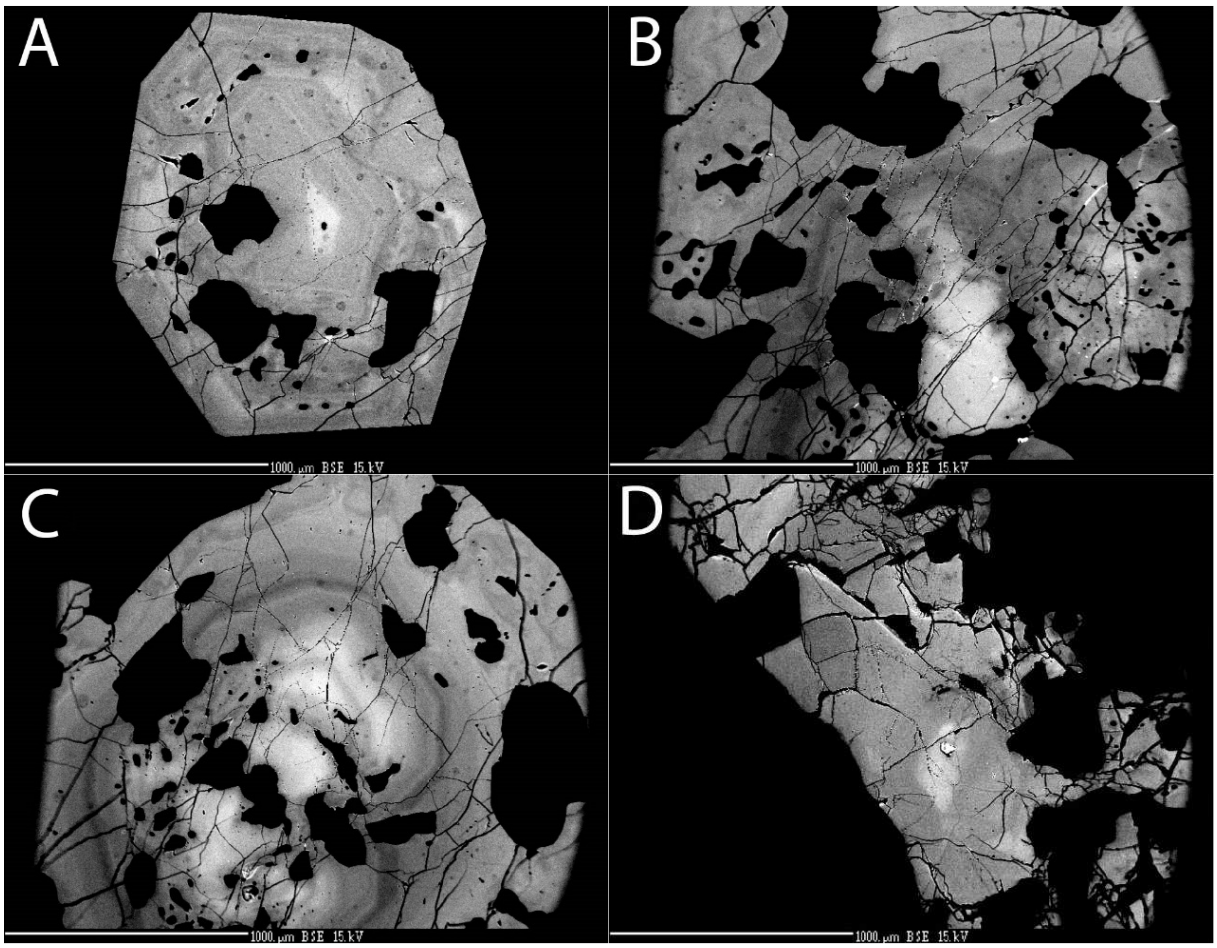

Figure 3.11: BSE images of group B garnets. A- Mjeltedalen 2a (grain 1), B - Mjeltedalen 2a (grain 3), C - Mjeltedalen 2a (grain 4), D - Storemyr 3.

Group C:

The prevalence of a resorption surface separating the bright core (inner step zone) and the darker margin (outer step zone) is characteristic for group C garnets. The bright cores commonly exhibit subordinate, concentric oscillatory zoning. Garnets of this group reside in the samples from the Kleppe Quarry, Bratterud, Sjauset, and Grønliheii pegmatites. In many cases truncating resorption surfaces are accompanied by numerous, concentrically arranged quartz inclusions (5-160 µm) (Fig. 3.12 A, B, C, and D), which may cause an amoeboid to skeletal crystal habit (Fig. 3.12 E). In some crystals the bright, cores are almost completely dissolved (Fig. 3.12 F-G) and there are crystals (in the same samples) which does not display bright cores at all. In those cases, the cores were presumably resorbed completely (Fig. 3.12 H and central crystal in Fig. 3.12 I). In few cases, crystals exhibit an additional, bright but narrow step zone (20 µm wide), which are features of dissolution (e.g. Fig. 3.12 J).

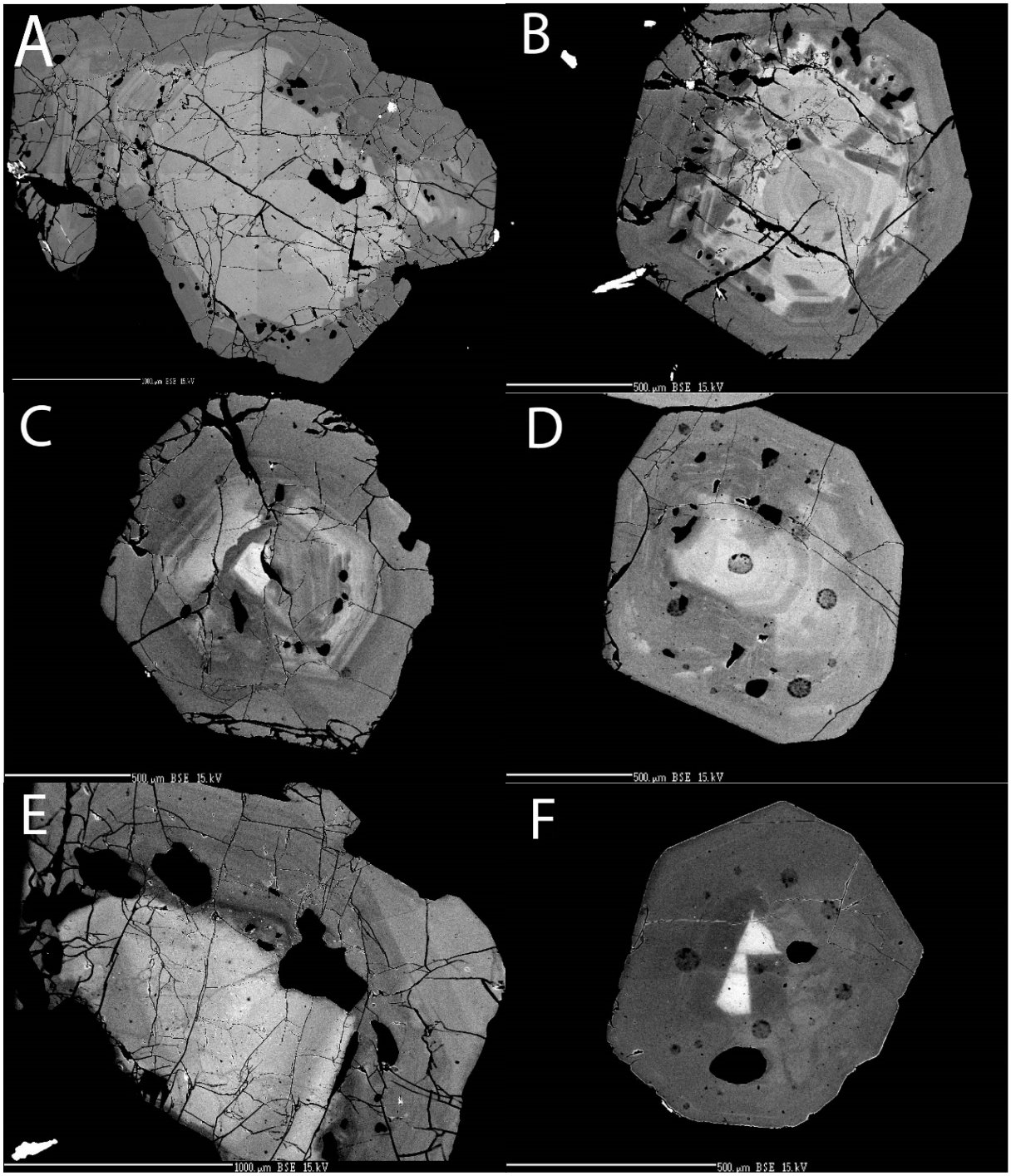
A
B
500 µm BSE 15 kV
C
500 µm BSE 15 kV
D
500 µm BSE 15 kV
E
1000 µm BSE 15 kV
F
500 µm BSE 15 kV

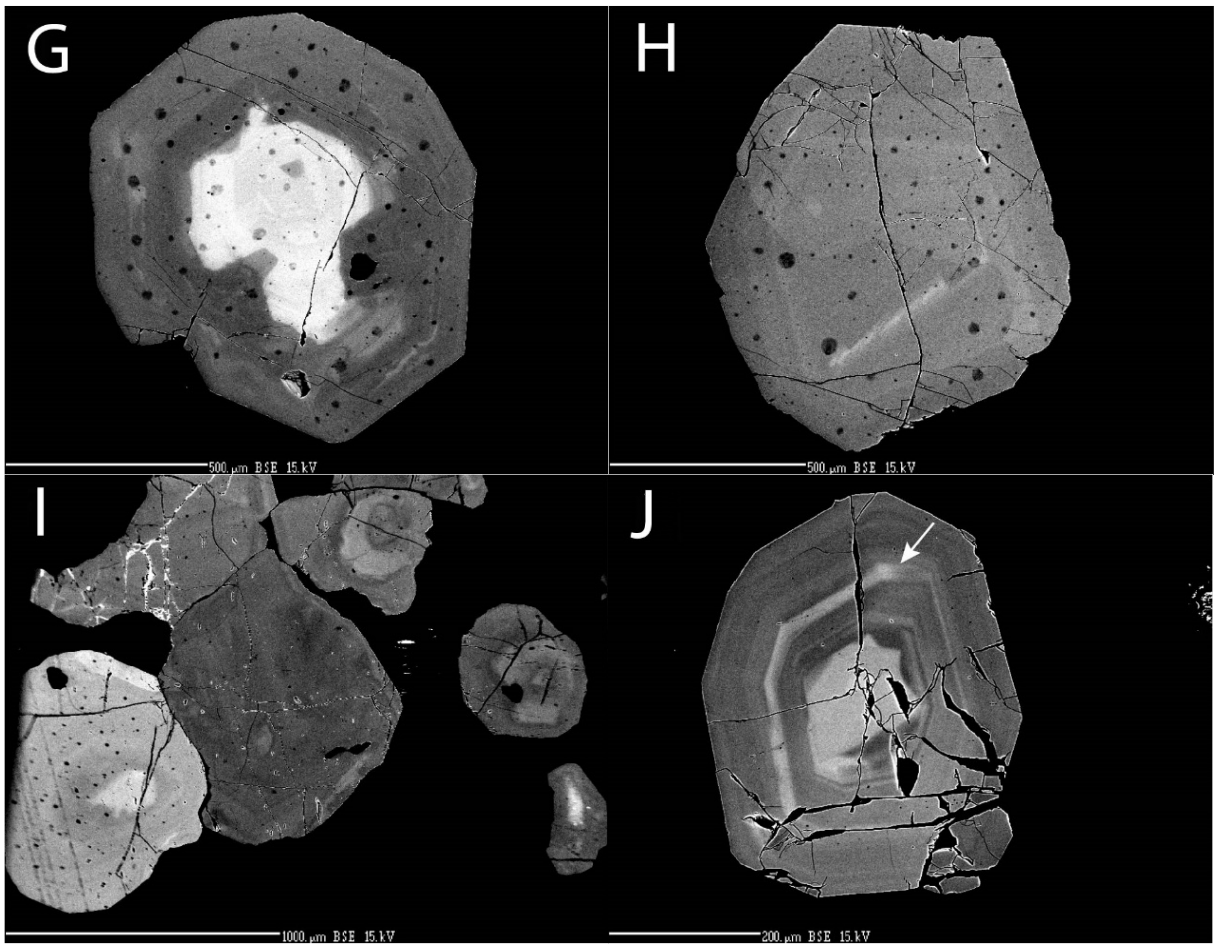

Figure 3.12: BSE images of group C garnets. A – Bratterud (grain 1) , B – Sjauset (grain 1), C - Sjauset (grain 2) , D - Grønliheii (grain 3) , E - Kleppe quarry (grain 2), F - Grønliheii (grain 2), G - Grønliheii (grain 4), H - Grønliheii (grain 4), I – cluster of garnet crystals from Kleppe quarry, J – Sjauset (grain 3): Displayed bright and narrow zone, which is a feature of dissolution (white arrow).

Group D:

Group D garnets, from the Storemyr pegmatite 1, exhibit fine-scale, contrast-poor oscillatory zoning. Step zoning cannot be identified in this group, due to the general gradual character of the individual zones. In general, the crystal core commonly appears slightly brighter than the margin, whereby the brightness continuously decreases from core to rim. Some large quartz inclusions (50-430 µm) occur in the outer margin of the crystal (Fig. 3.13 A).

Group E:

Group E garnets, from the Storemyr pegmatite 2, show fine-scale, contrast-poor, oscillatory zoning in general, similar to Group D garnets. However, the crystal core appears darker (expect the innermost center of the crystal) and the brightness increases more or less continuously from core to rim. Similar to Group D crystals, step zoning cannot be defined, due to the general gradual character of the individual zones. However, the relative bright center and darker intermediate zone and the bright margin might be interpreted as three individual step zones. Bright and fine-scale irregular growth zoning (<20 µm wide) resides in the inner dark step zone (Fig. 3.13 B). A minor resorption appears at the margin of the crystal

(Fig. 3.13 B). Bright zircons (white dots) are abundant and aligned in fractures transecting the crystal.

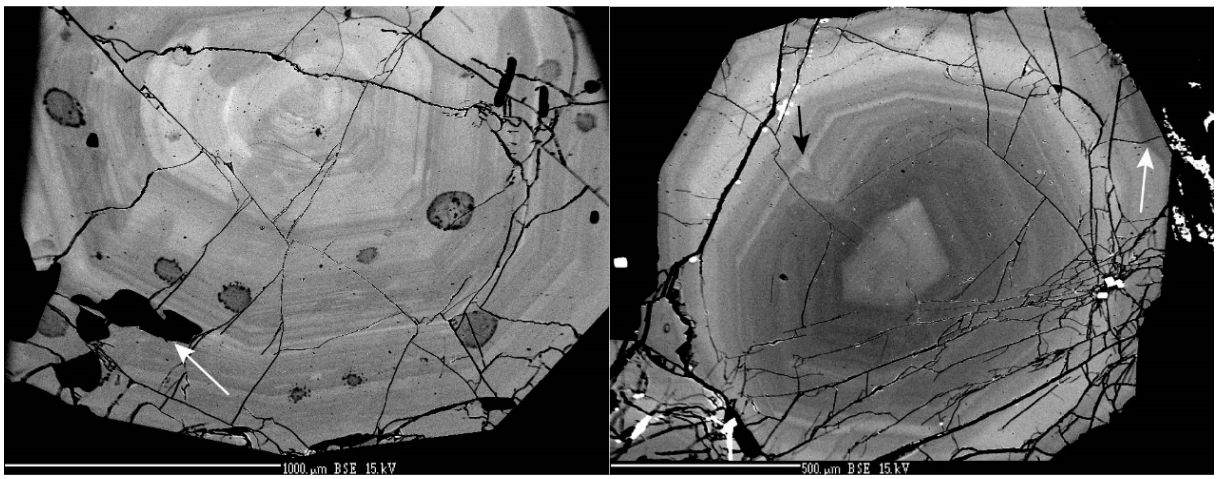

Figure 3.13: Left (A): BSE-image of a group D garnet crystal (grain 5) from the Storemyr pegmatite 1. Larger quartz inclusions appear at the outer margin of the crystal (white arrow). Right (B): BSE-image of a group E garnet crystal (grain 1) from the Storemyr pegmatite 2. Bright and fine-scale irregular growth zoning (<20 µm wide) residing in the inner darker step zone (black arrow). Minor truncating resorption surface appearing at the rim of the crystal (white arrow).

Group F:

Group F garnets include samples from the Butvatnet, Heftetjern and Heftetjern 2 pegmatites. These crystals are characterized by bright but contrast-poor crystal cores (step zone 1) overgrown by a relatively thin (up to 200 µm), dull margin (step zone 2; Fig. 3.14). Step zone 1 is bordered by a resorption surface, which is very distinctive for the crystals shown in Fig. 3.14 A-B. In Fig. 3.14 B, the resorption cause patchy structures (white arrows). Step zone 1 displays in some but not all cases subordinate, fine-scale oscillatory zoning (10-40µm wide). The crystals exhibit a slightly dark core within step zone 1 (Fig. 3.14 A), while others lack any fine-scale zoning (Fig. 3.14 B).

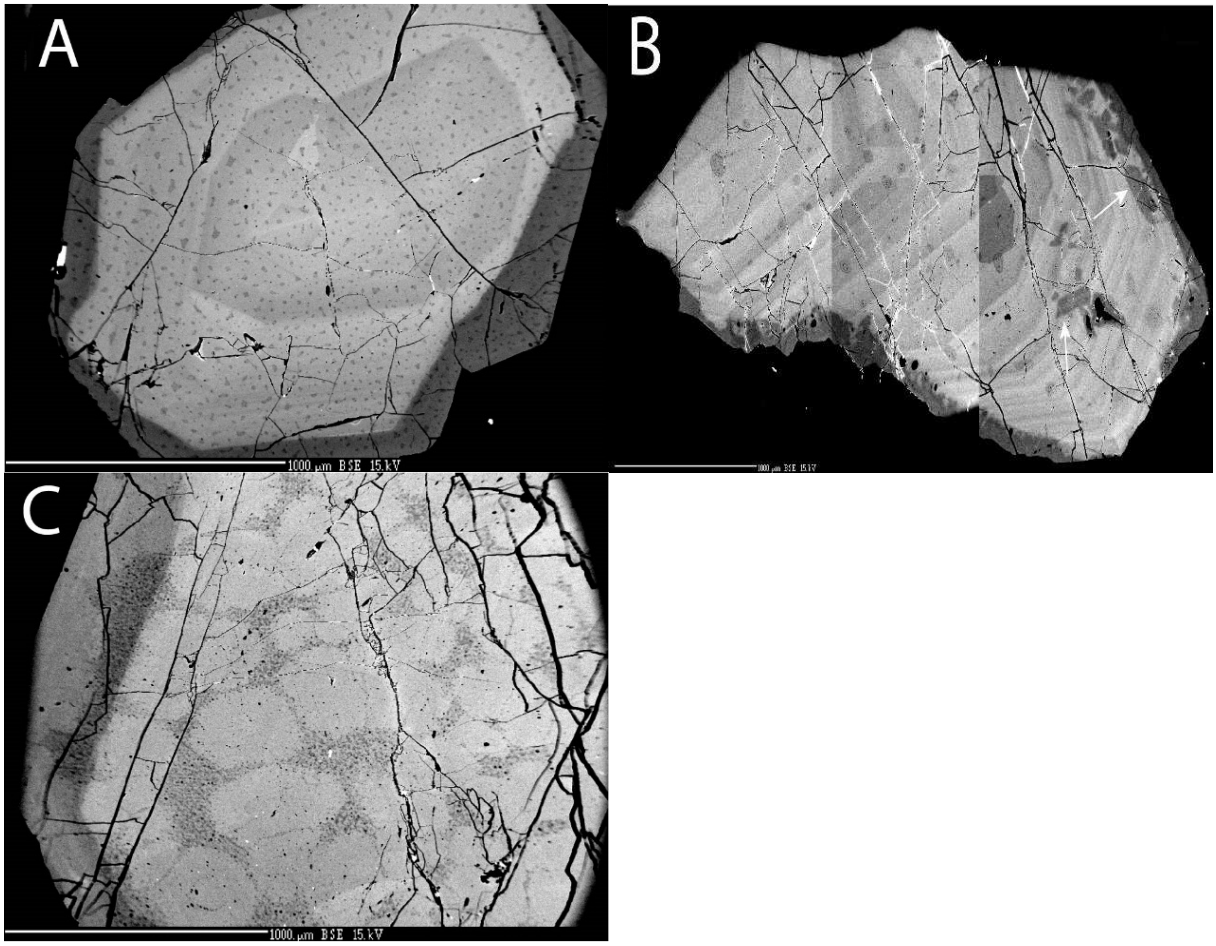

Figure 3.14: BSE images of Group F garnet. A - Butvatnet (grain 3), B - Heftetjern (grain 1), C - Heftetjern 2 (section of grain 1): The regular dots in the bright core of the crystal shown in (A) and the greyish, network-like structures on the crystal are sample surface contamination.

Group G:

This group of garnets comprises large crystals (1 – 2 cm), which does not show growth zoning in BSE imaging. Garnets of this group originate from the Upper Høydalen and Lower Høydalen pegmatites, with one sample from the intermediate zone (Upper Høydalen 1 sample), and two other garnets from the cleavelandite replacement zones of the Upper Høydalen and Lower Høydalen pegmatites (Upper Høydalen 12, and Lower Høydalen samples).

3.2.3 Micro inclusion inventory

A total of 49 Tørdal garnets from the 17 pegmatite samples were investigated by SEM. The micro inclusions residing in the garnet crystals appear in µm sizes. Table 3.4 summarizes the abundance and diversity of the micro inclusion inventory of the Tørdal garnets. The individual micro inclusion species, their appearance (size, habit, frequency) and chemistry are described in detail in this chapter.

Quartz, SiO_2

High abundances of anhedral quartz inclusions (5 - 330 µm) in garnet crystals are characteristic for the Svåheii 2, Storemyr 1, Kleppe Quarry, Heftetjern, Heftetjern 2, Bratterud, Sjauset, Grønliheii, Mjeltedalen 2a, and Storemyr 3 samples. Lesser abundances are observed in garnet crystals from the Svåheii 3, Butvatnet and Lislegrønlia pegmatites. The garnet crystals of the Storemyr 2, Upper Høydalen 1 (intermediate zone), Upper Høydalen 12 and Lower Høydalen samples (both latter garnets from the cleavelandite replacement zone) appear to be free of quartz inclusions.

Zircon, $Zr(SiO_4)$

Garnet crystals from the Svåheii 2, Storemyr 2 and Heftetjern pegmatites exhibit high abundances of both euhedral-subhedral tabular and acicular zircon inclusions (3 – 50 µm). Lesser abundances of zircon are observed in garnet crystals from the Svåheii 3, Butvatnet, Kleppe Quarry, Bratterud, Sjauset, Lislegrønlia, Grønliheii, Mjeltedalen 2a, and Storemyr 3 pegmatites. Garnet crystals from the Storemyr, Upper Høydalen (intermediate zone), Upper Høydalen 12 (cleavelandite replacement zone), and Lower Høydalen (cleavelandite replacement zone pegmatite) samples do not contain zircon inclusions.

Xenotime Group $Y(PO_4)$ / $Yb(PO_4)$

Both subhedral cubical and anhedral xenotime group inclusions (2 – 30 µm), with simple zoning, are sometimes present in some garnet crystals from the Svåheii 3, Butvatnet, Upper Høydalen 1 samples. Normalized atomic proportion percentages show a relatively consistent chemistry of xenotime with even Y and P levels, with some traces of Yb, Si, and Al. Inclusions of solid solutions between xenotime-(Y) and xenotime-(Yb) are sporadically found in some grains of the Butvatnet sample.

Gadolinite-(Y), $Y_2Fe^{2+}Be_2Si_2O_{10}$

Inclusions of gadolinite-(Y) are infrequently occurring in some garnet crystals from the Storemyr sample. Sizes of the mentioned inclusions are 6 µm, which exhibited subhedral cubical shapes. EDS analysis does not offer any detection of Be, but different ratios between Yei, and Si show clear ratios resembling the stoichiometry of gadolinite-(Y). The gadolinite-(Y) inclusions share traces of Nd, with additional traces of Ce for inclusions in garnets from the Bratterud sample.

Keiviite-(Y), $Y_2Si_2O_7$

Keiviite-(Y) frequently occurs in garnet crystals from the Upper Høydalen 1, Heftetjern 2, and Kleppe quarry samples. Occasionally these inclusions are seen to be located in some garnet crystals from the Svåheii 3, Butvatnet, Bratterud, Upper Høydalen 12, and Mjeltedalen 2a. The inclusions generally exhibit tabular euhedral-subhedral shapes with some instances of simple zoning. The sizes of the inclusions are in the range of 1 – 30 µm (with the exception of a 370 µm keiviite-(Y) found in the Heftetjern 2 sample). Most of these inclusions show consistent Y/Si ratio, with some exceptions where Y is substituted with common traces of Ca and Yb, and in some cases Fe, Ce, and Ta (thus a decrease in Y). In some instances, these keiviite-(Y) inclusions exhibit simple zonation. Intergrowths with unidentified Ca-Mn-oxides are sometimes observed.

Y-F-silicate

F-bearing Y-silicate inclusions are frequently observed in many grains from the Svåheii 3 and Heftetjern 2 sample, while sometimes appearing in the garnet crystal of the Upper Høydalen 1 sample. The shape of these inclusions is tabular euhedral-subhedral, with sizes in the range of 3 – 20µm Most of these inclusions show consistent and even ratio between Si, F, and Y. Calcium commonly occurs together with Yb, Mg, Ti, Na, Dy, and Sc in common trace concentrations.

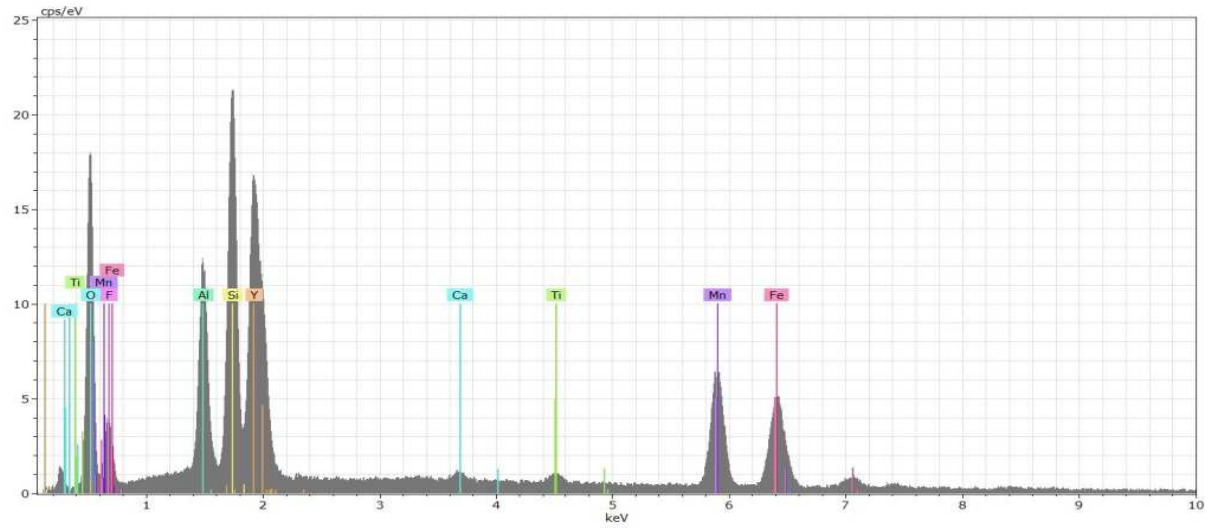

Figure 3.15: Representative EDS-spectra of the F-bearing Y-silicates from the Svåheii 3 sample. Manganese and Fe are remnants of the surrounding garnet chemistry.

Fluorite, CaF_2

Fluorite inclusions were only spotted in the Upper Høydalen 12 sample. These inclusions exhibited subhedral cubical shape with sizes of approximately 5 µm. In general, analyzed inclusions exhibited F twice as abundant as Ca.

Yttrofluorite, $(Ca_{1-x}Y_x)F_{2+x}$, $0.05 < x < 0.3$

Yttrofluorite inclusions frequently reside in garnet crystals from the Lower Høydalen sample, and sometimes occur in garnets from the Upper Høydalen 1 sample. The shapes of these inclusions are either anhedral or subhedral cubical, with sizes ranging from 9 – 23 µm. Analyzed inclusions show a consistent chemistry, resembling yttrofluorite.

Titanite, $CaTi(SiO_4)O$

Titanite is observed sporadically in a few garnets from the Svåheii 2 sample, in which their shapes are subhedral tabular or anhedral. Sizes of the titanites are 15 - 20 µm. Ca/Ti ratios are all approximately 2:1. Although, trace concentrations commonly found such as Al, Nb, Ta, and Fe may be substituting Ti, and thus, explaining the depletion of Ti.

Ca-Fe-LREE-silicate

This relatively large subhedral, bladed and heavily altered (approximately 300 µm) Al-bearing Ca-Fe-LREE-silicate is settled in one of the garnet grains from the Bratterud sample. Calcium and Fe concentrations are fairly even, with minor abundances of LREE (Ce, La, and Pr). Cerium is twice as abundant as La. Traces concentrations of Fe, Mn, Si, Al, and O are remnants of the surrounding garnet chemistry. Si is more abundant than Al, and the O/Si ratio is approximately 3.5:1.

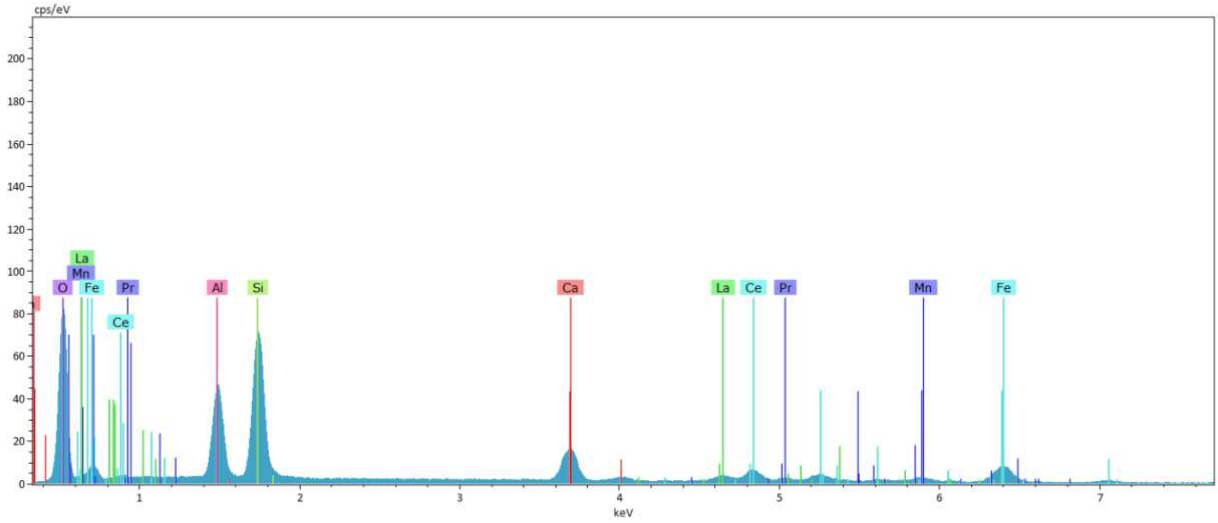

Figure 3.16: EDS spectra of an unidentified Ca-Fe-LREE-silicate from the Bratterud sample.

Ca-Y-LREE-oxide

These unidentified F-bearing Ca-Y-LREE oxides are sporadically spotted in the garnet fragments from the Upper Høydalen 12 sample. These oxides exhibit an anhedral and poikiloblastic shape, with sizes of approximately 10 µm. Calcium is the most abundant component with subordinate Y, in which the Ca/Y ratio is 3:1. LREE(La, and Ce)-contents appeared as minor abundances, where Ce is twice as abundant than La. O/Ca and O/F ratios are 3.4:1 and 6.2:1, respectively. Al and Th (seen as Ag) are barely detected during analysis.

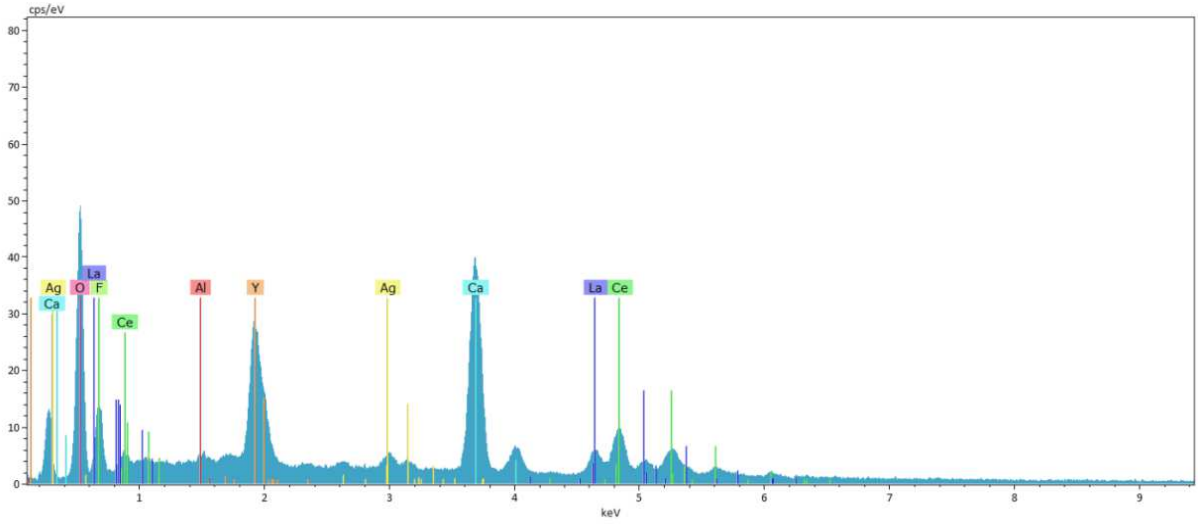

Figure 3.17: EDS spectra of an unidentified Ca-Y-LREE-oxide from the Upper Høydalen 12 sample.

Thortveitite ($REE_2Si_2O_7$)

These Sc-silicate inclusions occasionally reside in the garnet crystal from the Upper Høydalen 1 sample, and in a single grain of the Svåheii 2 sample. The inclusions are subhedral cubical shaped, with sizes of ~10 µm. Analysis of the inclusion of the Upper Høydalen 1 sample shows Sc being the major constituent with subordinate Y and Yb. The thortveitite inclusion from Svåheii 2 shows a consistently even ratio between Sc and Y, with minor traces of Yb. All inclusions of this group are considered members of the thortveitite group ($REE_2Si_2O_7$). The Sc-silicate inclusion from the Upper Høydalen 1 sample are considered a predominantly thortveitite ($Sc_2Si_2O_7$), while the inclusion from the Svåheii 2 location is determined to be solid solution between subordinate thortveitite ($Sc_2Si_2O_7$) and predominant keiviite-(Y) ($Y_2Si_2O_7$). Scandium, one of the main constituents making up thortveitite, is in many instances known to form solid solutions with other elements such as Y, and Yb. (Kristiansen, 2009; U.S. Geological Survey, 2016). The stoichiometric relationship between the three elements is again explained by a simple substitution mechanism where scandium replaces both Y and Yb ($Sc^{3+} \leftrightarrow (Y, Yb)^{3+}$), despite their relative differences in size (0.745 Å for Sc^{3+} in 6-coordination in comparison with 0.900 Å and 0.868 Å for Y^{3+} and Yb^{3+}, respectively) (Shannon, 1976; Raade et al., 2002).

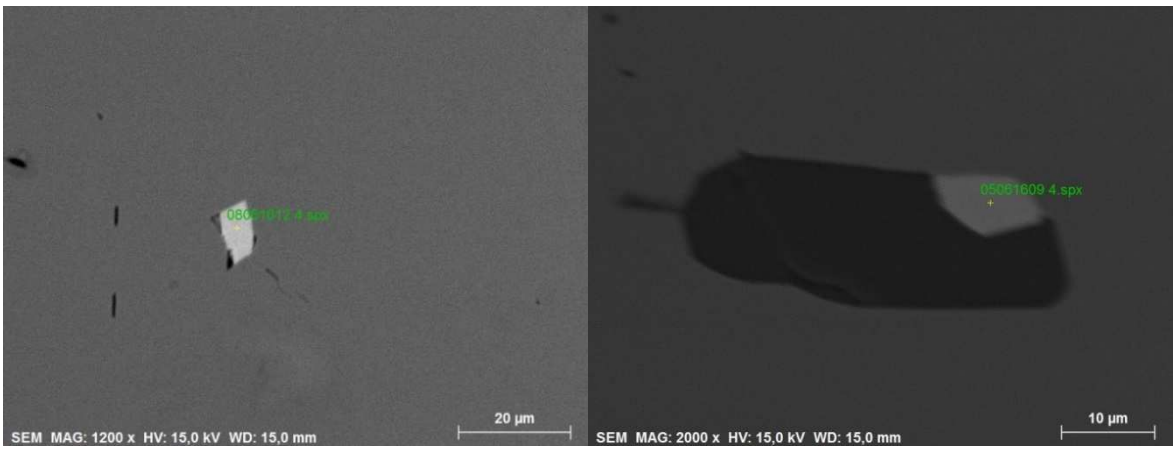

Figure 3.18: Displayed images of the thortveitite inclusions seen in garnets from the Upper Høydalen 1 and Svåheii 2 samples. A (left) – a thortveitite inclusion spotted in the garnet crystal from the Upper Høydalen sample. B (right) – thortveitite inclusion intergrown with quartz in a garnet grain from the Svåheii 2 sample.

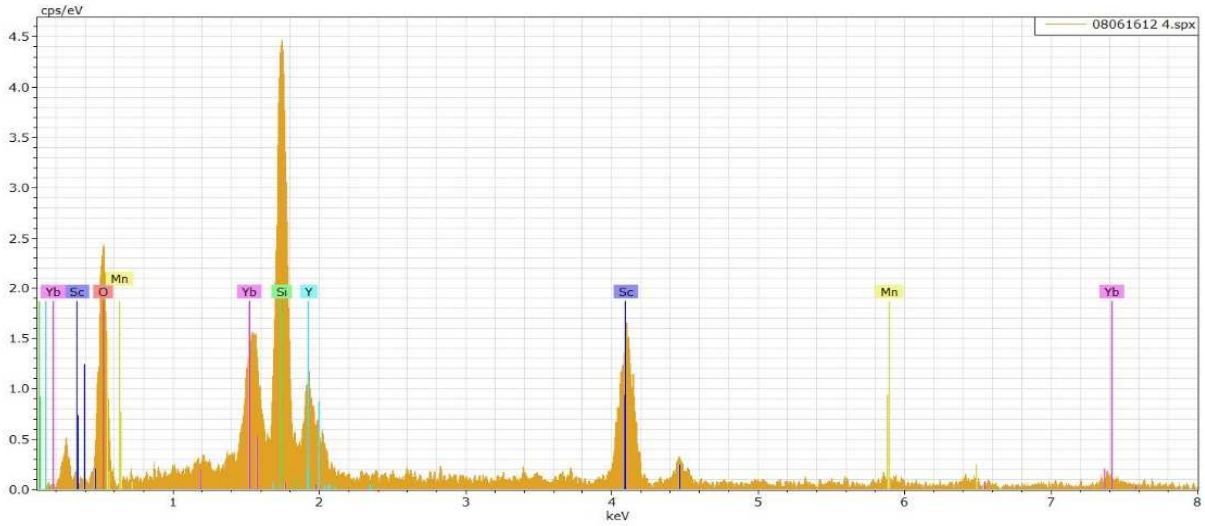

Figure 3.19: EDS spectra of the thortveitite inclusion from the Upper Høydalen 1 sample. Predominant Sc with subordinate Yb and Y, which reflects the solid solutions of between thortveitite ($Sc_2Si_2O_7$), keiviite-(Y) ($Y_2Si_2O_7$), and keiviite-(Yb) ($Yb_2Si_2O_7$).

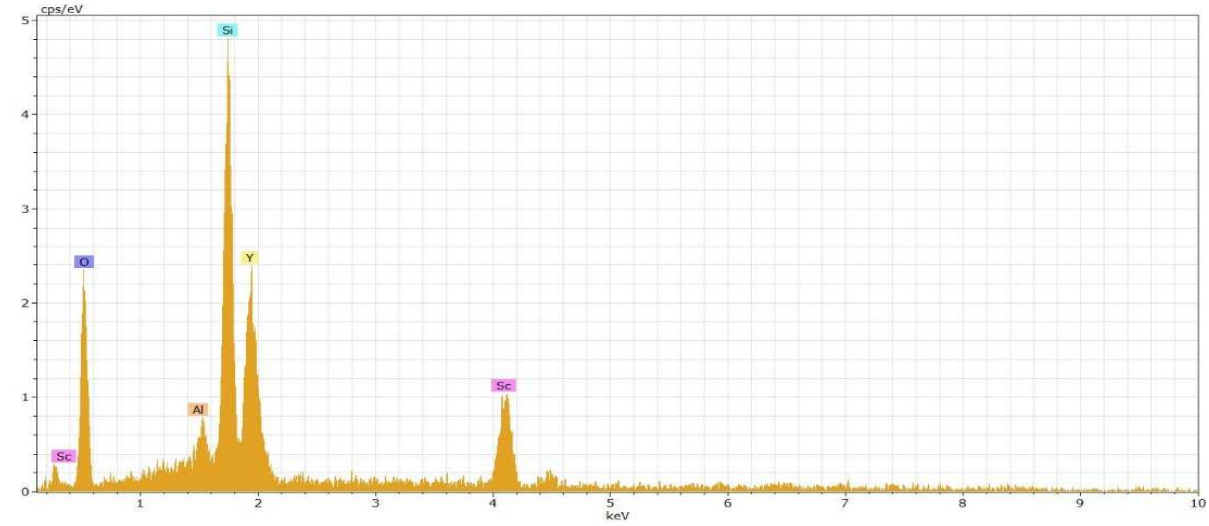

Figure 3.20: EDS spectra of the thortveitite, which are considered solid solutions between subordinate thortveitite ($Sc_2Si_2O_7$) and predominant keiviite-(Y) ($Y_2Si_2O_7$). The displayed EDS spectra is from a thortveitite inclusion from the Svåheii 2 sample.

Ti-Y-mineral

This group of unidentified inclusions includes both Ti-Y-oxides and Ti-Y-silicates. The shape of the inclusions is euhedral-subhedral cubical, with a size of 1 – 4 µm. These inclusions frequently reside in the garnet crystals from the Svåheii 3, Butvatnet, Storemyr 1, and Heftetjern 2 samples. Additionally, they infrequently appear in garnet grains from the Kleppe quarry, Bratterud, Heftetjern 1, Grønliheii, Mjeltedalen 2a, and Storemyr 3 samples. The oxides of this group generally exhibit Ti as a major constituent with subordinate Y, in which Y is in most instances slightly less abundant than Ti. Occasional traces such as Yb, Dy, Ca, Ni, As, Sn and U with additional remnants of the surrounding garnet chemistry, occur during analyses of these oxides. The Ti-Y-silicates exhibit in general consistent and even Ti/Y ratios. Common trace concentrations in these silicates include Sn, U, As, and remnants of the surrounding garnet chemistry, with occasional traces of Pb, Mg, and Ca.

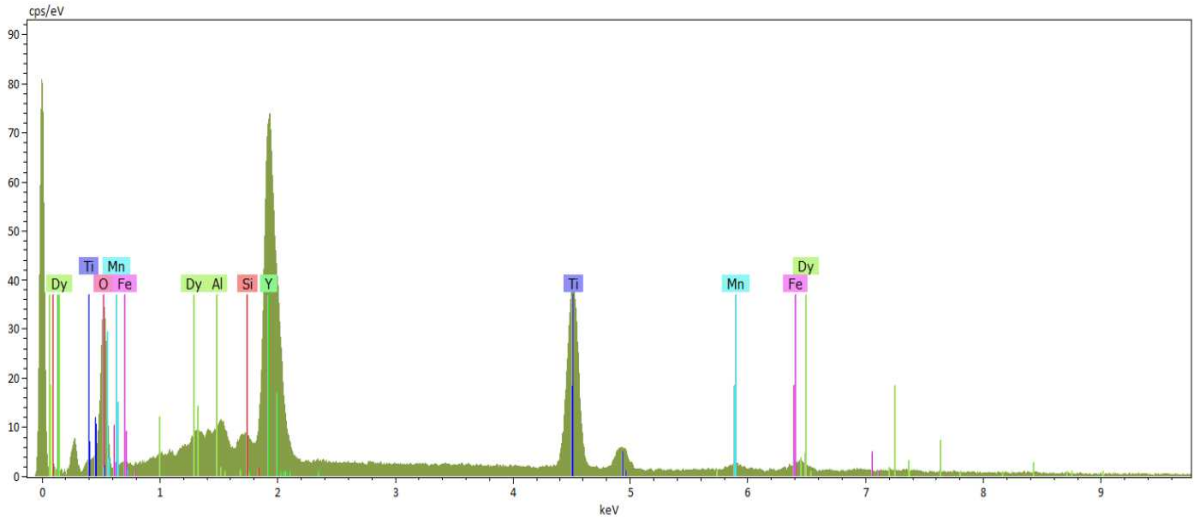

Figure 3.21: Representative EDS spectra of the Ti-Y-oxide inclusions from the Butvatnet sample.

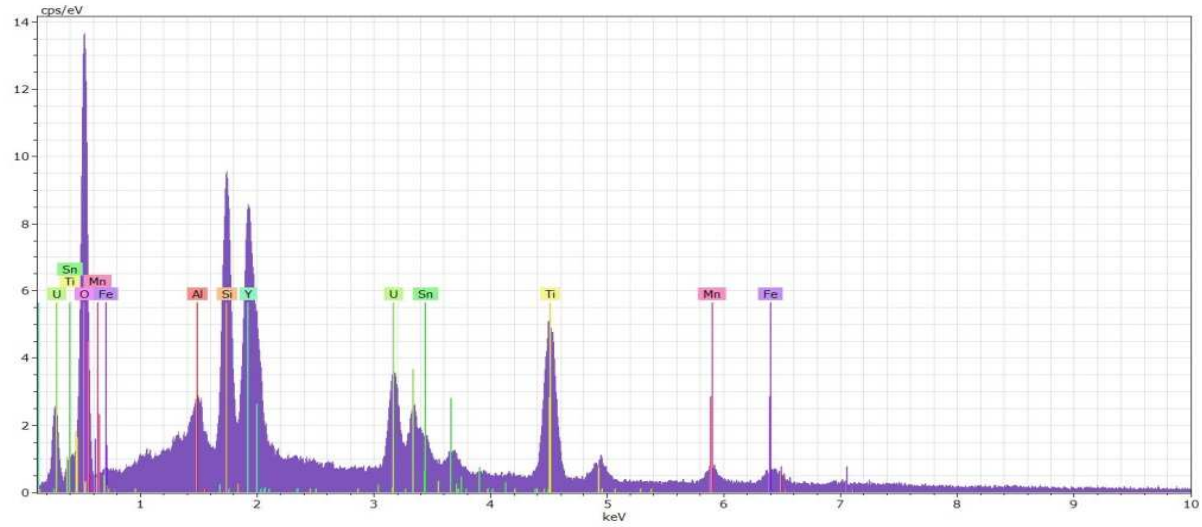

Figure 3.22: Representative EDS spectra of the Ti-Y-silicate inclusions from Mjeltedalen 2a sample.

Polycrase-(Y), $Y(Ti,Nb)_2(O,OH)_6$

Inclusions of polycrase sporadically appear in many of the grains of the Svåheii 2 sample, and in some grains from the Mjeltedalen 2a sample. These inclusions exhibit euhedral-anhedral shapes, in which the euhedral shapes appear cubical or tabular. Inclusions sizes are in the range of 15 – 85 µm. In the Svåheii 2 sample, these inclusions show a consistent chemistry resembling polycrase-(Y). Traces of U are present as in all inclusions in the latter sample, with some cases of trace concentrations of Ta, Ca, and Yb. In some instances, these inclusions are intergrown with other minerals such as hematite and zircon. Polycrase-(Y) inclusions from the Mjeltedalen 2a sample exhibit zoning or intergrowths with other mineral species. The zoned inclusion show the consistent chemistry of polycrase-(Y) in the light grey areas while exhibiting inconsistent chemistry with traces of Ca, Zr, and Fe in the dark gray rim. Another polycrase-(Y) inclusion is intergrown with several unidentified U-Y-Fe-oxides. The

polycrase-(Y) inclusion exhibits an inconsistent chemistry, in which Ti is subordinate in comparison to the even Y and Nb. Traces of Zr, Ca, Th, U, Si are observed at considerable concentrations. The general loss of Ti may be due to the substitution mechanism: $Ti^{4+} \leftrightarrow Si^{4+}$.

Ti-Mn-Fe-oxide

These inclusions are in some instances found in some garnet crystals from the Heftetjern 2, and Storemyr 3 samples. The inclusions are cubic euhedral-subhedral shaped with sizes in the range of 2 – 6 µm. Titanium is the major constituent with the subordinates of Mn and Fe. The inclusions from the Heftetjern 2 pegmatite show ratios of 1.8:1 for both Ti/Mn and Ti/Fe, whereas ratios of Mn and Fe are even. Ti/Mn and Ti/Fe ratios for the Storemyr 3 sample are 2.3:1 and 1.5:1, respectively. The Fe/Mn ratio from the same analysis is 1.5:1. In general, the Ti/O ratios for these inclusions from both pegmatites are approximately 3:1.

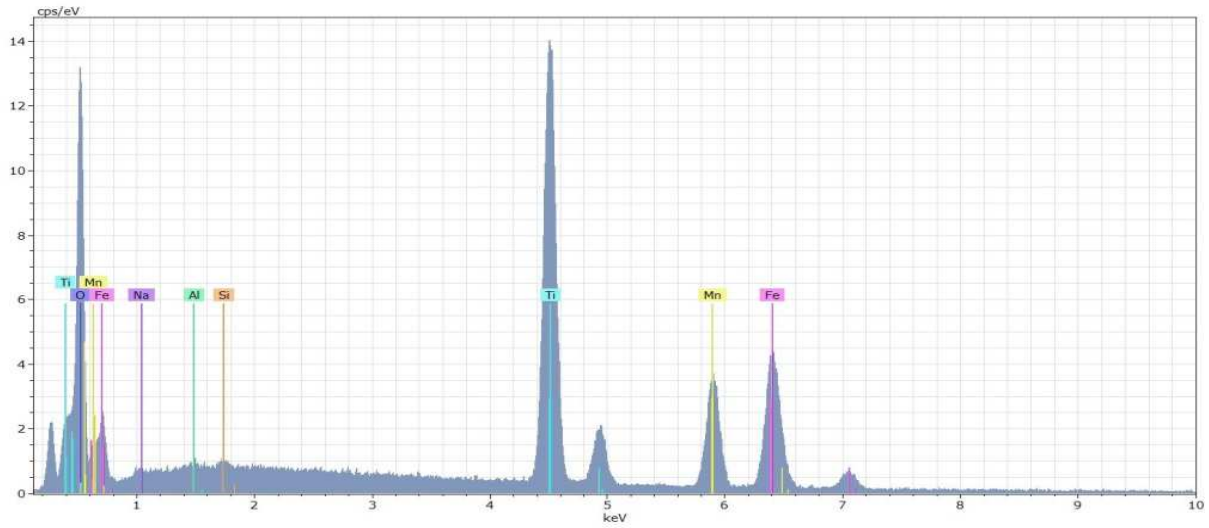

Figure 3.23: EDS spectra of an analyzed unidentified Ti-Mn-Fe-oxide inclusion from the Storemyr 3 sample.

Hematite, Fe_2O_3

Hematite inclusions are sometimes located in a few grains of the Svåheii 2 and Storemyr 3 samples. In the Svåheii 2 sample hematite appears as a dark subhedral cubical core (40 µm size), which is surrounded by a light grey rim of a euhedral tabular shaped polycrase-(Y) (70 µm size). The subhedral cubical hematites (50 µm sizes) residing in the garnet crystals of the Storemyr 3 sample are dark dull grey and free of zoning.

Fe-Cu-oxide

Unidentified inclusions of subhedral cubical shaped Fe-Cu-oxides (10 µm sizes) are sporadically present in the garnet crystal from the Lower Høydalen pegmatite. The major constituent is Fe with subordinate Cu, which exhibit a Fe/Cu ratio and Fe/O ratio of 3.7:1 and approximately 1:2. Traces of Mn, Ti, Si, P, S, and Sn are also present.

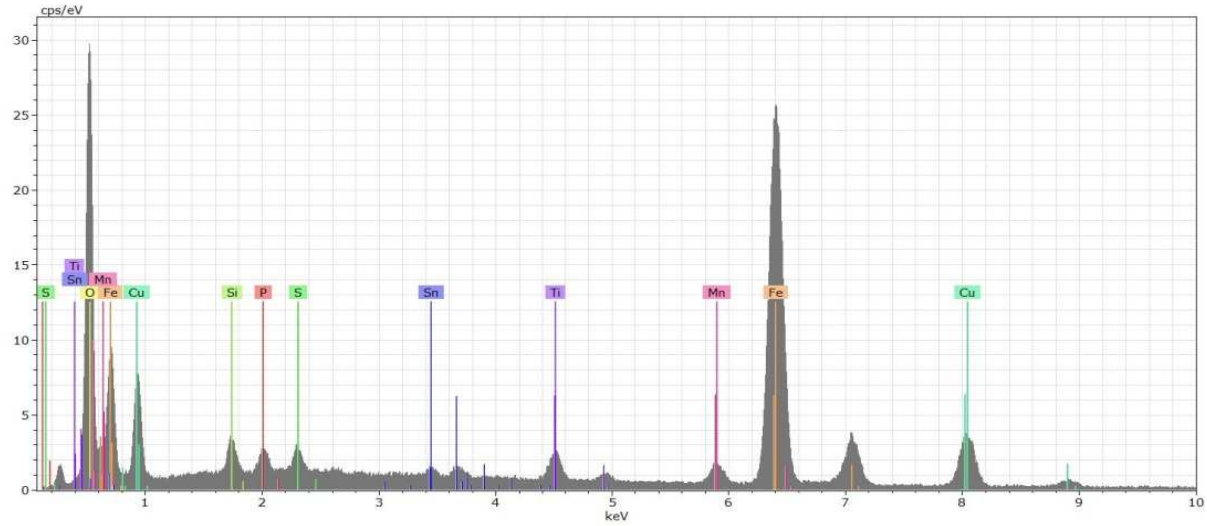

Figure 3.24: EDS spectra of an unidentified Fe-Cu-oxide inclusion from the Lower Høydalen sample.

Fe-REE-silicate

These unidentified Fe-REE-silicates frequently appear in some garnet crystals from the Grønliheii sample, while being sporadically present in an analyzed garnet grain from the Butvatnet sample. The silicates generally exhibit both euhedral acicular and subhedral equant shapes, with sizes in the range of 2 – 5 µm. Most inclusions share Fe as a major constituent with subordinate Ce, Nd, Y, and Ca. In some cases other subordinate constituents are Na and La. Cerium is generally 2-3 times as abundant in most cases in comparison with the other REEs (Y, Nd, and La) and Na. Some Fe, Al, Si, O and all Mn are considered remnants of the surrounding garnet chemistry. These silicates are undoubtedly Al-bearing, with a general Al/Si ratio of 0.7:1. The Si/O ratio for these inclusions is approximately 1:5.

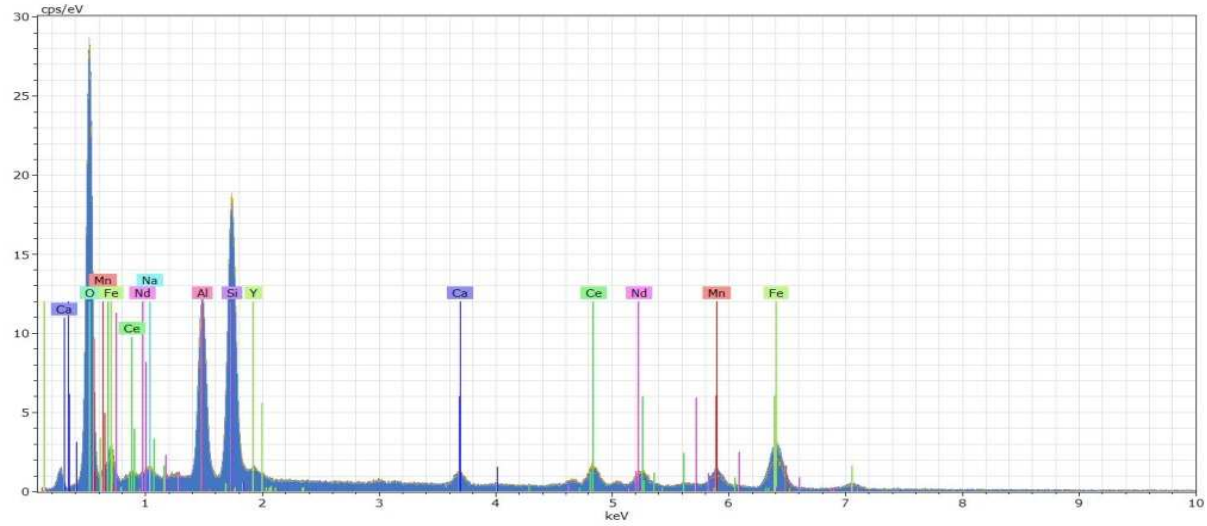

Figure 3.25: Representative EDS spectra of the unidentified Fe-REE-silicate inclusions from the Grønliheii sample.

Cu-S-oxide

Unidentified S-bearing anhedral Cu-oxides (10 µm sizes) is only observed in a garnet grain from the Heftetjern 1 sample. Copper is the major component with subordinate S, in which the Cu/S ratio is 2.8:1. The S/O ratio is 1:5. Mn, Fe, Al, Si are remnants of the surrounding garnet chemistry.

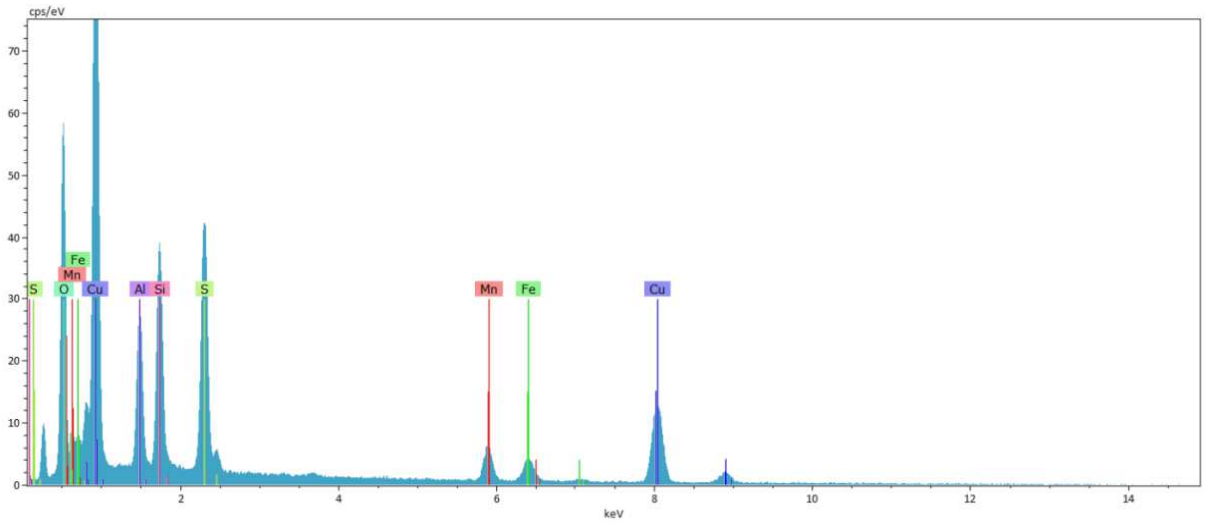

Figure 3.26: EDS spectra of an unidentified S-bearing Cu-oxide from the Heftetjern sample.

Ce-silicate

These unidentified Ce-silicates are only present in the garnet crystal of the Lower Høydalen sample, wherein they appear subhedral acicular shaped (10 – 15 µm sizes). Cerium is the major constituent with traces of Nb and P. Manganese, Fe, Si, and some O are considered an influence of the surrounding garnet chemistry. In some cases, these oxides are bordered by K-feldspars. Ce/O ratios for these inclusions are generally 1:5.4.

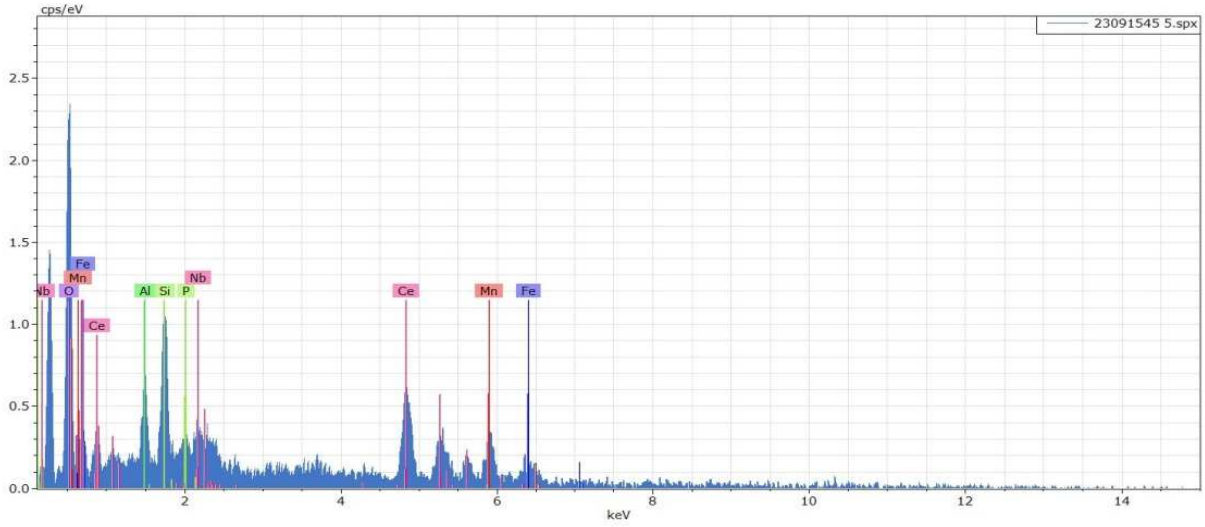

Figure 3.27: EDS spectra of an unidentified Ce-oxide inclusion from the Lower Høydalen sample.

Al-oxide

Al-oxide inclusions commonly occur in garnet fragments of the Upper Høydalen 12 (cleavelandite replacement zone) sample and in a grain from the Mjeltedalen 2a sample. Typical sizes of the inclusions from the these samples are 6 – 10 µm with subhedral equant shapes. The inclusions also sporadically appear in the garnet crystal from the Lower Høydalen sample, wherein they occur as anhedral masses (3 µm sizes) intergrown with subhedral cubical Ca-Y-fluorides (5 µm sizes). Al-oxide inclusions from the Mjeltedalen 2a and Upper Høydalen 12 samples show similar Al/O ratios of 1:1.3 and 1:1.5, respectively. Analysis of the Upper Høydalen 12 shows trace concentrations of Si, Ca, Mn, and Th. Al-oxide inclusions from the Lower Høydalen exhibit traces of F and Ca. The Al/O ratio of these inclusions is 1:1.8. Remnant garnet chemistry is reflected in contents of Fe, Mn, Si, and some Al and O.

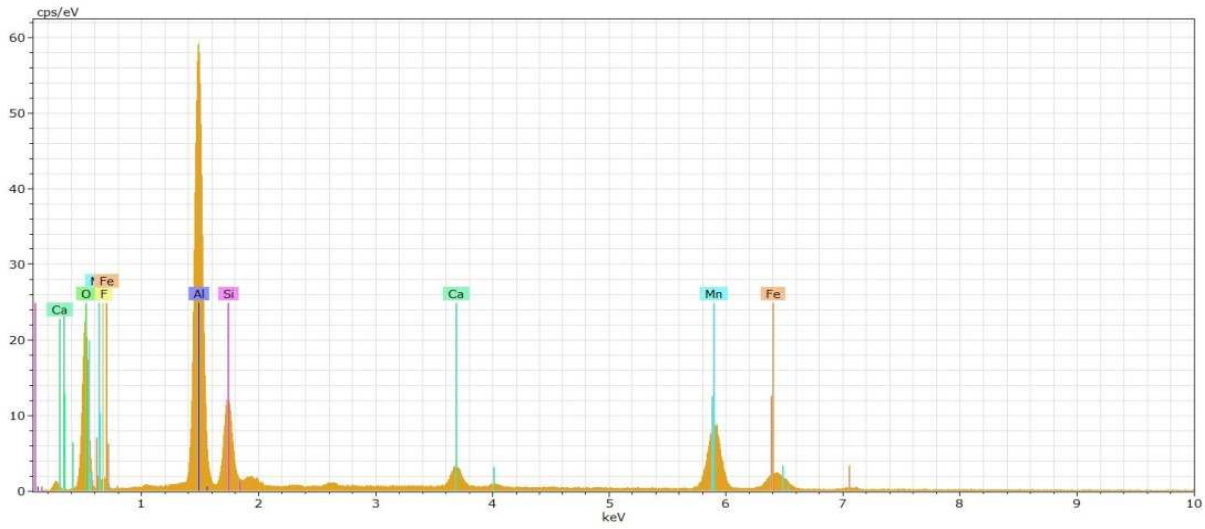

Figure 3.28: Representative EDS spectra of unidentified Al-oxide inclusions from the Lower Høydalen sample.

U-oxide

A U-oxide inclusion is only spotted sporadically in a single garnet grain from the Heftetjern 1 sample. This inclusion exhibits a euhedral cubical shape, with a size of 10 µm. The major constituent is U with subordinate Pb. Minor impurities of Y and Yb are also detected during the analysis. The U/O ratio is 1:2.8. A possible candidate for identification may be uranite, UO_2.

Ti-Fe-oxide

Ti-Fe-oxide inclusions are only infrequently present in most grains from the Storemyr 1 sample. The inclusions appear either euhedral acicular (8 µm sizes) or euhedral/subhedral cubical (2 – 3 µm sizes). Titanium is the major constituent with subordinate Fe in most analyses, with a few instances of Fe being the major constituent with subordinate Ti. Ti/Fe ratios are in the range of 0.7-1.7:1. Traces of Y and Zn are common in some of these oxides. Manganese, Al, Si and partly Fe and O are remnants of the surrounding garnet chemistry. These Ti-Fe-oxides may potentially be ilmenites.

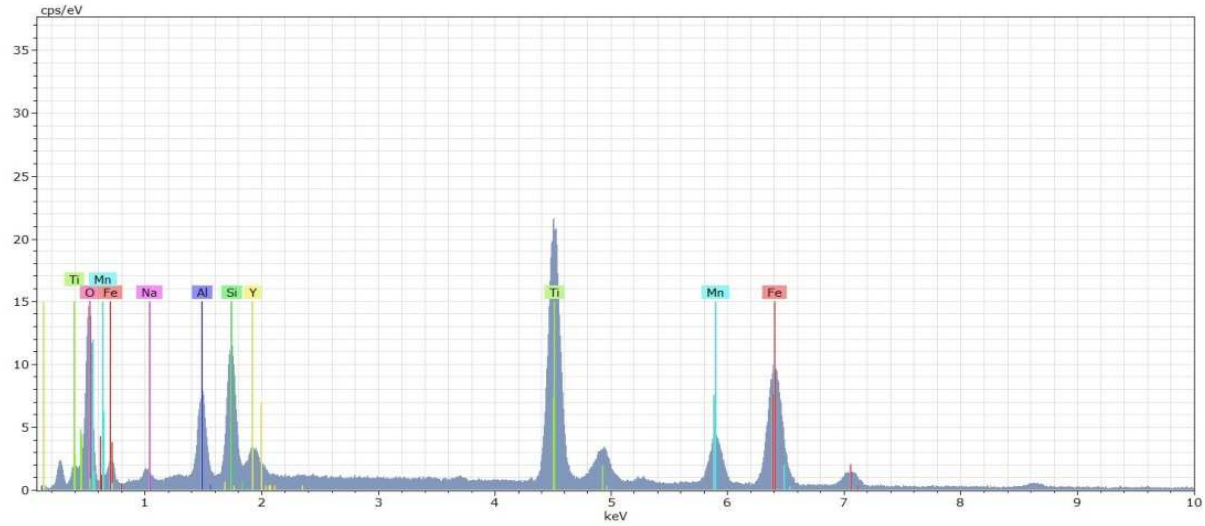

Figure 3.29: EDS spectra of an unidentified Fe-Ti-oxide inclusion, with the possibility of being ilmenite, from the Storemyr 1 sample

.

Thorite, $Th(SiO_4)$

A thorite inclusion is only recognized in a single grain from the Bratterud sample. The thorite appears as a fractured subhedral equant inclusion with a size of 100 µm, which shows consistent chemistry resembling thorite.

Th-Y-silicate

These Th-Y-silicate inclusions are sometimes located in a few garnet grains of the Bratterud sample. Both anhedral masses (5 µm sizes) and subhedral cubical shaped inclusions (40 µm) intergrown with both anhedral zircon (30 µm) and hematite (10 µm thick surrounding rim) are observed. The major constituent for all inclusions is Th with subordinate Y. Thorium is approximately three times as abundant for the inclusions in some of the grains, while Y is twice as abundant for the latter inclusions. Th/Y and Si/O ratios are in the range of 2-2.8:1 and 1.6-3.6:1, respectively. Traces of Ce, Nd, Fe, and Ca are in some instances detected.

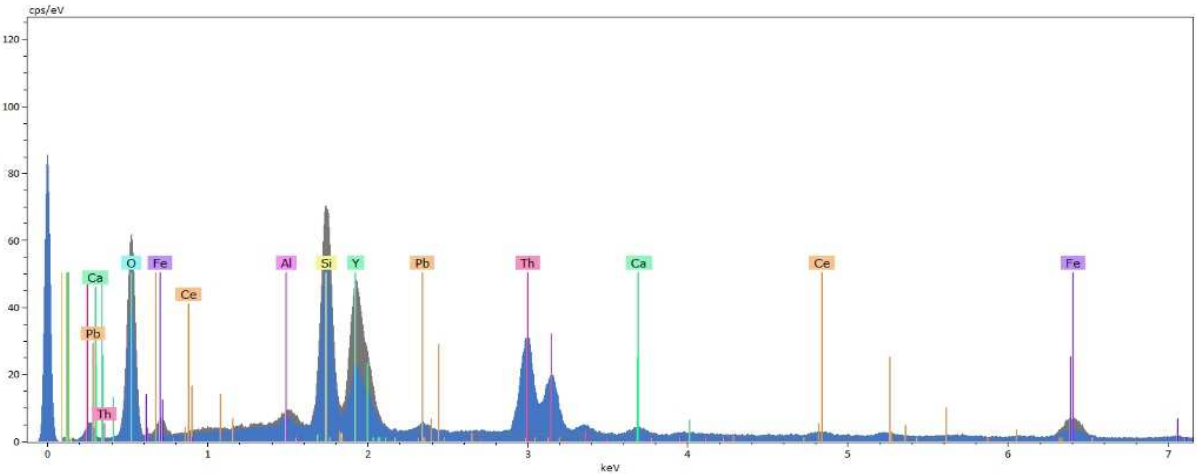

Figure 3.30: EDS spectra of an unidentified Th-Y-silicate inclusion from the Bratterud sample (marked in dark blue).

Th-U-silicate

A Th-U-silicate inclusion is only observed in a single grain from the Heftetjern 1 sample. The size of the subhedral cubical inclusions is 10 µm, where it is intergrown with acicular zircon (size of 8 µm). The major constituent is Th with subordinate U. The Th/U ratio is 1.5:1, with Th/Si and Si/O ratios of 1:1.8 and 1:3.3, respectively. Trace concentrations detected in the analyzed inclusion include Pb and Y. This inclusion may potentially be a U-rich thorite.

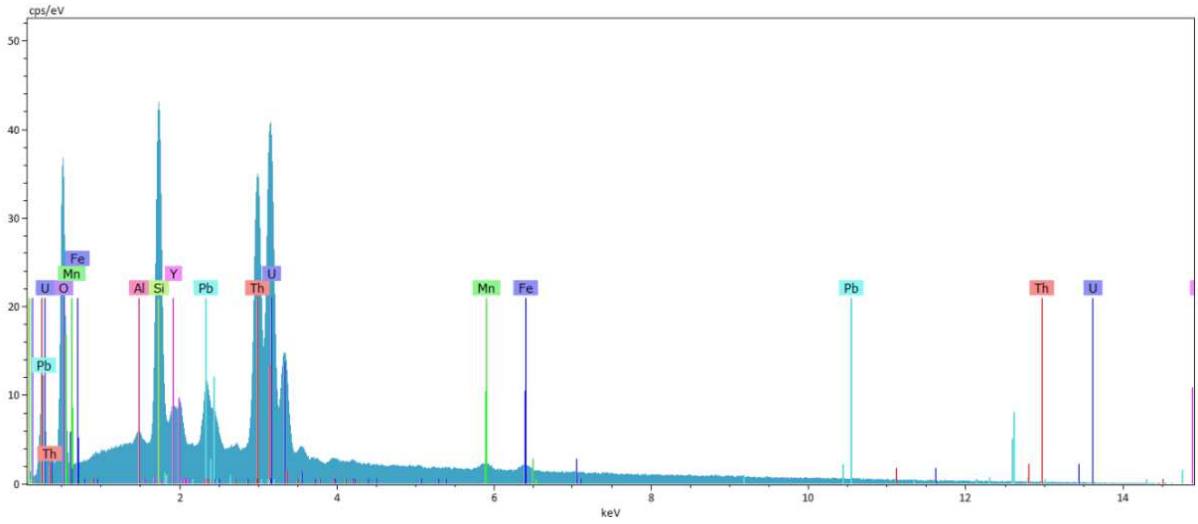

Figure 3.31: EDS spectra of an unidentified Th-U-silicate, probably a U-rich thorite, from the Heftetjern 1 sample.

K-feldspar, $K(AlSi_3O_8)$

K-feldspars are sometimes present in the garnet crystal from the Upper Høydalen 1 sample, while commonly appearing within garnet fragments from the Upper Høydalen 12 sample. The general sizes of the K-feldspars are 3 – 10 µm, with subhedral acicular shapes in the Upper Høydalen 1 sample (instances of intergrowth with keiviite-(Y)) and anhedral masses in the Upper Høydalen 12 sample.

Albite, $Na(AlSi_3O_8)$

An albite inclusion only appears in a garnet grain from the Svåheii 2 sample, where it is commonly adjacent to other zircon inclusions. The albite inclusion appears as an anhedral mass, with a size of 10 µm. Calcium contents are relatively minuscule (>1.0 norm. at. %), suggesting it is a relatively pure albite.

In summary, various micro inclusions were observed in the Tørdal garnets. Mainly these inclusions comprise quartz, zircon, Y-rich minerals, F-rich minerals and a few Sc-rich inclusions. Spatially, the abundance of quartz is generally high in garnets for most locations throughout Tørdal, with the exception of the quartz-poor Butvatnet, Storemyr 2, Svåheii 3, and Høydalen locations. Mostly the NE-garnets from the Heftetjern, Sjauset, Bratterud, and some of the Storemyr garnets (Storemyr 2) are highly abundant in zircons. The abundance of zircons generally decreases towards the S-SW-areas of the study (the zircon-poor Svåheii 3, Butvatnet, Grønliheii, Lislegrønlia, Mjeltedalen, Kleppe quarry, Storemyr 3 locations), whereas the Storemyr 1 and all the Høydalen garnets lack zircons. The Y-rich inclusions found mainly comprise keiviite-(Y), Y-F-silicates, (yttrofluorite) and Ti-Y-minerals. The abundance of these minerals is high for some garnets of the SW-area (Svåheii 3, Butvatnet, Upper Høydalen 1, Lower Høydalen and Heftetjern 2 samples). Garnets from other locations of the study area either exhibit low abundances of Y-rich micro inclusions or completely lacking them. The F-rich minerals, comprising Y-F-silicate, fluorite, and yttrofluorite, are only found in the Heftetjern-Høydalen area. The “cleavelandite”-zone garnet from the Lower Høydalen pegmatite exhibit high abundances of yttrofluorite, whereas the Heftetjern 2 garnets exhibit a large quantity of Y-F-silicates. Low abundances of yttrofluorite and fluorite are exhibited for the wall zone garnet and “cleavelandite”-zone garnet, respectively. The only species of Sc-rich micro inclusions were thortveitite, which only appears in the most SW-garnets (Svåheii 2 location) and NE-garnets (Upper Høydalen location), and in no other garnets of the study area.

Table 3.4 Inclusion mineralogy and commonality

Inclusions	*Svåheii 2*	*Svåheii 3*	*Butvatnet*	*Grønliheii*	*Lislegrønlia*	*Mjeltdalen 2a*	*Kleppe Quarry*	*Storemyr 1*	*Storemyr 2*
Quartz	xxx	x	x	xx	xx	xxx	xx	xxx	-
Zircon	xx	x	x	x	x	x	x	-	xxx
Xenotime-(Y)	-	x	x	-	-	-	-	-	-
Gadolinite-(Y)	-	-	-	-	-	-	-	x	-
Keiviite-(Y)	-	x	xxx	-	-	x	x	-	-
Y-F-silicate	-	xxx	-	-	-	-	-	-	-
Fluorite	-	-	-	-	-	-	-	-	-
Yttrofluorite	-	-	-	-	-	-	-	-	-
Titanite	x	-	-	-	-	-	-	-	-
Ca-Fe-LREE-silicate	-	-	-	-	-	-	-	-	-
Ca-REE-oxide	-	-	-	-	-	-	-	-	-
Thortveitite	x	-	-	-	-	-	-	-	-
Ti-Y-minerals	-	xx	xxx	xx	-	xx	x	xx	-
Polycrase-(Y)	x	-	-	-	-	x	-	-	-
Ti-Mn-Fe-oxide	-	-	-	-	-	-	-	-	-
Hematite	x	-	-	-	-	-	-	-	-
Fe-Cu-oxide	-	-	-	-	-	-	-	-	-
Fe-REE-silicate	-	-	x	xx	-	-	-	-	-
Cu-S-oxide	-	-	-	-	-	-	-	-	-
Ce-silicate	-	-	-	-	-	-	-	-	-
Al-oxide	-	-	-	-	-	x	-	-	-
U-oxide	-	-	-	-	-	x	-	-	-
Ti-Fe-oxide	-	-	-	-	-	-	-	x	-
Thorite	-	-	-	-	-	-	-	-	-
Th-Y-minerals	-	-	-	-	-	-	-	-	-
U-thorite	-	-	-	-	-	-	-	-	-
K-feldspar	-	-	-	-	-	-	-	-	-
Albite	x	-	-	-	-	-	-	-	-

Table 3.4 Continued

Inclusions	*Storemyr 3*	*Upper Høydalen 1*	*Upper Høydalen 12*	*Lower Høydalen*	*Heftetjern 1*	*Heftetjern 2*	*Bratterud*	*Sjauset*
Quartz	xxx	-	-	-	xxx	xxx	xxx	xxx
Zircon	x	-	-	-	xxx	xx	x	xx
Xenotime-(Y)	-	x	-	-	-	-	-	-
Gadolinite-(Y)	-	-	-	-	-	-	-	-
Keiviite-(Y)	-	xx	x	-	-	xxx	x	-
Y-F-silicate	-	x	-	-	-	xxx	-	-
Fluorite	-	-	x	-	-	-	-	-
Yttrofluorite	-	x	-	xxx	-	-	-	-
Titanite	-	-	-	-	-	-	-	-
Ca-Fe-LREE-silicate	-	-	-	-	-	-	x	-
Ca-REE-oxide	-	-	x	-	-	-	-	-
Thortveitite	-	x	-	-	-	-	-	-
Ti-Y-mineral	x	-	-	-	xx	xx	x	-
Polycrase-(Y)	-	-	-	-	-	-	-	-
Ti-Mn-Fe-oxide	x	-	-	-	-	x	-	-
Hematite	x	-	-	-	-	-	-	-
Fe-Cu-oxide	-	-	-	x	-	-	-	-
Fe-REE-silicate	-	-	-	-	-	-	-	-
Cu-S-oxide	-	-	-	-	x	-	-	-
Ce-silicate	-	-	-	x	-	-	-	-
Al-oxide	-	-	xx	x	-	-	-	-
U-oxide	-	-	-	-	x	-	-	-
Ti-Fe-oxide	-	-	-	-	-	-	-	-
Thorite	-	-	-	-	-	-	x	-
Th-Y-mineral	-	-	-	-	-	-	x	-
U-thorite	-	-	-	-	x	-	-	-
K-feldspar	-	x	xx	-	-	-	-	-
Albite	-	-	-	-	-	-	-	-

Table 3.4: Displayed microinclusions residing in the garnets from the different pegmatite locations in Tørdal. The microinclusion inventory in the garnets reflect the general geochemistry of the various pegmatites. Inclusion commonality is illustrated as: x - rare, xx - common, and xxx - very common.

3.3 Chemistry of garnets in the Tørdal pegmatites

3.3.1 Major element distribution

The 33 analyzed garnets from 16 different locations in Tørdal exhibit an average spessartine component of ~ 48 mol.%., ranging from 29.8 to 93.2 mol.%. Average core-rim compositions of major elements in all analyzed garnet crystals are presented in Table 3.5. Garnet crystals from the Svåheii 2, Storemyr, Storemyr 2, Bratterud, Heftetjern 1, Heftetjern 2, and Upper Høydalen 1 samples all exhibit predominant spessartine components with subordinate almandine components (e.g. 57.6 mol.% spess *versus* 37.9 mol.% alm). The spessartine component is also predominant in the garnet core from the Svåheii 3 sample (56.6 mol.% spess *versus* 38.6 mol.% alm), which has a rim of predominant almandine component 47.7 mol.% spess *versus* 48.4 mol.% alm). In garnet grains from the Sjauset, Upper Høydalen 12, and Lower Høydalen samples the spessartine component is dominating (e.g. 80.1.% spess *versus* 15.5 mol.% alm). Prevailing almandine components with subordinate spessartine components are exhibited for garnets from the Lislegrønlia, Mjeltedalen 2a, Storemyr 3, Kleppe quarry, Grønliheii, and Butvatnet locations (e.g. 39.5 mol.% spess *versus* 54.5 mol.% alm). Components such as pyrope, grossular, yttrogarnet, and andradite are all below 6 mol.%. Other presented garnet components containing Ti and Na are mostly negligible, besides TiO_2 and Na_2O, which in some grains are maximum <0.11 wt. % and <0.10 wt. %, respectively.

Garnet compositions in a spessartine versus almandine plot (Fig. 3.32) show two parallel linear trends evolving from Fe-rich and Mn-poor to Mn-rich and Fe-poor garnets. The first trend generated by the samples from the Svåheii 3, Bratterud, Heftetjern 1, Heftetjern 2, Upper Høydalen 1, Upper Høydalen 12, Lower Høydalen and Sjauset locations. Garnets from the Mjeltedalen 2a, Kleppe quarry, Storemyr, Storemyr 2, Storemyr 3, Svåheii 2, Lislegrønlia, Grønliheii, and Butvatnet locations form the second trend (shifted to slightly lower almandine component). These garnets have in general a much lower spessartine component. This shift is mainly due to the pyrope component, which is in the range of 1.9-5.5 mol. % in these garnet crystals. Figure 3.33 shows a pyrope vs spessartine plot, which again reflects this pyrope shift of the Mn-poor garnet crystals forming the second trend. These slightly Mg-enriched garnets exhibit *apfu* core-rim compositions of Mg which are either relatively constant (<0.02 *apfu* difference), decreasing or increasing (Fig. 3.36). The Kleppe quarry and Lislegrønlia garnets show variability within each sample. Magnesium *apfu* values increase in grain 1A, C, and E decreases in grains 1B and 2 and is more or less constant in grain 1D. In the Lislegrønlia sample, the core-rim *apfu* value for Mg is consistent for grain 1 and 3, whereas decreases in grain 2. All crystals from the Storemyr, Storemyr 2, Svåheii 2 and Butvatnet samples exhibit decreasing *apfu* core-rim Mg values. Constant core-rim *apfu* values for Mg are exhibited for the garnets from the Grønliheii, Mjeltedalen 2a, and Storemyr 3 samples. Calcium-rich garnets include crystals from the Kleppe quarry, Storemyr 3, and Mjeltedalen samples (1.00 – 1.36 CaO wt.%, 0.093 – 0.124 *apfu*), corresponding to an andradite component of 0.6 to 3.4 mol.%.

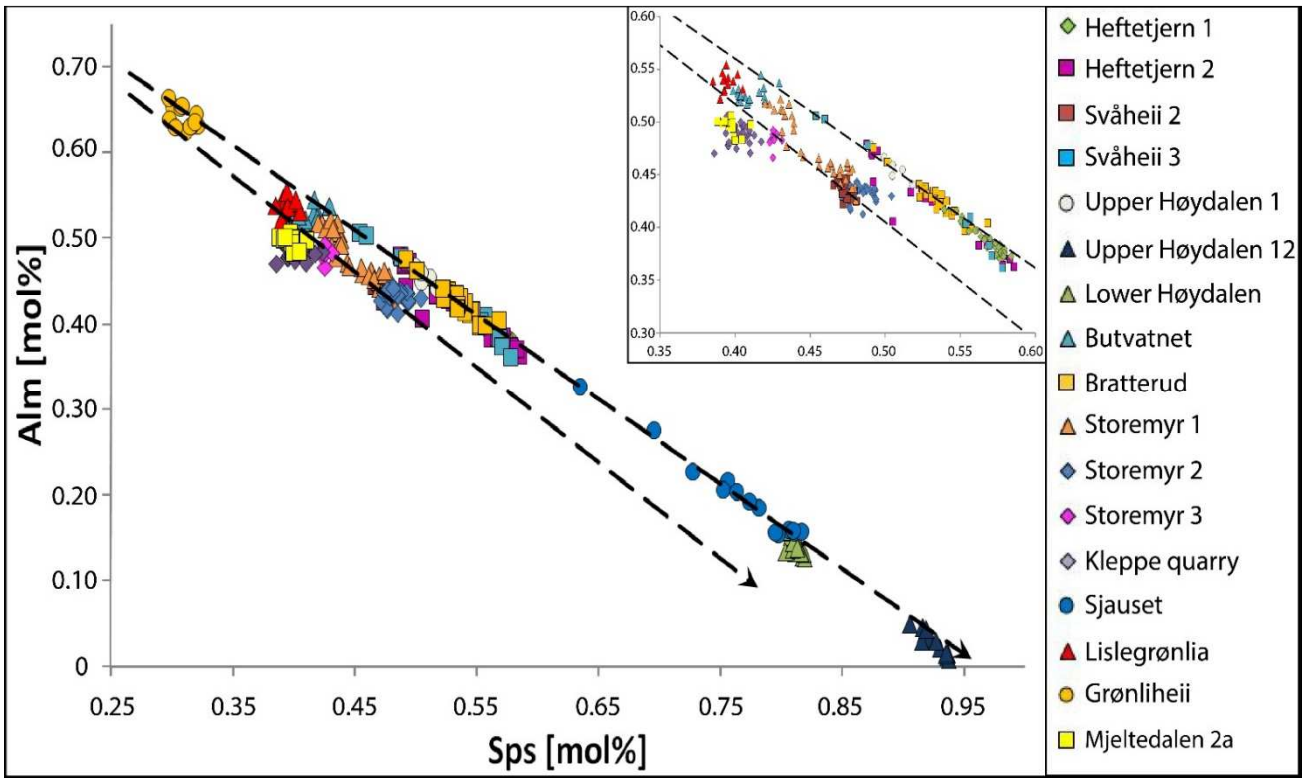

Figure 3.32: Spessartine versus almandine plot of analyzed garnets from the different pegmatite samples. The plotted data show to parallel trends. The shift towards both slightly lower spessartine and almandine mol.% is mainly because of the presence of the pyrope component in the garnet crystals from the Mjeltedalen 2a, Kleppe quarry, Storemyr 1, Storemyr 2, Storemyr 3, Svåheii 2, Lislegrønlia, Grønliheii, and Butvatnet samples.

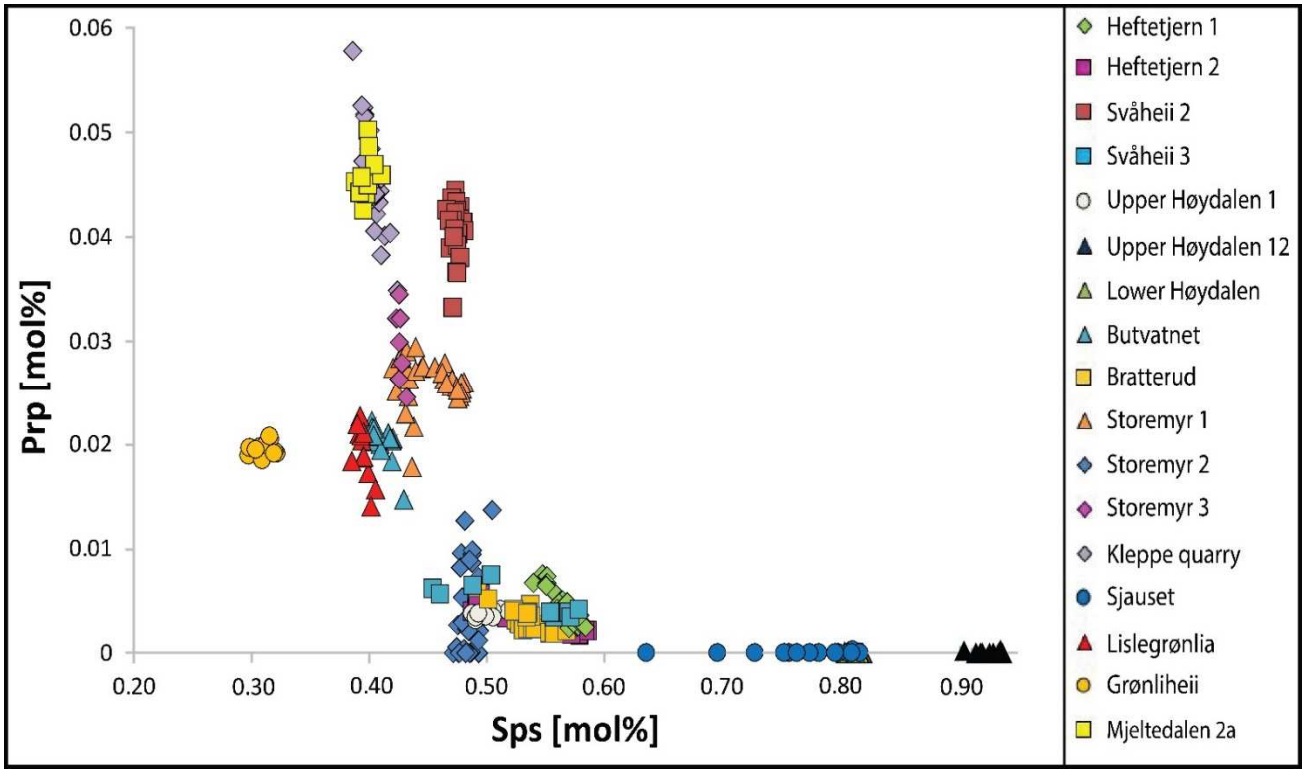

Figure 3.33: Spessartine versus pyrope plot of analyzed garnets from the different pegmatite samples. The pyrope shift as seen in Figure 3.32 is evident for Mjeltedalen 2a, Kleppe quarry, Storemyr 1, Storemyr 2, Storemyr 3, Svåheii 2, Lislegrønlia, Grønliheii, and Butvatnet samples, which form a data cluster clearly separated from the low-pyrope, high-spessartine-component-bearing samples.

Mn/(Mn+Fe) *apfu* values from the core to the rim of the 33 analyzed garnet crystals (Fig. 3.36) are either more or less constant (<0.02 *apfu* difference) or decreasing from the core to the rim. The relative lowest Mn/(Mn+Fe) *apfu* core values (0.308-0.335 *apfu*) are exhibited for the crystals from the Grønliheii location. These garnets exhibit no considerable change in these *apfu* values towards the rim. Garnet crystals with intermediate Mn/(Mn+Fe) *apfu* core values are from the locations of Lislegrønlia (core value ranges of 0.406-0.408 *apfu*), Mjeltedalen (core value ranges of 0.421-0.438 *apfu*), Kleppe quarry (core value ranges of 0.428-0.453 *apfu*), Butvatnet (0.442 *apfu*), and Storemyr 3 (0.455 *apfu*). These values remain more or less constant from the core to the rim for garnet crystals from Lislegrønlia, Mjeltedalen 2a, Butvatnet, and the Storemyr 3 samples. The Kleppe quarry crystals mostly exhibit no changes in these values (Fig. 3.36 B-F), with the exception of Kleppe grain 1A (Fig. 3.36 A) exhibit a steadily decreasing Mn/(Mn+Fe) value of 0.445 *apfu* at the core and 0.425 *apfu* at the rim.

Relatively higher Mn/(Mn+Fe) core values exhibit the crystals from the Storemyr (0.494 *apfu)*, Storemyr 2 (core value ranges of 0.510-0.514 *apfu*), Svåheii 2 (0.503 *apfu)*, Svåheii 3 (0.581 *apfu*), Upper Høydalen (0.514), Bratterud (0.575 *apfu*), Heftetjern (0.586 *apfu*), and Heftetjern 2 (0.597 *apfu*) locations. Garnet crystals from the Svåheii pegmatites (Svåheii 2 and 3) show different trends from the core to the rim. Mn/(Mn+Fe) values of grain 1 from the Svåheii 2 pegmatite are more or less constant (<0.02 *apfu difference)*, while the garnet crystal from Svåheii 3 shows a decrease from the core to the rim (Fig. 3.36 H). In the core of this crystal, the Mn/(Mn+Fe) value is 0.581. Towards the grain margin, the Mn/(Mn+Fe) *apfu* value steadily decreases to 0.464 and abruptly increases to 0.512 *apfu* at the outermost rim of the crystal. Grain 1 from the Storemyr sample (Fig. 3.36 I) appears distinctly different from garnet crystals from the Storemyr 2 location. In the core of this crystal, the Mn/(Mn+Fe) *apfu* value is 0.494, which is more or less constant across the inner part of the crystal. Towards the margin, the value drops down to 0.435 *apfu*, and increases to 0.452 at the outermost rim. The other garnet grains from Storemyr 2 (grain 1 and 5) show relatively consistent *apfu* values for Mn/(Mn+Fe), with the exception of grain 5 (Fig. 3.36 K), which shows a slight increase at the outermost rim to 0.526 *apfu*. The garnet crystal from Upper Høydalen shows more or less the same Mn/(Mn+Fe) *apfu* values (core-rim: 0.514-0.506 *apfu*). However, mid-grain of this crystal the *apfu* values are variable with a maximum difference of 0.027 *apfu* (Fig. 3.36 AE). Analyzed crystals from the Bratterud, Heftetjern and Heftetjern 2 samples exhibit steadily decreasing *apfu* values from the core to the rim (Fig. 3.36 X, AC, and AD).

The highest Mn/(Mn+Fe) *apfu* core values are observed in crystals from the Sjauset (core value ranges of 0.794-0.824 *apfu*), Lower Høydalen (0.821 *apfu*), and Upper Høydalen 12 (0.931 *apfu*) locations. The Sjauset crystals (Fig. 3.36 U-W) exhibit variations in the Mn/(Mn+Fe) values within the grains. The core of crystal 1 contains 0.824 *apfu* Mn/(Mn+Fe), which drops abruptly to 0.698 *apfu* towards the grain margin, and then increases to 0.808 *apfu* at the outermost margin. The other Sjauset crystals (grain 2 and 3) show a general decline in the Mn/(Mn+Fe) *apfu* values from the core to the rim. Grain 2 shows a more or less consistent *apfu* value from the core (0.809 *apfu*) to the proximity of the rim but then drops to 0.750 *apfu*

at the outermost rim (Fig. 3.36 V). Mn/(Mn+Fe) *apfu* values in grain 3 steadily decrease from the core to the rim (0.794-0-634 *apfu*). Both garnet crystals from the Lower Høydalen and Upper Høydalen 12 locations exhibit no apparent change in Mn/(Mn+Fe) *apfu* values from the core to the rim.

3.3.2 Trace element distribution

Concentrations of rare earth elements and rare metals are both presented as average core-rim compositions in Table 3.5-6. The elements of major interest for this study are Sc, Y, and REEs. These elements are therefore presented in more detail than other elements.

The highest average Sc concentrations in garnet analyzed by EPMA were detected in grain 1 from the Heftetjern 1 location (0.29 wt.% Sc_2O_3, 0.021 *apfu*), while the highest concentration analyzed by LA-ICP-MS was 2197.19 ppm in grain 3 also from the Heftetjern 1 location. EPMA analyzed contents of Sc in all garnets show a bulk average of 0.08 wt.% Sc_2O_3. Average core-rim concentrations of Sc determined by EPMA show the highest abundance (in the range of 0.20-0.29 Sc_2O_3 wt.%) for garnet crystals from the Heftetjern 1, Heftetjern 2, Upper Høydalen 1 samples. Average Sc concentrations of garnets of all investigated locations are displayed in the regional map (Fig. 3.35). Concentrations of 987 to 1895 ppm are classified as high, 392 to 987 ppm as medium, and 14 to 392 ppm as low.

Garnet crystals with high Sc concentrations are from the Heftetjern 1, Heftetjern 2 and Upper Høydalen 1 samples (bulk averages of 1568, 1895, and 1460 ppm, respectively). Scandium concentrations in these garnets from the Heftetjern area (Heftetjern 1, and Heftetjern 2 samples) may show some significant differences (max. ~699 ppm core differences) , whereas Sc abundance in garnets from the Høydalen area (Upper Høydalen, Upper Høydalen 12, and Lower Høydalen samples) are much more variable (max bulk average ppm difference of 1408 ppm). The Upper Høydalen crystal shows high concentrations of Sc, while both the garnets from the Upper Høydalen 12 and Lower Høydalen garnet exhibit low Sc concentrations. The Svåheii garnets exhibit large variations in Sc concentrations. Garnets grains from the Svåheii 2 pegmatite exhibit an average medium-high Sc content, while the Sc concentration in the garnet crystal from the Svåheii 3 pegmatite is relatively low. Other garnets with medium-high Sc contents comprise the locations Butvatnet, Lislegrønlia, Kleppe quarry, Mjeltedalen 2a, and all Storemyr occurrences. The Storemyr samples (Storemyr, Storemyr 2, and Storemyr 3) show slight variations in the Sc concentrations, with both Storemyr and Storemyr 3 having slightly lower concentrations. Garnets from the Grønliheii, Sjauset and Bratterud samples all exhibit low contents of Sc.

The Sc concentration increases from 0.01 to 0.34 Sc_2O_3 wt.% in garnets with increasing spessartine component from 0.3 to 0.6 MnO/(MnO+FeO) (Fig. 3.34 A). For this spessartine component range, the Sc content increases with increasing fractionation of the pegmatite melt (because increasing spessartine component reflects an increasing fractionation degree of the pegmatite melt). With further fractionation (>0.60 mol.% spessartine component) the Sc concentration drops drastically down to concentrations <0.03 Sc_2O_3 wt.%. With further increasing spessartine component Sc in these garnets becomes almost 0 wt.%. The Sc concentrations in the various garnets from the different pegmatites indicate that Sc concentrations are highest in garnets from the wall zone of the chemically most evolved pegmatites (although the Bratterud garnets, which also exhibit the same MnO/(MnO+FeO) ratios as those that are Sc-rich, are Sc-poor). However, garnets from the "cleavelandite" replacement zones of the same pegmatites show the lowest Sc content, which is similar to garnets from less evolved pegmatites from Grønliheii, and Svåheii 3.

The Ca *versus* Sc plot in Fig. 3.34 B shows a positive correlation (both up to 0.06 Ca *apfu*, and ~ 0.025 Sc *apfu*) with a subsequent negative correlation (0.06 – 0.13 Ca *apfu*, and ~0.14 – 0.005 Sc *apfu).* Both Ca and Sc increases from relatively Sc-poor garnets (both from the wall zone from less evolved pegmatites, and the highly fractionated 'cleavelandite' garnets) to the Sc-rich garnets). However, Sc contents drop for a considerable portion of the "pyrope-rich" garnets (from the Svåheii 2, Kleppe quarry, Storemyr 2, Storemyr 3, and Mjeltedalen locations). Three distinct circles are displayed in the Mg *versus* Sc plot (Fig. 3.34 C): the red circle 1, green circle 2, and turquoise circle 3. The most Sc-rich garnets from the wall zones of the Upper Høydalen and Heftetjern 1 and 2 locations, situated within the red circle 1 (<0.02 Mg *apfu* and 0.12 – 0.025 Sc *apfu*), exhibit distinctively low Mg content and high Sc contents. Within the green circle 2 (0 – 0.20 Mg *apfu*, 0 – 0.003 Sc *apfu*) both Mg- and Sc-poor garnets from the cleavelandite replacement zones of the Høydalen pegmatites, and in addition garnets from the wall zones of the highly and intermediately fractionated pegmatites (Sjauset, Bratterud, and Svåheii 3 locations, respectively). All the garnets considered to be "pyrope-rich" are situated within the turquoise circle 3 (mainly within the ranges 0.04 - 0.16 Mg *apfu* and 0 – 0.17 Sc *apfu*).

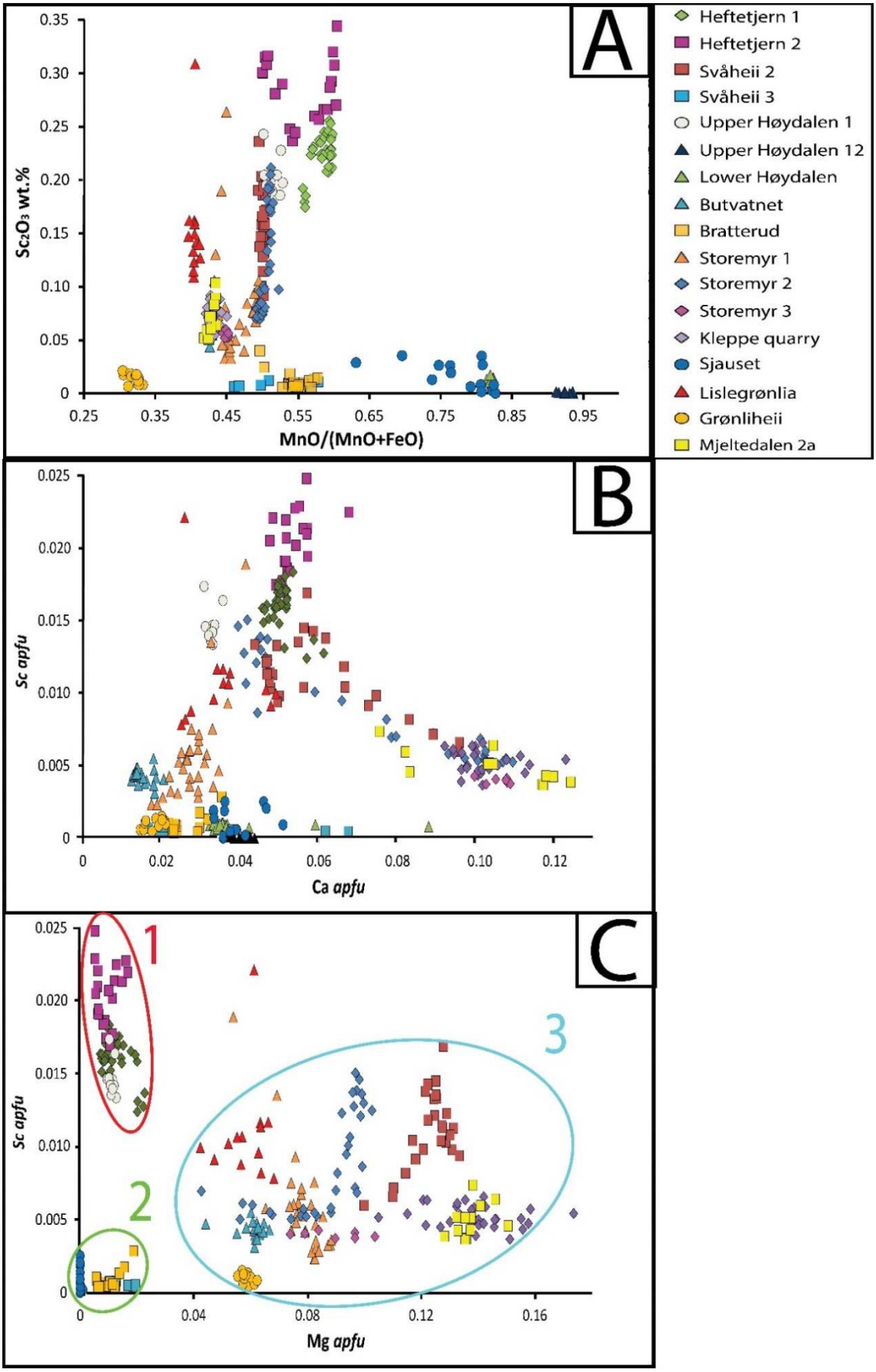

Figure 3.34: Composition diagrams of garnets from Tørdal pegmatites. Data were obtained with EPMA. A - MnO/(MnO+FeO) versus Sc_2O_3 wt.% plot. B – Sc versus Ca apfu plot. C – Sc versus Mg apfu plot.

Core-rim Sc *apfu* values presented in Fig. 3.36 are relatively consistent (<0.02 *apfu* differences). High precision LA-ICP-MS data gives better insight into the mineral scale distribution of Sc throughout the crystals compared to EPMA, which have a much higher detection limit and uncertainty. These acquired data indicate that Sc mostly decreases from the core to the rim and in some instances slightly increases towards the rim. Garnets with high Sc concentrations (Heftetjern 1, Heftetjern 2, and Upper Høydalen 1 samples) show variability within each sample between grains in core-rim compositions. All analyzed crystals from the Heftetjern 1 samples exhibit a general decline for Sc from the core to the rim (differences ranging from 154 to 688 ppm). The two analyzed garnets, grain 1 and 2 from the Heftetjern 2 sample, exhibit slight differences in the distribution of Sc. Grain 1, similarly like the Heftetjern 1 crystals, show a decline from the core to the rim (155 ppm difference in concentration). Grain 2 exhibit a slight increase from the core to the rim, with a ~20 ppm difference. The garnet crystal from the Upper Høydalen 1 exhibit a decline in Sc-contents from the core to the rim (difference of ~ 156 ppm).

No consistent core-rim variations of Sc in the moderately Sc-abundant garnets (from the Svåheii 2, Kleppe quarry, Butvatnet, Lislegrønlia, Mjeltedalen, Storemyr 1-3 locations) were evident among the garnets from the different locations. The Svåheii 2 grains generally exhibit a decline of Sc from the core to the rim (max. ~ 410 ppm difference). Scandium contents in the Kleppe quarry garnets generally increase from the core to the rim (compositional differences of 16 to 55 ppm). The Butvatnet garnets show a general core-rim decrease in Sc with differences of 3 to 115 ppm. No consistent intracrystalline distribution for Sc is shown for the Lislegrønlia garnets, while the Mjeltedalen crystals exhibit both relatively constant and decreasing core-rim concentrations of scandium (0.02 Sc_2O_3 wt.% difference). The garnets from the different Storemyr samples show significant variations of the intracrystalline Sc distribution. Grain 1 from the Storemyr shows an increase from the core to the rim (0.02 Sc_2O_3 wt.% difference). Both grain 1 and 5 show a decrease for Sc from the core towards the rim (differences of 0.08-0.09 Sc_2O_3 wt.%), while the Sc distribution in the garnet from Storemyr 3 appears homogenous throughout the crystal.

The Sc-poor garnets of the Lower Høydalen, Upper Høydalen 12, Sjauset, Bratterud, and Grønliheii show relatively low core-rim variations. No compositional core-rim difference was detected in the Upper Høydalen crystal, while the crystal from Upper Høydalen 12 exhibits no difference. The Sjauset garnets exhibit a slight increase in Sc from the core to the rim, with a difference of 0.01 wt.% Sc_2O_3. Core-rim compositions of Sc are variable for the Bratterud garnets (maximum difference of ~62 ppm). Most of the Grønliheii garnets do not exhibit any compositional core-rim differences of Sc. The analyzed Sc-poor garnet from the Svåheii 3 location shows no variation from the core to the rim in Sc-concentration.

The generally the most abundant rare metal detected in the garnet crystals is Y, with the highest concentrations in the Butvatnet sample. These concentrations are 2.6 Y_2O_3 wt.% (0.117 *apfu)* in grain 3 determined with EPMA, and 24935 ppm analyzed with LA-ICP-MS in grain 2. The abundance of Y in garnet from other locations is variable. The relatively yttrium-rich garnets (≥1.0 Y_2O_3 wt.%, ≥10000 ppm Y) include most of the Kleppe quarry grains (grain 1B-E, grain 2), Svåheii 2 (grain 1), Svåheii 3, Storemyr 1, Storemyr 2 (grain 1 and 5), Storemyr 3, Lislegrønlia grains, most of the Mjeltedalen 2a grains (grain 1, 3, and 4), Butvatnet (grain 1, 2, and 3), Bratterud (grain 1, and 4), Grønliheii (grain 2-4), Heftetjern 1 (grain 1, 3, and 5), Upper Høydalen 1 (1 and 12) and Lower Høydalen garnet crystals. Figure 3.36 shows that Y either remains relatively constant (<0.02 *apfu* difference), or decreases from the core to the rim, in particular for the Y-rich crystals. Crystals with more or less consistent Y comprise the Kleppe quarry, Svåheii 2 (grain 1), Storemyr 2 (grain 1 and 5), Lislegrønlia (grain 1, 2, and 3), Mjeltedalen 2a (grain 1 and 2), Upper Høydalen 1, and Lower Høydalen samples. Although many of these crystals show consistent Y core-rim compositions, some crystals show variability within crystals. These include the Storemyr 2 (grain 1), Lislegrønlia (grain 3), and Storemyr 3 (grain cluster), which show *apfu* value differences of < 0.02. The Mjeltedalen (grain 3 and 4), Butvatnet, Svåheii 3, Storemyr (grain 1, Bratterud, Grønliheii (grain 2-4), Heftetjern 1-2 garnets exhibit a decrease of Y from the core to the rim. The Y-poor garnets (<1.0 Y_2O_3 wt.%, ≤10000 ppm Y) from the Sjauset (grain 1, 2, and 3), Grønliheii (grain 1), Upper Høydalen 12 samples show either constant or decreasing Y. Both grain 2 and 3 from the Sjauset sample show a general decrease of Y, while grain 1 exhibit an increase in Y. Both the Grønliheii (grain 1) and Upper Høydalen 12 samples show consistent Y values at the core and rim.

Figures 3.37 A-R display chondrite-normalized REE patterns of 18 selected garnet crystals. Europium is below the limit of detection (<0.06 ppm) in all analyzed grains. The shape of REE patterns for all grains are relatively consistent and exhibit enrichment of the HREEs, and relatively low concentrations of LREEs. The highest HREEs content was detected in a garnet from the Butvatnet location (ΣHREE = 12839 ppm, grain 3). The same sample also shows the highest LREE abundances (ΣLREE = 147 ppm, grain 2). Significant core-rim variations of HREEs (largely owing to Yb) are observed for many of the analyzed crystals. For example, the grain 1 from the Bratterud sample exhibits a significant increase in the HREE contents from the core towards the rim (difference of ΣHREE = 8204 ppm, Fig. 3.37 I). A significant concentration decrease from the core to the rim (ΣHREE from 5155 to 3171 ppm) show garnets from the Svåheii 2 (Fig. 3.37 C) , Kleppe quarry (Fig. 3.37 E), Butvatnet (Fig. 3.37 G-H), and Heftetjern 2 (Fig. 3.37 N-O) locations.

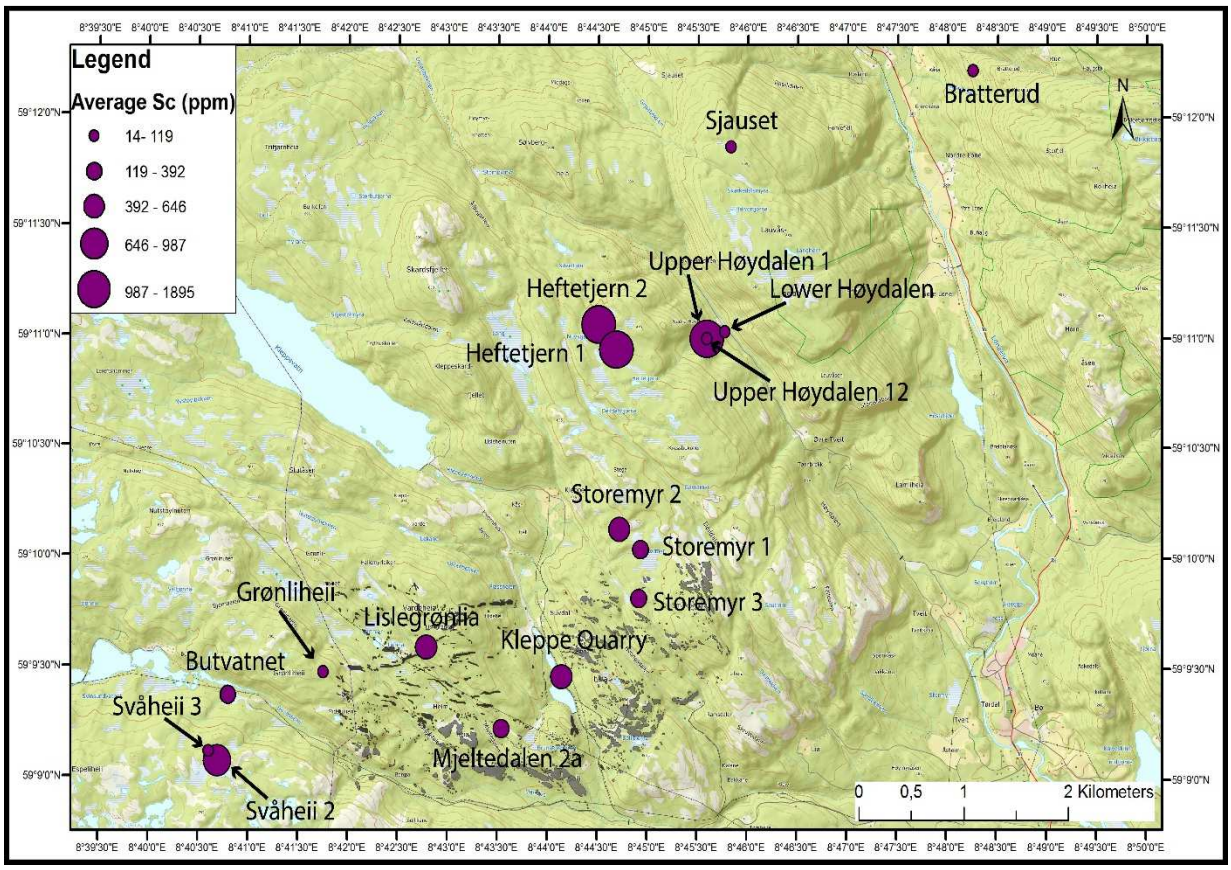

Figure 3.35: Map of the regional scandium distribution based on EPMA, and LA-ICP-MS analyzes. The displayed grey shaded bodies in the southern part of the map represent the pegmatites residing in the mapped area (Figure 3.4).

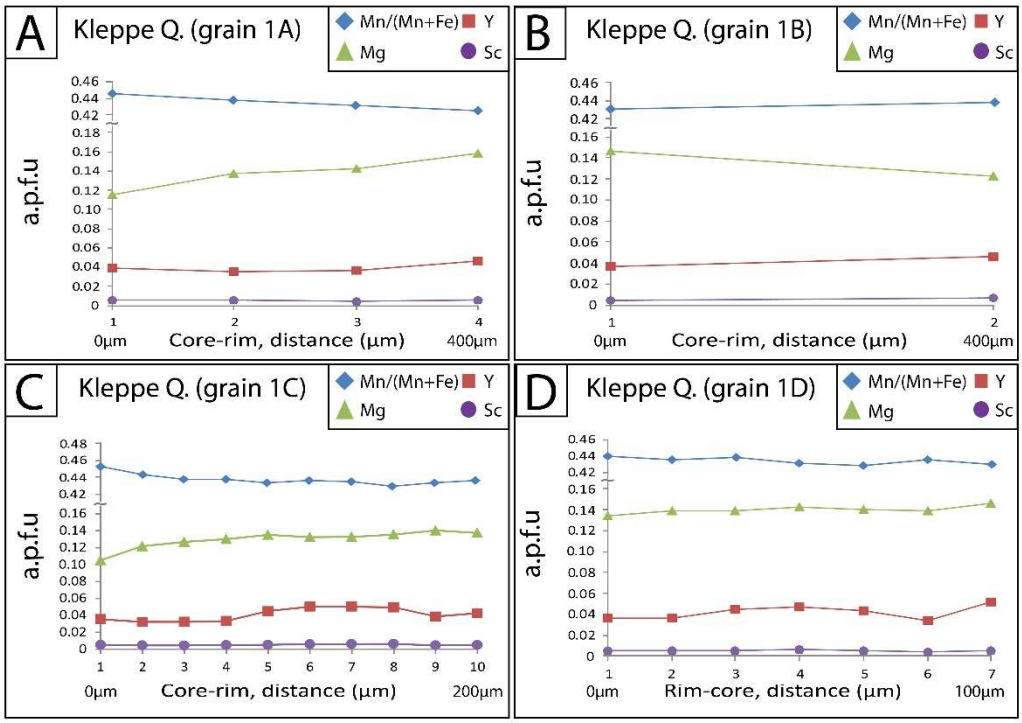

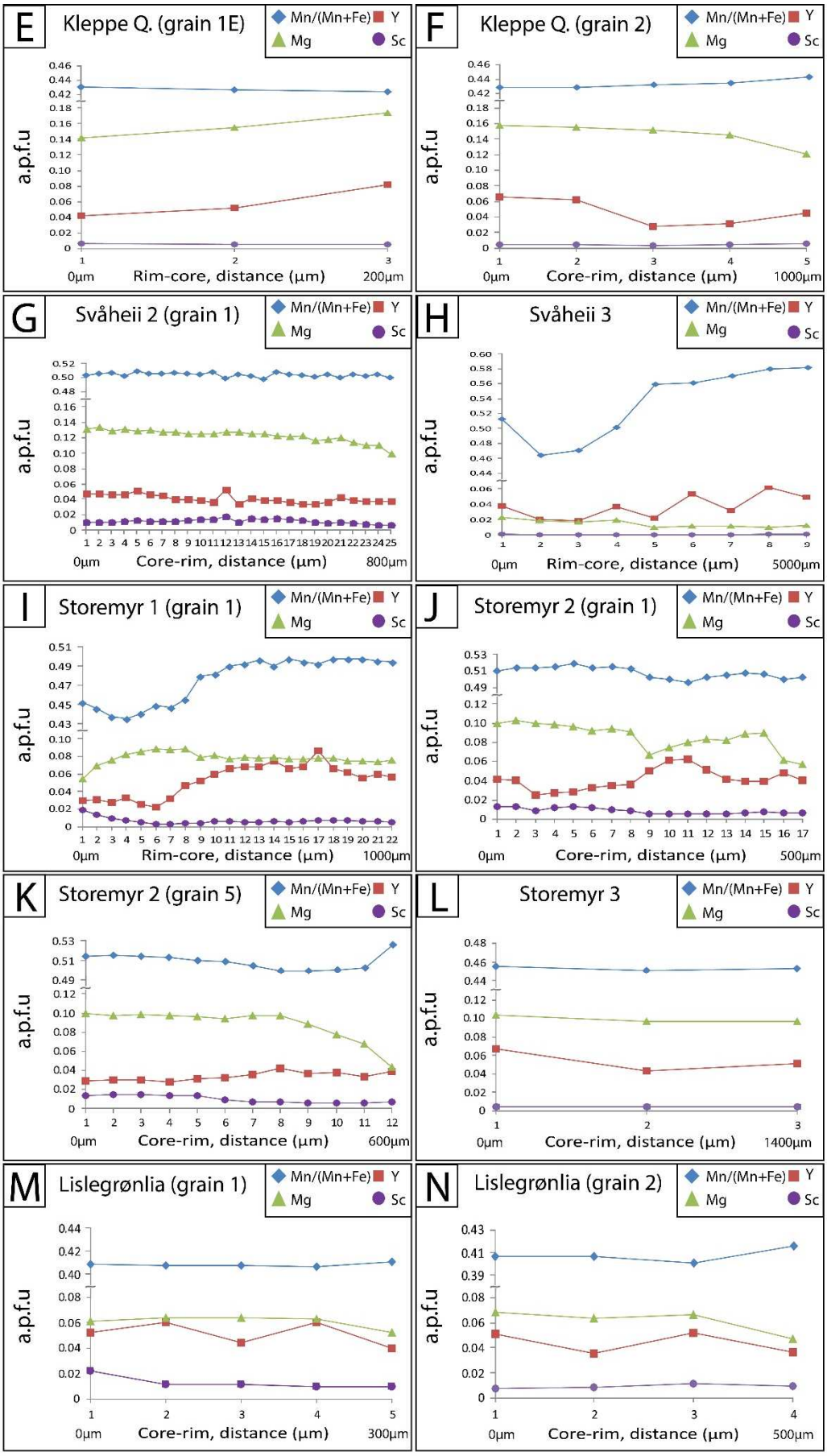
E
Kleppe Q. (grain 1E)
Mn/(Mn+Fe)
Y
Mg
Sc
a.p.f.u
0µm
Rim-core, distance (µm)
200µm
F
Kleppe Q. (grain 2)
Mn/(Mn+Fe)
Y
Mg
Sc
a.p.f.u
0µm
Core-rim, distance (µm)
1000µm
G
Svåheii 2 (grain 1)
Mn/(Mn+Fe)
Y
Mg
Sc
a.p.f.u
0µm
Core-rim, distance (µm)
800µm
H
Svåheii 3
Mn/(Mn+Fe)
Y
Mg
Sc
a.p.f.u
0µm
Rim-core, distance (µm)
5000µm
I
Storemyr 1 (grain 1)
Mn/(Mn+Fe)
Y
Mg
Sc
a.p.f.u
0µm
Rim-core, distance (µm)
1000µm
J
Storemyr 2 (grain 1)
Mn/(Mn+Fe)
Y
Mg
Sc
a.p.f.u
0µm
Core-rim, distance (µm)
500µm
K
Storemyr 2 (grain 5)
Mn/(Mn+Fe)
Y
Mg
Sc
a.p.f.u
0µm
Core-rim, distance (µm)
600µm
L
Storemyr 3
Mn/(Mn+Fe)
Y
Mg
Sc
a.p.f.u
0µm
Core-rim, distance (µm)
1400µm
M
Lislegrønlia (grain 1)
Mn/(Mn+Fe)
Y
Mg
Sc
a.p.f.u
0µm
Core-rim, distance (µm)
300µm
N
Lislegrønlia (grain 2)
Mn/(Mn+Fe)
Y
Mg
Sc
a.p.f.u
0µm
Core-rim, distance (µm)
500µm

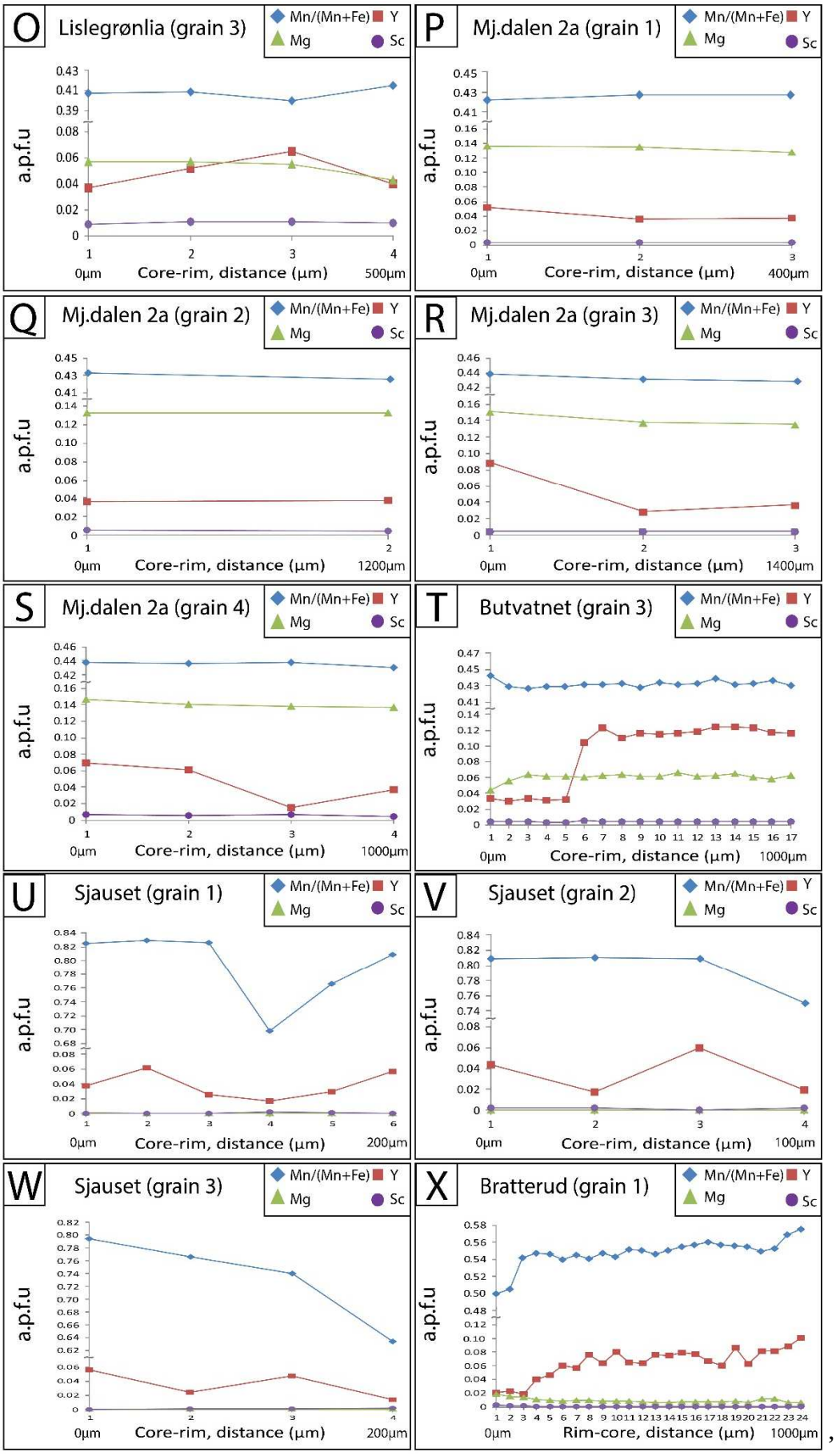
O
Lislegrønlia (grain 3)
Mn/(Mn+Fe)
Y
Mg
Sc
a.p.f.u
0µm
Core-rim, distance (µm)
500µm
P
Mj.dalen 2a (grain 1)
400µm
Q
Mj.dalen 2a (grain 2)
1200µm
R
Mj.dalen 2a (grain 3)
1400µm
S
Mj.dalen 2a (grain 4)
1000µm
T
Butvatnet (grain 3)
1000µm
U
Sjauset (grain 1)
200µm
V
Sjauset (grain 2)
100µm
W
Sjauset (grain 3)
200µm
X
Bratterud (grain 1)
Rim-core, distance (µm)
1000µm

,

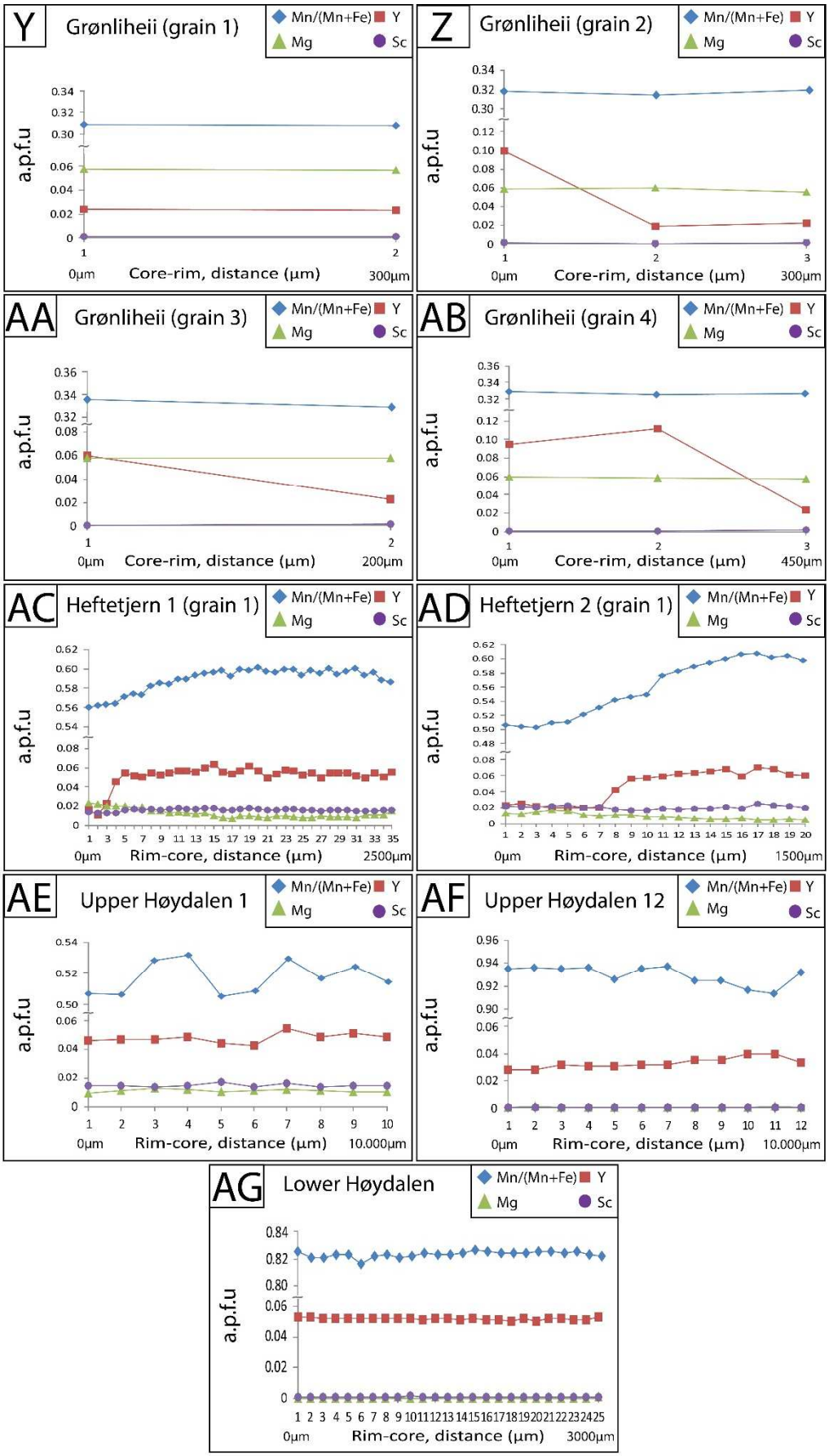

Figure 3.36: EPMA acquired average core-rim apfu compositions of the 33 analyzed garnet crystals.

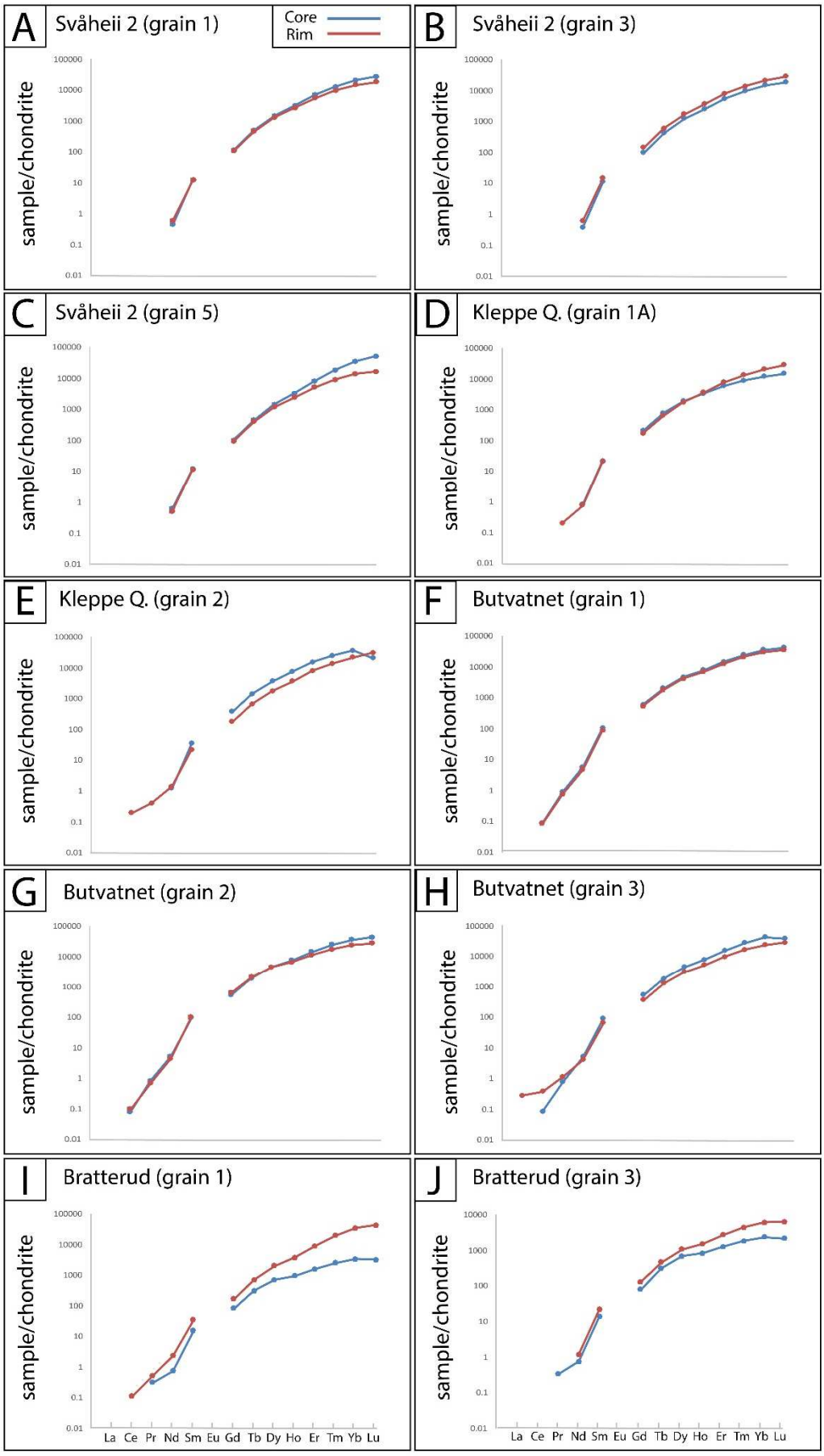
A
Svåheii 2 (grain 1)
Core
Rim
B
Svåheii 2 (grain 3)
C
Svåheii 2 (grain 5)
D
Kleppe Q. (grain 1A)
E
Kleppe Q. (grain 2)
F
Butvatnet (grain 1)
G
Butvatnet (grain 2)
H
Butvatnet (grain 3)
I
Bratterud (grain 1)
J
Bratterud (grain 3)
sample/chondrite
100000
10000
1000
100
10
1
0.1
0.01
La Ce Pr Nd Sm Eu Gd Tb Dy Ho Er Tm Yb Lu

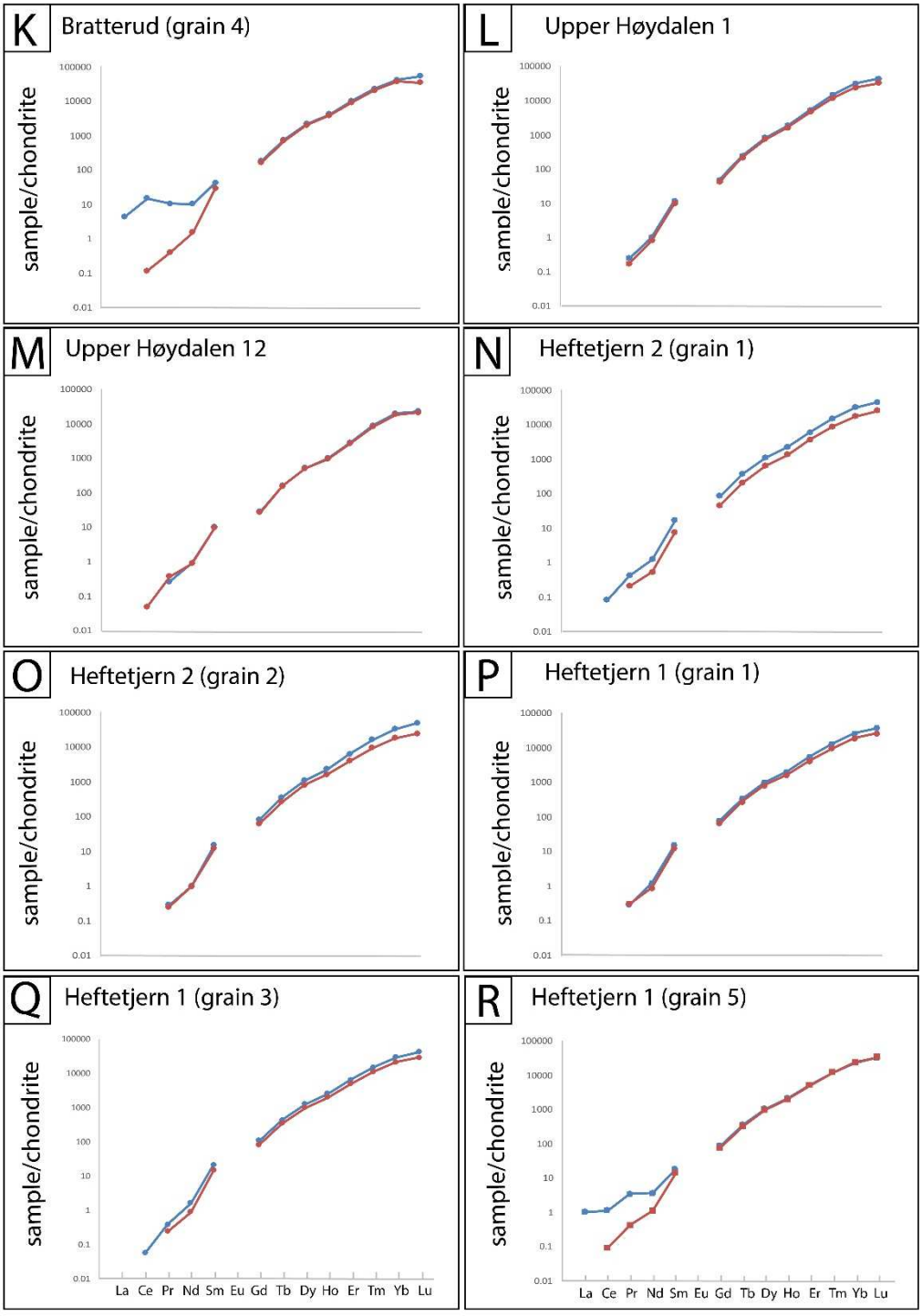

Figure 3.37: Chondrite normalized plots of the lanthanides (La-Lu) acquired through LA-ICP-MS of the 18 analyzed garnet grains. The data is normalized to lanthanide contents in chondrites by (Anders and Grevesse, 1989).

Table 3.5 Average garnet compositions

	Kleppe Quarry (grain 1A)		Kleppe Quarry (grain 1B)		Kleppe Quarry (grain 1C)		Kleppe Quarry (grain 1D)		Kleppe Quarry (grain 1E)		Kleppe Quarry (grain 2)		Svåheii 2 (grain 1)		Svåheii 3		Storemyr 1 (grain 1)	
	Core	Rim	Core	Rim	Core	Rim	Core	Rim	Core	Rim	Core	Rim	Core	Rim	Core	Rim	Core	Rim
n	2	2	1	1	5	5	4	3	2	1	2	3	12	13	5	4	14	8
(wt.%)																		
SiO_2	36.1(3)	36.10(4)	35.76	35.93	35.8(1)	35.9(2)	36.0(4)	35.8(4)	35.8(6)	36.07	35.58(9)	36.0(5)	35.9(2)	35.9(4)	36.1(4)	36.3(2)	35.8(4)	36.3(4)
FeO	23.1(4)	22.5(3)	23.25	22.71	23.1(3)	22.8(4)	23.1(4)	22.9(1)	22.9(5)	22.89	22.95(4)	22.8(3)	20.4(2)	20.5(2)	18.7(8)	22(1)	21.2(5)	23.4(6)
MnO	17.14(4)	17.6(3)	17.36	17.49	17.5(2)	17.8(7)	17.3(2)	17.6(1)	16.8(6)	17.07	16.99(8)	17.5(4)	20.5(4)	20.5(3)	24.5(8)	20(1)	20.4(5)	18.6(5)
Al_2O_3	20.7(3)	20.9(1)	20.54	20.73	20.28(2)	20.5(1)	20.4(3)	20.4(1)	19.7(1)	20.48	20.1(2)	20.6(2)	20.7(1)	20.7(3)	20.5(3)	20.5(1)	20.6(3)	20.5(3)
MgO	1.2(1)	1.0(1)	1.19	1.00	1.11(5)	1.0(1)	1.16(4)	1.12(3)	1.3(1)	1.16	1.27(2)	1.1(2)	1.05(4)	0.9(1)	0.09(2)	0.16(3)	0.63(3)	0.6(1)
CaO	1.15(3)	1.25(4)	1.20	1.14	1.13(7)	1.15(6)	1.12(6)	1.13(9)	1.33(9)	1.15	1.11(4)	1.1(2)	0.55(7)	0.8(3)	0.22(3)	0.5(3)	0.31(3)	0.3(1)
TiO_2	0.03(5)	0.00(1)	<0.01	0.02	0.02(1)	0.01(2)	0.02(3)	0.02(1)	0.04(3)	<0.01	0.04(3)	<0.01	0.03(5)	0.01(2)	0.08(3)	0.02(4)	0.0(1)	0.02(4)
Na_2O	0.06(1)	0.06	0.06	0.07	0.06(1)	0.06(1)	0.06(1)	0.06(0)	0.09(2)	0.05	0.09(1)	0.06(0)	0.08(3)	0.07(5)	0.05(3)	0.04(2)	0.06(2)	0.04(1)
Sc_2O_3	0.07(1)	0.08	0.07	0.09	0.08(2)	0.07(1)	0.07(2)	0.08(1)	0.07(0)	0.09	0.06(1)	0.07(3)	0.17(5)	0.15(8)	0.01(0)	0.01(0)	0.08(2)	0.1(1)
Y_2O_3	0.9(2)	0.85(9)	0.85	1.05	1.0(2)	0.8(2)	1.0(2)	0.8(1)	1.5(6)	0.96	1.46(9)	0.8(3)	1.0(2)	0.8(1)	1.0(6)	0.6(4)	1.4(3)	0.7(3)
Yb_2O_3	0.4(1)	0.43(1)	0.35	0.54	0.3(2)	0.29(9)	0.2(1)	0.3(1)	0.6(3)	0.30	0.67(4)	0.3(2)	0.4(2)	0.3(2)	0.0(1)	0.18(4)	0.2(1)	0.07(7)
SnO_2	N.D.	N.D.	N.D.	N.D.	N.D.	N.D.	N.D.	N.D.	N.D.	N.D.	N.D.	N.D.	N.D.	N.D.	N.D.	N.D.	N.D.	N.D.
Total	101.06	100.99	100.64	100.75	100.38	100.38	100.43	100.21	100.13	100.22	100.32	100.33	100.78	100.63	101.25	100.31	101.17	101.01
Si apfu	2.952	2.947	2.938	2.947	2.951	2.953	2.957	2.947	2.960	2.965	2.940	2.956	2.945	2.942	2.963	2.978	2.941	2.976
^{IV}Al	0.048	0.053	0.062	0.053	0.049	0.047	0.043	0.053	0.040	0.035	0.060	0.044	0.055	0.058	0.037	0.022	0.059	0.024
Total Z	3.000	3.000	3.000	3.000	3.000	3.000	3.000	3.000	3.000	3.000	3.000	3.000	3.000	3.000	3.000	3.000	3.000	3.000
^{VI}Al	1.943	1.964	1.927	1.951	1.918	1.942	1.931	1.929	1.887	1.949	1.906	1.948	1.945	1.943	1.948	1.963	1.942	1.960
Ti	0.002	0.000	0.000	0.001	0.001	0.000	0.001	0.001	0.003	0.000	0.003	0.000	0.002	0.001	0.005	0.001	0.005	0.001
Sc	0.005	0.006	0.005	0.006	0.006	0.005	0.005	0.005	0.005	0.007	0.005	0.005	0.012	0.010	0.001	0.001	0.006	0.008
Total Y	1.950	1.970	1.933	1.958	1.925	1.948	1.937	1.936	1.895	1.956	1.913	1.953	1.959	1.955	1.953	1.966	1.953	1.969
Fe^{2-}	1.580	1.541	1.598	1.558	1.591	1.569	1.588	1.580	1.587	1.574	1.586	1.567	1.397	1.410	1.282	1.508	1.460	1.605
Mn^{21}	1.185	1.219	1.208	1.215	1.221	1.239	1.205	1.230	1.176	1.189	1.189	1.216	1.425	1.425	1.701	1.431	1.420	1.290
Mg	0.005	0.006	0.005	0.006	0.006	0.005	0.005	0.005	0.005	0.007	0.005	0.005	0.012	0.010	0.001	0.001	0.006	0.008
Ca	0.100	0.109	0.105	0.100	0.099	0.102	0.098	0.100	0.118	0.102	0.098	0.102	0.048	0.072	0.019	0.051	0.027	0.032
Na	0.009	0.009	0.010	0.010	0.010	0.009	0.010	0.010	0.014	0.008	0.015	0.009	0.012	0.011	0.007	0.007	0.010	0.006
Y	0.041	0.037	0.037	0.046	0.046	0.036	0.044	0.039	0.067	0.042	0.064	0.035	0.044	0.037	0.044	0.028	0.065	0.031
Yb	0.010	0.011	0.009	0.013	0.009	0.007	0.007	0.008	0.015	0.007	0.017	0.008	0.011	0.008	0.002	0.005	0.007	0.002
Total X	2.932	2.931	2.973	2.948	2.983	2.966	2.957	2.972	2.983	2.928	2.974	2.942	2.950	2.972	3.057	3.030	2.994	2.974
(mol. %)																		
Yttrogarnet	1.4	1.2	1.2	1.5	1.5	1.2	1.5	1.3	1.6	1.3	2.1	1.2	1.5	1.2	1.3	0.8	2.0	0.7
Schorlomite-Al	0.1	0.0	0.0	0.1	0.1	0.0	0.1	0.1	0.0	0.0	0.1	0.0	0.1	0.0	0.1	0.0	0.1	0.0
Morimotoite	0.0	0.0	0.0	0.0	0.0	0.0	0.0	0.0	0.3	0.0	0.0	0.0	0.0	0.0	0.1	0.1	0.1	0.0
NaTi garnet	0.0	0.0	0.0	0.0	0.0	0.0	0.0	0.0	0.0	0.0	0.0	0.0	0.0	0.0	0.0	0.0	0.1	0.0
Morimotoite-Fe	0.0	0.0	0.0	0.0	0.0	0.0	0.0	0.0	0.0	0.0	0.0	0.0	0.0	0.0	0.0	0.0	0.0	0.0
Sc garnet	0.3	0.3	0.3	0.3	0.3	0.2	0.2	0.3	0.3	0.3	0.2	0.2	0.5	0.5	0.0	0.0	0.3	0.4
Spessartine	39.4	40.6	40.1	40.5	40.6	41.2	40.0	40.8	39.1	39.6	39.5	40.4	47.4	47.3	56.6	47.7	47.3	43.0
Pyrope	5.0	4.2	4.9	4.1	4.5	4.1	4.7	4.6	5.5	4.7	5.2	4.6	4.3	3.9	0.4	0.6	2.6	2.6
Almandine	49.8	49.1	48.4	49.6	48.4	48.9	49.2	48.5	47.5	50.5	47.7	49.2	43.6	43.3	38.6	48.4	44.9	51.3
Grossular	1.1	2.8	0.7	1.6	0.0	1.0	0.4	0.5	0.0	1.0	0.0	1.3	0.0	0.6	0.0	0.5	0.0	0.1
Andradite	1.9	0.6	2.6	1.4	2.9	2.1	2.6	2.6	3.4	2.1	2.9	1.8	0.9	1.3	0.4	1.1	0.4	0.5
Skiagite	0.1	0.0	0,0	0.0	0.6	0.0	0.4	0.1	1.3	0.0	1.0	0.0	0.3	0.1	1.8	0.3	1.7	0.6

Table 3.5 Continued

	Storemyr 2 (grain 1)		Storemyr 2 (grain 5)		Storemyr 3 (grain cluster)		Lislegrønlia (grain 1)		Lislegrønlia (grain 2)		Lislegrønlia (grain 3)		Mjeltedalen 2a (grain 1)		Mjeltedalen 2a (grain 2)		Mjeltedalen 2a (grain 3)	
	Core	Rim	Core	Rim	Core	Rim	Core	Rim	Core	Rim	Core	Rim	Core	Rim	Core	Rim	Core	Rim
n	8	9	6	6	1	2	3	2	2	2	2	2	2	1	1	1	2	1
(wt.%)																		
SiO_2	35.8(2)	35.7(3)	35.9(4)	35.7(2)	35.17	35.9(2)	35.5(2)	35.4(4)	35.8(1)	35.52(2)	35.8(5)	35.6(9)	36.0(2)	36.03	36.23	35.90	35.8(7)	36.00
FeO	20.2(2)	20.6(3)	20.4(1)	20.6(6)	21.96	22.4(1)	24.81(4)	24.89(8)	25.0(3)	25.0(5)	25.1(1)	24.9(1)	23.33(3)	23.17	22.86	23.17	22.6(9)	23.36
MnO	21.1(4)	20.5(4)	21.2(3)	20.8(9)	18.17	18.3(1)	16.91(9)	16.9(2)	16.9(2)	17.0(6)	17.07(2)	16.9(9)	16.9(4)	17.05	17.19	16.96	17.2(2)	17.34
Al_2O_3	20.8(3)	20.1(4)	20.9(2)	20.4(4)	20.35	20.3(3)	20.9(4)	20.6(2)	20.6(1)	20.4(3)	20.81(1)	20.66(1)	20.4(1)	20.38	20.63	20.65	20.5(3)	20.73
MgO	0.79(6)	0.6(1)	0.79(3)	0.6(3)	0.84	0.79(0)	0.51(2)	0.47(9)	0.54(3)	0.4(1)	0.46(0)	0.4(1)	1.11(0)	1.05	1.08	1.09	1.18(9)	1.11
CaO	0.5(2)	1.1(1)	0.5(2)	1.1(1)	1.21	1.23(1)	0.3(1)	0.4(1)	0.29(1)	0.4(1)	0.36(9)	0.4(1)	1.33(1)	1.41	1.18	1.36	1.0(2)	1.17
TiO_2	0.01(3)	0.02(4)	0.01(2)	0.01(4)	0.03	0.05(1)	0.03(4)	0.02(4)	0.02(1)	0.04(3)	0.01(1)	0.03(6)	0.03(3)	0.01	0.01	0.03	0.05(6)	0.02
Na_2O	0.06(2)	0.08(2)	0.06(1)	0.06(2)	0.10	0.07(1)	0.05(2)	0.05(2)	0.07(2)	0.06(1)	0.05(1)	0.06(1)	0.08(2)	0.07	0.07	0.06	0.10(7)	0.06
Sc_2O_3	0.16(5)	0.08(2)	0.19(5)	0.09(2)	0.05	0.05(1)	0.2(1)	0.14(1)	0.11(1)	0.14(4)	0.14(3)	0.14(1)	0.05(0)	0.05	0.07	0.06	0.07(1)	0.07
Y_2O_3	0.7(2)	1.1(3)	0.69(7)	0.8(1)	1.50	1.0(1)	1.1(3)	1.1(4)	1.0(3)	1.0(3)	1.0(3)	1.1(5)	1.0(3)	0.84	0.84	0.86	1(1)	0.85
Yb_2O_3	0.3(2)	0.5(1)	0.20(9)	0.3(1)	0.86	0.59(1)	0.3(2)	0.4(2)	0.4(3)	0.3(1)	0.25(8)	0.4(1)	0.5(2)	0.45	0.35	0.34	0.5(4)	0.32
SnO_2	N.D.	N.D.	N.D.	N.D.	<0.01	<0.01	<0.01	<0.01	<0.01	<0.01	0.00(1)	0.00(1)	0.00(1)	<0.01	<0.01	<0.01	<0.01	<0.01
Total	100.42	100.38	100.84	100.46	100.26	100.68	100.58	100.37	100.73	100.26	101.05	100.59	100.73	100.51	100.51	100.47	100.00	101.03
Si apfu	2.944	2.953	2.940	2.943	2.922	2.953	2.924	2.933	2.946	2.936	2.944	2.938	2.952	2.961	2.968	2.948	2.949	2.943
^{IV}Al	0.056	0.047	0.060	0.057	0.078	0.047	0.076	0.067	0.054	0.064	0.056	0.062	0.048	0.039	0.032	0.052	0.051	0.057
Total Z	3.000	3.000	3.000	3.000	3.000	3.000	3.000	3.000	3.000	3.000	3.000	3.000	3.000	3.000	3.000	3.000	3.000	3.000
^{VI}Al	1.958	1.916	1.958	1.930	1.915	1.925	1.954	1.942	1.950	1.932	1.957	1.946	1.927	1.935	1.960	1.946	1.936	1.940
Ti	0.001	0.001	0.001	0.001	0.002	0.003	0.002	0.001	0.001	0.002	0.001	0.002	0.002	0.001	0.000	0.002	0.003	0.001
Sc	0.011	0.006	0.013	0.006	0.004	0.004	0.015	0.010	0.008	0.010	0.010	0.010	0.004	0.004	0.005	0.004	0.005	0.005
Total Y	1.970	1.922	1.972	1.937	1.921	1.932	1.971	1.953	1.960	1.945	1.967	1.958	1.933	1.940	1.965	1.952	1.944	1.947
Fe^{2-}	1.389	1.428	1.398	1.420	1.526	1.543	1.709	1.721	1.725	1.735	1.722	1.720	1.600	1.592	1.566	1.591	1.558	1.597
Mn^{21}	1.470	1.440	1.473	1.452	1.279	1.276	1.180	1.189	1.183	1.197	1.186	1.182	1.179	1.187	1.193	1.179	1.198	1.200
Mg	0.011	0.006	0.013	0.006	0.004	0.004	0.015	0.010	0.008	0.010	0.010	0.010	0.004	0.004	0.005	0.004	0.005	0.005
Ca	0.051	0.098	0.047	0.098	0.108	0.108	0.033	0.040	0.026	0.041	0.032	0.043	0.117	0.124	0.103	0.120	0.094	0.103
Na	0.010	0.012	0.009	0.010	0.016	0.012	0.008	0.008	0.010	0.010	0.008	0.009	0.012	0.011	0.011	0.009	0.016	0.009
Y	0.033	0.048	0.030	0.037	0.067	0.047	0.052	0.050	0.044	0.044	0.044	0.052	0.044	0.037	0.036	0.038	0.059	0.037
Yb	0.008	0.013	0.005	0.009	0.022	0.015	0.010	0.011	0.010	0.009	0.006	0.011	0.013	0.011	0.009	0.009	0.013	0.008
Total X	2.972	3.045	2.976	3.032	3.021	3.005	3.006	3.029	3.006	3.045	3.008	3.027	2.969	2.966	2.924	2.950	2.941	2.959
(mol. %)																		
Yttrogarnet	1.1	1.5	1.0	1.2	2.2	1.4	1.7	1.7	1.5	1.5	1.5	1.7	1.5	1.2	1.2	1.3	1.5	1.2
Schorlomite-Al	0.0	0.0	0.0	0.0	0.1	0.1	0.1	0.1	0.1	0.1	0.0	0.1	0.1	0.0	0.0	0.1	0.0	0.1
Morimotoite	0.0	0.0	0.0	0.0	0.0	0.1	0.0	0.0	0.0	0.0	0.0	0.0	0.0	0.0	0.0	0.0	0.0	0.0
NaTi garnet	0.0	0.0	0.0	0.0	0.0	0.0	0.0	0.0	0.0	0.0	0.0	0.0	0.0	0.0	0.0	0.0	0.0	0.0
Morimotoite-Fe	0.0	0.0	0.0	0.0	0.0	0.0	0.0	0.0	0.0	0.0	0.0	0.0	0.0	0.0	0.0	0.0	0.0	0.0
Sc garnet	0.6	0.3	0.7	0.3	0.2	0.2	0,7	0.5	0.4	0.5	0.5	0.5	0.2	0.2	0.3	0.2	0.2	0.3
Spessartine	48.9	47.9	48.9	48.2	42.5	42.5	39.3	39.6	39.4	39.8	39.5	39.3	39.2	39.5	39.7	39.2	39.9	39.9
Pyrope	3.2	2.5	3.2	2.6	3.5	3.2	2.1	1.9	2.2	1.9	1.9	1.6	4.5	4.3	4.4	4.4	4.8	4.5
Almandine	43.5	43.1	43.3	42.8	46.6	48.2	53.9	53.4	54.1	52.7	54.5	54.2	49.8	49.9	50.6	49.8	49.3	49.4
Grossular	0.5	0.0	0.6	0.6	0.4	0.5	0.2	0.0	0.0	0.0	0.0	0.0	0.7	1.3	1.9	1.9	0.9	1.2
Andradite	0.5	2.9	0.3	2.3	2.9	2.7	0.2	0.8	0.4	0.7	0.5	0.8	2.9	2.6	1.3	1.8	1.7	1.9
Skiagite	0.0	0.6	0.0	0.2	0.0	0.1	0.5	0.8	0.9	1.3	0.5	0.6	0.0	0.0	0.0	0.0	0.0	0.0

Table 3.5 Continued

	Mjeltedalen 2a (grain 4)		Butvatnet (grain 3)		Sjauset (grain 1)		Sjauset (grain 2)		Sjauset (grain 3)		Bratterud (grain 1)		Grønliheii (grain 1)		Grønliheii (grain 2)		Grønliheii (grain 3)	
	Core	Rim	Core	Rim	Core	Rim	Core	Rim	Core	Rim	Core	Rim	Core	Rim	Core	Rim	Core	Rim
n	2	2	10	7	3	3	3	1	2	2	6	22	1	1	2	1	1	1
(wt.%)																		
SiO_2	35.6(1)	36.23(3)	35.1(2)	36.0(6)	36.0(6)	36.2(2)	35.7(7)	35.90	36.0(2)	35.8(4)	35.6(4)	36.0(5)	36.38	36.50	35(1)	36.43	36.26	36.69
FeO	22.6(3)	23.0(4)	22.9(3)	24(1)	7.4(3)	9(4)	8.2(1)	10.98	9(1)	13(4)	18(1)	19(1)	29.65	29.62	28(1)	28.93	27.81	28.72
MnO	17.3(1)	17.4(8)	17.2(3)	18.0(8)	35.0(8)	33(3)	34.6(8)	32.55	33.3(2)	29(3)	23.2(9)	22(1)	13.06	12.96	12.9(6)	13.39	13.85	13.93
Al_2O_3	20.4(2)	20.84(5)	20.9(2)	20.6(2)	20.81(9)	20.9(2)	20.83(9)	20.62	20.88(1)	20.6(1)	20.8(4)	20.6(2)	20.72	21.05	20.6(5)	20.97	20.56	20.77
MgO	1.17(5)	1.13(1)	0.50(3)	0.4(1)	0.01(1)	<0.01	<0.01	<0.01	<0.01	<0.01	0.07(5)	0.08(5)	0.47	0.47	0.48(1)	0.46	0.47	0.48
CaO	1.0(2)	1.1(4)	0.16(3)	0.20(5)	0.44(5)	0.42(5)	0.4(1)	0.41	0.40(5)	0.55(5)	0.26(2)	0.28(9)	0.24	0.23	0.20(1)	0.24	0.17	0.24
TiO_2	0.07(4)	0.01(0)	0.09(2)	0.02(4)	0.01(2)	0.02(3)	0.02(1)	0.02	0.02(4)	0.01(1)	0.06(4)	0.04(3)	0.02	<0.01	0.03(7)	<0.01	0.04	<0.01
Na_2O	0.10(1)	0.05(2)	0.12(7)	0.04(5)	0.03(1)	0.03(2)	0.05(4)	0.03	0.04(3)	0.04(6)	0.09(2)	0.07(4)	0.02	0.02	0.06(4)	0.03	0.07	0.03
Sc_2O_3	0.09(1)	0.08(4)	0.06(1)	0.05(1)	0.01(1)	0.02(2)	0.02(3)	0.03	0.01(1)	0.02(2)	0.01(1)	0.01(2)	0.02	0.02	0.01(1)	0.02	0.01	0.01
Y_2O_3	1.4(2)	0.6(4)	2.6(2)	0(1)	0.9(6)	0.7(6)	0.9(8)	0.45	0.9(7)	0.7(7)	2.0(3)	1.3(9)	0.56	0.54	1(1)	0.52	1.36	0.52
Yb_2O_3	0.6(1)	0.2(2)	0.7(1)	0.1(2)	0.4(4)	0.2(4)	0.4(5)	0.12	0.3(5)	0.2(4)	0.6(2)	0.2(2)	0.09	0.09	0.4(7)	0.07	0.18	0.04
SnO_2	<0.01	<0.01	N.D.	N.D.	0.01(1)	0.01(1)	0.01(1)	0.01	0.01(1)	0.01(1)	N.D.	N.D.	0.01	<0.01	0.01(1)	<0.01	0.01	<0.01
Total	100.33	100.64	100.33	99.41	101.02	100.50	101.13	101.11	100.86	99.93	100.69	99.58	101.23	101.52	98.69	101.04	100.78	101.44
Si apfu	2.937	2.957	2.913	2.965	2.957	2.959	2.938	2.952	2.950	2.949	2.937	2.966	2.975	2.971	2.956	2.976	2.979	2.988
^{IV}Al	0.063	0.043	0.087	0.035	0.043	0.041	0.062	0.048	0.050	0.051	0.063	0.034	0.025	0.029	0.044	0.024	0.021	0.012
Total Z	3.000	3.000	3.000	3.000	3.000	3.000	3.000	3.000	3.000	3.000	3.000	3.000	3.000	3.000	3.000	3.000	3.000	3.000
^{VI}Al	1.919	1.962	1.960	1.966	1.969	1.972	1.954	1.949	1.965	1.953	1.962	1.961	1.971	1.990	1.972	1.995	1.970	1.981
Ti	0.005	0.000	0.006	0.001	0.001	0.002	0.002	0.001	0.001	0.000	0.004	0.002	0.001	0.000	0.002	0.000	0.002	0.000
Sc	0.006	0.006	0.004	0.004	0.000	0.002	0.002	0.002	0.001	0.001	0.001	0.001	0.001	0.002	0.001	0.001	0.001	0.001
Total Y	1.930	1.968	1.970	1.971	1.970	1.976	1.957	1.952	1.967	1.955	1.967	1.965	1.974	1.991	1.975	1.996	1.973	1.982
Fe^{2+}	1.558	1.574	1.587	1.658	0.511	0.718	0.565	0.755	0.650	0.935	1.257	1.333	2.027	2.016	1.963	1.977	1.911	1.956
Mn^{2-}	1.208	1.208	1.210	1.254	2.434	2.235	2.409	2.267	2.309	2.050	1.625	1.601	0.904	0.894	0.908	0.926	0.964	0.960
Mg	0.006	0.006	0.004	0.004	0.000	0.002	0.002	0.002	0.001	0.001	0.001	0.001	0.001	0.002	0.001	0.001	0.001	0.001
Ca	0.093	0.097	0.014	0.018	0.039	0.036	0.038	0.036	0.035	0.049	0.023	0.024	0.021	0.020	0.018	0.021	0.015	0.021
Na	0.016	0.008	0.019	0.007	0.005	0.005	0.008	0.004	0.006	0.006	0.015	0.012	0.003	0.004	0.009	0.005	0.012	0.005
Y	0.065	0.026	0.117	0.041	0.041	0.035	0.040	0.020	0.040	0.031	0.090	0.058	0.024	0.024	0.059	0.023	0.059	0.022
Yb	0.017	0.006	0.018	0.005	0.011	0.008	0.011	0.003	0.009	0.007	0.016	0.006	0.002	0.002	0.011	0.002	0.004	0.001
Total X	2.963	2.925	2.970	2.986	3.041	3.038	3.074	3.087	3.052	3.078	3.026	3.035	2.983	2.961	2.969	2.954	2.966	2.967
(mol. %)																		
Yttrogarnet	2.2	0.9	2.6	1.0	1.2	1.0	1.3	0.7	1.3	1.0	1.9	1.1	0.8	0.8	1.4	0.8	0.6	0.5
Schorlomite-Al	0.1	0.0	0.0	0.0	0.0	0.0	0.1	0.1	0.0	0.0	0.0	0.0	0.1	0,0	0.0	0.0	0.0	0.0
Morimotoite	0.0	0.0	0.4	0.1	0.0	0.1	0.0	0.0	0.0	0.0	0.3	0.2	0.0	0.0	0.2	0.0	0.3	0.0
NaTi garnet	0.1	0.0	0.0	0.0	0.0	0.0	0.0	0.0	0.1	0.0	0.0	0.0	0.0	0.0	0.0	0.0	0.0	0.0
Morimotoite-Fe	0.0	0.0	0.1	0.0	0.0	0.0	0.0	0.0	0.0	0.0	0.0	0.0	0.0	0.0	0.0	0.0	0.0	0.0
Sc garnet	0.3	0.3	0.0	0.2	0.0	0.1	0.1	0.1	0.0	0.1	0,0	0.0	0.1	0.1	0.0	0.1	0.0	0.1
Spessartine	40.2	40.2	40.5	41.8	81.1	74.5	80.1	75.2	76.9	68.1	54.3	53.3	30.1	29.8	30.3	30.9	32.2	32.0
Pyrope	4.8	4.6	2.1	2.0	0.0	0.0	0.0	0.0	0.0	0.0	0.3	0.3	1.9	1.9	2.0	1.9	1.9	1.9
Almandine	48.3	49.9	52.3	53.1	15.7	22.5	15.5	20.5	19.7	27.6	41.0	43.0	65.4	66.4	64.5	65.4	63.1	64.5
Grossular	0.1	2.0	0.0	0.0	0.3	0.3	0.1	0.0	0.1	0.1	0.3	0.2	0.0	0.5	0.0	0.6	0.2	0.1
Andradite	2.5	0.9	0.0	0.3	0.9	0.6	1.0	1.0	1.0	1.4	0.1	0.4	0.6	0.1	0.3	0.0	0.0	0.6
Skiagite	0.4	0.0	0.1	0.7	0.0	0.0	0.3	0.8	0.1	0.3	0.1	0.2	0.7	0.0	0.3	0.0	0.0	0.0

Table 3.5 Continued

	Grønliheii (grain 4)		Heftetjern 1 (grain 1)		Heftetjern 2 (grain 1)		Upper Høydalen 1		Upper Høydalen 12		Lower Høydalen	
	core	rim	Core	Rim	Core	Rim	Core	Rim	Core	Rim	Core	Rim
n	4	1	20	15	10	10	4	6	7	5	15	10
(wt.%)												
SiO_2	35.8(4)	36.22	36.0(2)	36.1(4)	35.8(2)	36.1(4)	35.9(1)	36.0(4)	35.5(4)	35.5(4)	35.6(2)	35.6(1)
FeO	27.6(6)	28.85	17.0(4)	17(1)	16.90(9)	20(1)	20.0(8)	20.4(9)	3.2(7)	2.9(3)	7.61(8)	7.6(2)
MnO	13.3(5)	13.80	24.8(3)	24.1(7)	24.6(7)	21(1)	21.5(2)	21.4(9)	39.9(7)	40.3(4)	35.2(4)	35.0(4)
Al_2O_3	20.61(3)	20.70	20.6(2)	20.6(2)	20.5(1)	20.6(2)	20.6(2)	20.6(1)	20.9(1)	20.9(1)	20.8(1)	20.8(3)
MgO	0.49(3)	0.47	0.08(3)	0.13(7)	0.05(2)	0.10(4)	0.09(1)	0.09(2)	<0.01	0.00(1)	<0.01	<0.01
CaO	0.19(4)	0.23	0.56(4)	0.59(9)	0.60(7)	0.6(1)	0.38(3)	0.36(2)	0.47(2)	0.46(6)	0.4(3)	0.39(3)
TiO_2	0.04(2)	<0.01	0.10(4)	0.09(8)	0.11(5)	0.04(7)	0.04(4)	0.04(3)	0.02(1)	0.02(1)	0.03(2)	0.03(3)
Na_2O	0.10(2)	0.02	0.07(2)	0.06(3)	0.10(8)	0.1(2)	0.06(1)	0.05(1)	0.03(1)	0.03(1)	0.04(1)	0.04(1)
Sc_2O_3	0.01(1)	0.02	0.23(2)	0.22(5)	0.29(6)	0.28(6)	0.20(3)	0.20(4)	<0.01	<0.01	0.01(0)	0.01(0)
Y_2O_3	1.9(8)	0.54	1.2(1)	1.0(7)	1.4(1)	0.7(6)	1.1(1)	1.05(8)	0.8(1)	0.68(7)	1.18(2)	1.19(2)
Yb_2O_3	0.4(4)	0.07	0.47(6)	0.3(3)	0.4(1)	0.2(2)	0.5(1)	0.4(1)	0.35(2)	0.31(6)	0.22(3)	0.24(3)
SnO_2	0.01(1)	<0.01	N.D.	N.D.	N.D.	N.D.	N.D.	N.D.	0.01(1)	0.01(2)	N.D.	N.D.
Total	100.45	100.92	101.11	100.19	100.75	99.72	100.37	100.59	101.18	101.11	101.09	100.90
Si apfu	2.956	2.971	2.957	2.964	2.950	2.965	2.964	2.968	2.924	2.923	2.930	2.934
^{IV}Al	0.044	0.029	0.043	0.036	0.050	0.035	0.036	0.032	0.076	0.077	0.070	0.066
Total Z	3.000	3.000	3.000	3.000	3.000	3.000	3.000	3.000	3.000	3.000	3.000	3.000
^{VI}Al	1.959	1.972	1.950	1.955	1.945	1.961	1.970	1.969	1.950	1.952	1.949	1.958
Ti	0.002	0.000	0.006	0.005	0.007	0.002	0.003	0.003	0.001	0.001	0.002	0.002
Sc	0.001	0.001	0.016	0.016	0.021	0.020	0.015	0.015	0.000	0.000	0.001	0.001
Total Y	1.963	1.973	1.972	1.976	1.973	1.983	1.987	1.987	1.951	1.953	1.951	1.961
Fe^{2+}	1.909	1.979	1.169	1.217	1.165	1.390	1.383	1.410	0.222	0.200	0.523	0.528
Mn^{2+}	0.933	0.959	1.728	1.675	1.718	1.520	1.505	1.493	2.778	2.807	2.454	2.436
Mg	0.001	0.001	0.016	0.016	0.021	0.020	0.015	0.015	0.000	0.000	0.001	0.001
Ca	0.017	0.020	0.049	0.052	0.053	0.054	0.034	0.032	0.041	0.041	0.041	0.035
Na	0.017	0.003	0.011	0.010	0.015	0.018	0.010	0.008	0.004	0.004	0.006	0.006
Y	0.087	0.024	0.054	0.047	0.064	0.031	0.051	0.046	0.035	0.030	0.052	0.052
Yb	0.012	0.002	0.012	0.010	0.012	0.006	0.014	0.011	0.009	0.008	0.006	0.006
Total X	2.975	2.988	3.039	3.027	3.047	3.040	3.012	3.014	3.090	3.090	3.082	3.064
(mol. %)												
Yttrogarnet	1.3	0.8	1.3	1.0	1.6	0.9	1.0	0.9	1.2	1.0	1.7	1.7
Schorlomite-Al	0.0	0.0	0.0	0.0	0.0	0.0	0.0	0.0	0.1	0.1	0.1	0.1
Morimotoite	0.2	0.0	0.4	0.4	0.2	0.0	0.1	0.1	0.0	0.0	0.0	0.0
NaTi garnet	0.0	0.0	0.1	0.1	0.3	0.0	0.1	0.1	0.0	0.0	0.0	0.0
Morimotoite-Fe	0.0	0.0	0.0	0.0	0.0	0.0	0.0	0.0	0.0	0.0	0.0	0.0
Sc garnet	0.0	0.1	0.8	0.8	1.0	1.0	0.7	0.7	0.0	0.0	0.0	0.0
Spessartine	31.2	31.9	57.6	55.9	57.3	50.6	50.3	49.8	92.2	93.2	81.5	81.0
Pyrope	2.0	1.9	0.3	0.5	0.2	0.4	0.4	0.4	0.0	0.0	0.0	0.0
Almandine	62.8	63.5	37.9	39.7	37.7	44.6	45.9	46.7	3.1	2.1	13.3	14.5
Grossular	0.2	0.0	0.1	0.2	0.1	0.5	0.2	0.2	0.2	0.2	0.0	0.1
Andradite	0.1	0.6	0.3	0.3	0.3	0.2	0.1	0.0	1.1	1.1	1.2	0.9
Skiagite	0.0	0.6	0.2	0.1	0.2	0.0	0.0	0.1	0.2	0.1	0.8	0.7

Table 3.5: Dipslayed average core-rim concentrations of various elements presented as oxide weight percentages (wt.%), apfu values for the X(A)-, Y(B)-, Z-sites of the garnet stoichiometry, and various garnet endmembers (mol.%). The term N.D.(Not detected) is only used for SnO2 , which was not analyzed for many of the samples. In apfu calculations Sn below 0,01 and is therefore not included.

Table 3.6 Average rare earth and rare metals concentrations

	MDL	Svåheii 2 (grain 1)		Svåheii 2 (grain 5)		Svåheii 2 (grain 3)		Kleppe q (grain 1A)		Kleppe q (grain 2)		Butvatnet (grain 3)		Butvatnet (grain 1)	
		core	rim	core	rim	core	rim	core	rim	core	rim	core	rim	core	rim
n		2	2	2	2	2	2	1	1	2	4	2	2	1	2
Na	152.42	534.40	663.70	847.01	571.17	456.73	596.83	405.31	471.11	686.49	419.10	827.10	606.32	835.82	801.56
Sc	1.27	1131.99	1010.67	907.72	1011.25	1136.66	726.51	466.96	483.15	508.18	453.32	432.88	436.48	420.60	364.39
Ti	56.78	168.80	<56.78	314.53	58.67	<56.78	<56.78	79.24	70.42	394.41	<56.78	574.32	324.10	613.22	487.93
Y	1.33	8665.78	6851.67	10658.44	6995.83	7044.33	7799.29	7315.87	6933.42	14164.69	7049.02	24682.93	16442.17	25404.76	23241.74
Nb	0.03	<0.03	<0.03	0.59	<0.03	<0.03	<0.03	<0.03	<0.03	<0.03	0.92	0.15	0.14	0.13	0.08
Sn	0.68	14.09	3.00	38.37	4.06	2.62	3.65	2.82	0.68	12.33	0.76	54.28	24.54	43.40	44.36
La	0.06	<0.06	<0.06	<0.06	<0.06	<0.06	<0.06	<0.06	<0.06	<0.06	<0.06	<0.06	0.07	<0.06	<0.06
Ce	0.03	<0.03	<0.03	<0.03	<0.03	<0.03	<0.03	<0.03	<0.03	<0.03	0.12	0.05	0.23	0.05	0.05
Pr	0.02	<0.02	<0.02	<0.02	<0.02	<0.02	<0.02	<0.02	0.02	<0.02	0.04	0.07	0.11	0.08	0.07
Nd	0.14	0.21	0.28	0.28	0.23	0.17	0.28	0.38	0.35	0.57	0.65	2.33	1.89	2.65	2.14
Sm	0.11	1.91	1.85	1.81	1.69	1.74	2.30	3.38	3.16	5.25	3.33	14.01	9.89	15.71	13.31
Eu	0.06	<0.06	<0.06	<0.06	<0.06	<0.06	<0.06	<0.06	<0.06	<0.06	<0.06	<0.06	<0.06	<0.06	<0.06
Gd	0.15	22.75	21.48	20.32	18.60	19.84	29.33	42.40	35.35	77.21	35.77	106.81	74.46	119.84	106.96
Tb	0.02	18.29	16.89	16.71	15.08	15.82	22.48	29.04	24.58	53.20	24.86	67.87	46.83	74.82	67.29
Dy	0.07	367.52	328.11	355.80	297.95	313.08	435.94	482.59	447.41	927.87	448.52	1097.42	749.03	1166.65	1050.24
Ho	0.02	177.02	149.25	182.31	136.59	144.52	209.28	193.26	208.98	432.11	211.81	439.20	292.87	443.50	394.33
Er	0.06	1139.53	904.09	1334.93	833.77	901.35	1322.34	990.68	1277.91	2541.95	1305.27	2506.05	1597.92	2374.91	2072.03
Tm	0.02	319.01	240.18	447.53	224.92	242.88	348.77	223.53	333.07	630.76	346.24	686.49	409.20	606.85	523.58
Yb	0.10	3440.34	2452.48	5752.14	2294.48	2503.36	3596.30	2040.73	3464.77	6176.62	3633.98	7071.22	3983.42	5922.10	5077.52
Lu	0.04	679.50	449.42	1276.67	408.95	463.97	729.90	371.51	730.49	514.05	779.37	971.16	704.21	1031.57	885.86
Hf	0.13	0.15	<0.13	17.90	<0.13	<0.13	<0.13	0.13	<0.13	0.29	0.13	1.15	0.94	1.23	1.04
Ta	0.02	0.03	<0.02	1.02	<0.02	<0.02	<0.02	0.02	<0.02	0.05	0.08	0.71	0.75	0.85	0.52
Th	0.02	<0.02	<0.02	0.39	<0.02	<0.02	<0.02	<0.02	<0.02	<0.02	0.07	<0.02	0.89	<0.02	<0.02
ΣLREE		24.87	23.63	22.42	20.52	21.76	31.91	46.16	38.88	83.06	39.94	123.27	86.64	138.33	122.53
ΣHREE		6141.19	4540.40	9366.08	4211.73	4584.97	6665.00	4331.34	6487.21	11276.55	6750.06	12839.39	7783.47	11620.40	10070.83

Table 3.6 Continued

	MDL	Butvatnet (grain 2)		Bratterud (grain 1)		Bratterud (grain 3)		Bratterud (grain 4)		Upper Høydalen 12		Upper Høydalen 1		Heftetjern 2 (grain 1)	
		core	rim	core	core	core	rim	core	rim	core	rim	core	rim	core	rim
n		1	3	3	3	1	2	1	2	6	6	6	6	4	2
Na	152.42	727.93	653.22	334.64	603.86	343.93	399.43	854.00	663.36	310.02	316.35	516.01	431.30	569.31	392.70
Sc	1.27	407.33	292.32	130.97	77.86	121.17	183.39	105.11	94.96	15.19	14.38	1538.46	1382.42	1961.86	1806.44
Ti	56.78	571.04	446.34	132.69	408.98	97.52	237.81	526.49	418.22	151.36	155.08	271.44	227.27	548.52	217.17
Y	1.33	24935.85	21282.60	6005.72	18823.38	5573.46	7728.36	21693.57	18646.95	7994.90	6812.57	11233.55	10191.14	13119.29	7367.67
Nb	0.03	0.11	0.10	<0.03	0.24	<0.03	<0.03	3.93	0.32	0.56	0.56	0.13	0.07	0.15	<0.03
Sn	0.68	49.42	43.63	10.12	99.54	7.51	23.09	144.28	113.58	120.29	114.65	23.80	19.68	33.85	9.30
La	0.06	<0.06	<0.06	<0.06	<0.06	<0.06	<0.06	1.06	<0.06	<0.06	<0.06	<0.06	<0.06	<0.06	<0.06
Ce	0.03	0.05	0.06	<0.03	0.07	<0.03	<0.03	9.29	0.07	<0.03	0.03	<0.03	<0.03	0.05	<0.03
Pr	0.02	0.08	0.06	0.03	0.05	0.03	<0.02	0.97	0.04	0.02	0.03	0.02	0.02	0.04	0.02
Nd	0.14	2.42	2.04	0.35	1.06	0.35	0.55	4.75	0.73	0.42	0.41	0.46	0.37	0.58	0.25
Sm	0.11	14.16	15.33	2.31	5.28	2.08	3.35	6.54	4.51	1.51	1.50	1.77	1.45	2.51	1.17
Eu	0.06	<0.06	<0.06	<0.06	<0.06	<0.06	<0.06	<0.06	<0.06	<0.06	<0.06	<0.06	<0.06	<0.06	<0.06
Gd	0.15	110.07	129.62	16.37	33.54	16.08	25.74	36.60	33.31	5.69	5.48	9.55	8.42	17.20	9.17
Tb	0.02	69.87	76.46	11.46	25.83	11.56	17.27	28.36	26.54	5.88	5.74	8.96	8.01	13.61	7.56
Dy	0.07	1115.81	1106.11	174.31	493.87	171.09	265.00	554.35	510.50	132.75	128.46	205.73	183.90	271.99	157.79
Ho	0.02	432.79	380.13	53.64	211.95	47.46	86.72	243.51	221.66	57.38	54.43	103.69	91.43	128.18	76.99
Er	0.06	2361.07	1859.43	255.30	1443.03	201.70	438.39	1694.54	1525.55	474.36	443.35	874.74	744.65	977.86	589.17
Tm	0.02	613.59	437.50	61.29	477.86	45.33	109.59	576.00	516.10	222.80	207.21	367.62	298.51	371.89	216.91
Yb	0.10	6084.10	4040.22	553.17	5669.39	392.80	1013.79	6976.00	6257.36	3352.09	3122.62	5253.07	4064.79	5110.56	2875.37
Lu	0.04	1079.41	685.83	79.74	1070.23	52.69	157.42	1354.71	867.29	580.15	531.35	1100.34	810.95	1113.43	626.31
Hf	0.13	0.97	1.27	<0.13	1.12	0.13	0.25	3.66	1.24	0.83	0.76	0.52	0.46	0.38	0.09
Ta	0.02	0.54	1.55	0.10	1.51	0.03	0.18	7.47	2.01	6.56	6.11	0.70	0.37	0.55	0.09
Th	0.02	<0.02	<0.02	<0.02	0.04	<0.02	<0.02	19.99	<0.02	<0.02	<0.02	<0.02	<0.02	<0.02	<0.02
ΣLREE		126.78	147.12	19.07	39.99	18.54	29.63	59.21	38.66	7.67	7.45	11.81	10.27	20.39	10.60
ΣHREE		11756.64	8585.68	1188.91	9392.16	922.63	2088.16	11427.47	9924.98	4825.41	4493.15	7914.14	6202.25	7987.51	4550.08

Table 3.6 Continued

	MDL	Heftetjern 2 (grain 2)		Heftetjern 1 (grain 1)		Heftetjern 1 (grain 5)		Heftetjern 1 (grain 3)	
		core	rim	core	rim	core	rim	core	rim
n		2	4	2	2	2	2	1	2
Na	152.42	548.84	420.79	579.11	512.33	525.07	498.02	581.11	474.84
Sc	1.27	1895.09	1915.61	1561.06	1298.41	1498.39	1344.80	2197.19	1509.91
Ti	56.78	566.23	362.08	599.43	476.11	533.50	587.28	743.61	608.61
Y	1.33	13309.72	9058.23	11900.28	9766.15	10883.71	10616.97	13335.92	10548.73
Nb	0.03	0.13	0.07	0.11	0.09	0.17	0.11	0.16	0.07
Sn	0.68	33.88	20.49	9.39	8.82	8.94	9.74	9.81	8.85
La	0.06	<0.06	<0.06	<0.06	<0.06	0.25	<0.06	<0.06	<0.06
Ce	0.03	<0.03	<0.03	<0.03	<0.03	0.71	0.06	0.03	<0.03
Pr	0.02	0.03	0.02	0.03	0.03	0.32	0.04	0.03	0.02
Nd	0.14	0.47	0.46	0.58	0.42	1.68	0.52	0.75	0.41
Sm	0.11	2.36	1.84	2.43	1.86	2.75	2.06	3.24	2.20
Eu	0.06	<0.06	<0.06	<0.06	<0.06	<0.06	<0.06	<0.06	<0.06
Gd	0.15	16.64	12.81	16.37	13.42	17.37	15.43	21.84	16.78
Tb	0.02	13.34	9.98	12.61	10.55	13.27	12.00	16.24	12.79
Dy	0.07	271.06	199.18	249.12	205.58	258.02	238.62	316.46	249.54
Ho	0.02	131.82	91.29	118.44	94.82	120.08	111.74	145.95	114.89
Er	0.06	1028.49	654.57	885.40	681.47	850.67	819.91	1056.14	811.65
Tm	0.02	397.15	231.64	327.76	243.22	295.65	294.45	380.16	280.94
Yb	0.10	5527.36	2978.03	4450.92	3190.92	3813.25	3906.70	5081.16	3605.79
Lu	0.04	1219.37	603.24	943.84	662.00	802.62	835.94	1074.91	742.49
Hf	0.13	0.38	0.16	0.29	0.23	0.75	0.32	0.45	0.30
Ta	0.02	0.46	0.31	0.43	0.33	0.46	0.38	0.58	0.29
Th	0.02	<0.02	<0.02	<0.02	<0.02	1.81	0.15	<0.02	<0.02
ΣLREE		19.50	15.14	19.42	15.73	23.06	18.13	25.90	19.42
ΣHREE		8588.58	4767.92	6988.08	5088.55	6153.54	6219.35	8071.02	5818.07

Table 3.6: Acquired LA-ICP-MS measurments presented as average core-rim compositions for 18 selected garnet crystals. MDL = mean detection limit.

3.3.3 Intracrystalline element distribution visualized by spatial imaging

Intracrystalline distribution maps of the seven elements including Mn, Fe, Ca, Sc, Y, Yb, and Ti were determined with ion beam microanalysis. These maps are presented in Fig. 3.38-40. Three garnet crystals from the Svåheii 2, Heftetjern, and Heftetjern 2 locations were chosen because of their relatively high abundances of Sc, detected by both EPMA and LA-ICP-MS. These maps provide insight into the spatial distribution of these elements, which reflect the crystallization conditions and their changes.

Manganese and Fe appear to be homogeneously distributed across all investigated crystals (Fig. 3.38-40 A and B). Both elements are equally abundant in grain 2 from the Svåheii 2 location, which was also observed with EPMA of grain 1 from this location. In grain 6 from Heftetjern Mn is slightly more abundant (30 counts higher) than Fe, while Mn is slightly less abundant (10 counts less) than Fe in grain 3 from Heftetjern 2. Calcium in all grains is generally more abundant at the grain margin than in the core (Fig. 3.38-40 C). The core of grain 2 from Svåheii 2 exhibits low contents of Ca (2000 counts), which abruptly increases outwards towards the grain margin (6000 counts). Grain 6 from Heftetjern shows patchy zones of both high and low abundances throughout the crystal, with high contents at the outmost grain margin. In grain 3 from Heftetjern 2 Ca is less abundant (2000 counts) in the grain core compared to the margin (4000 counts).

The distribution of Sc within the three analyzed grains exhibit different trends. In the grain from Svåheii the content of Sc is relatively high in the core (1200 counts), which slightly decreases towards the rim (averaging 800 counts) (Fig. 3.38D). Scandium is generally homogeneously distributed in grain 6 from Heftetjern (averaging 2000 counts), with the exceptions of patches of lower abundances near the grain margin (500 counts) (Fig. 3.39 D). Both the core and rim of grain 3 from Heftetjern 2 exhibit equally high abundances (2000 counts) of Sc, but Sc is a less abundant the intermediate zone (500 counts) (Fig. 3.40 D).

Other elements, which include Y, Yb, and Ti, show similarities in respect to element distribution patterns in all analyzed garnet crystals. These three elements are less abundant in the inner core of grain 2 from Svåheii 2 (Fig. 3.38 E-G). Concentrations of these elements increase abruptly in the outer core. Yttrium is enriched in a narrow zone around the core compared to the rest of the crystal. Ytterbium, on the other hand, is abundant in the intermediate zone, which is overgrown by an outer zone richer in this element. (Fig. 3.38 F). Titanium shows a weak concentric enrichment at the core, which is also enriched in an open crack crosscutting the crystal. Both Y and Yb distribution in grain 6 from the Heftetjern 1 location is patchy with a slightly higher abundance in the crystal ores (Fig. 3.39 E-F). Titanium shows a similar pattern (Fig. 3.39 G). In grain 3 from the Heftetjern 2 location, the distribution patterns of Y, Yb, and Ti are similar (Fig. 3.40 E-G). All these elements are enriched in the core, which exhibits an irregular, non-concentric shape. Both Y and Y concentrations abruptly decrease outwards the crystal margin. Titanium being slightly enriched in the core becomes less and less abundant towards the rim.

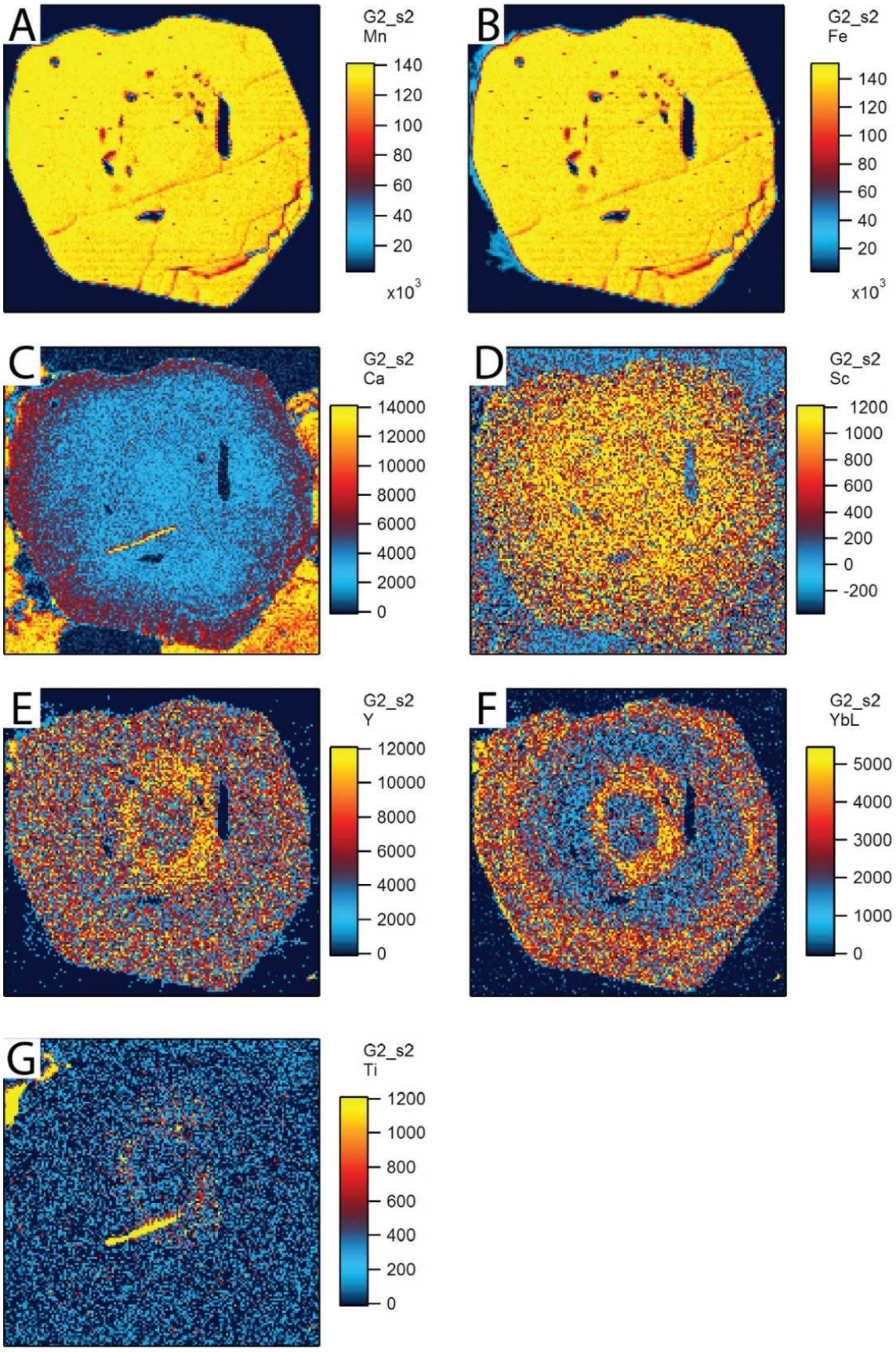

Figure 3.38: Ion beam microanalysis mapping of Svåheii 2 (05061609), grain 2. A - Distribution (Mn), B – (Fe), C – (Ca), D – (Sc), E – (Y), F – (Yb), G –(Ti). Stripes seen in images A and B are instrument artifacts.

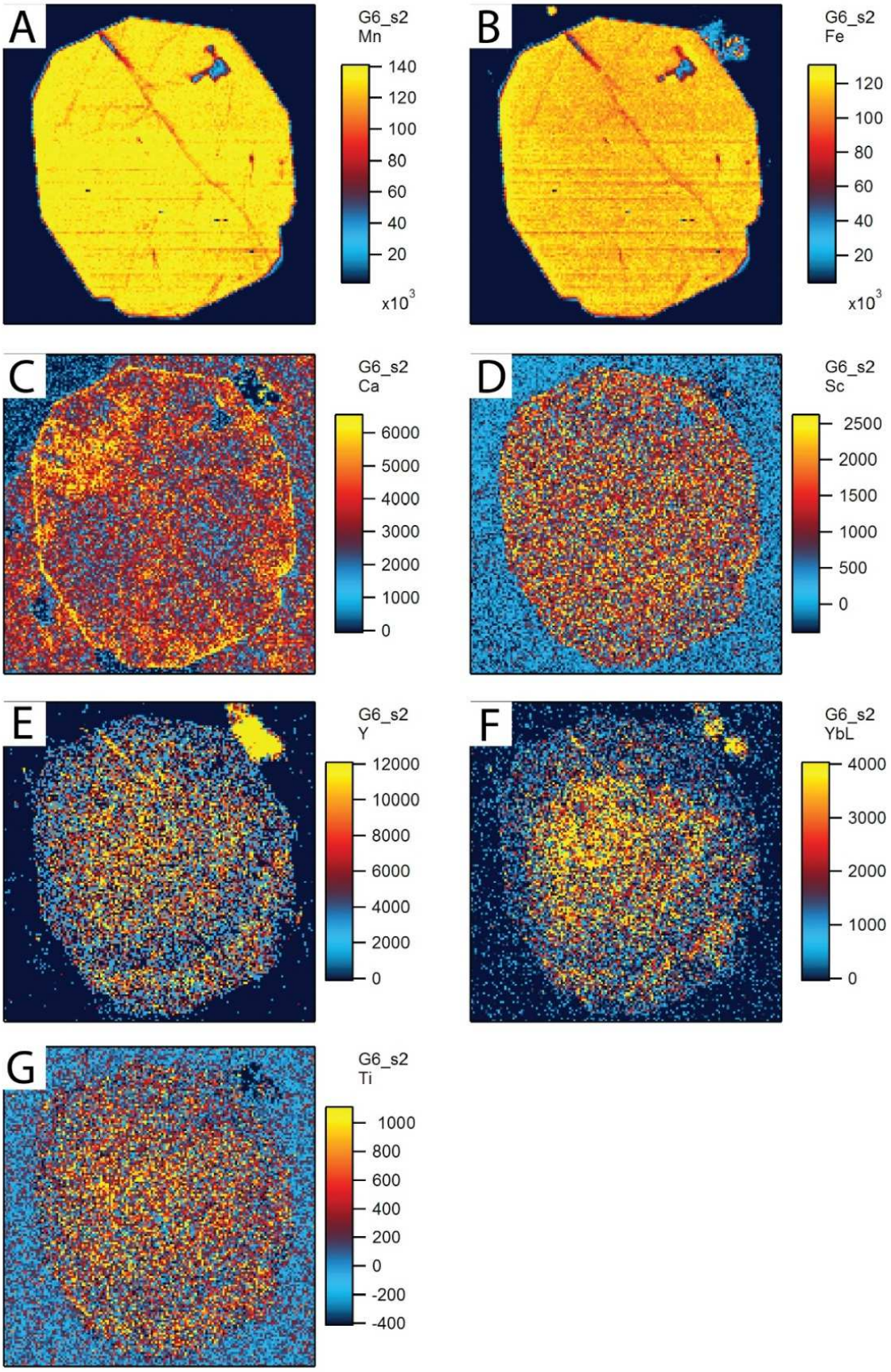

Figure 3.39: Ion beam microanalysis mapping of Heftetjern 1 (20091508), grain 6. A - Distribution (Mn), B – (Fe), C – (Ca), D – (Sc), E – (Y), F – (Yb), G – (Ti). Stripes seen in images A and B are instrument artifacts.

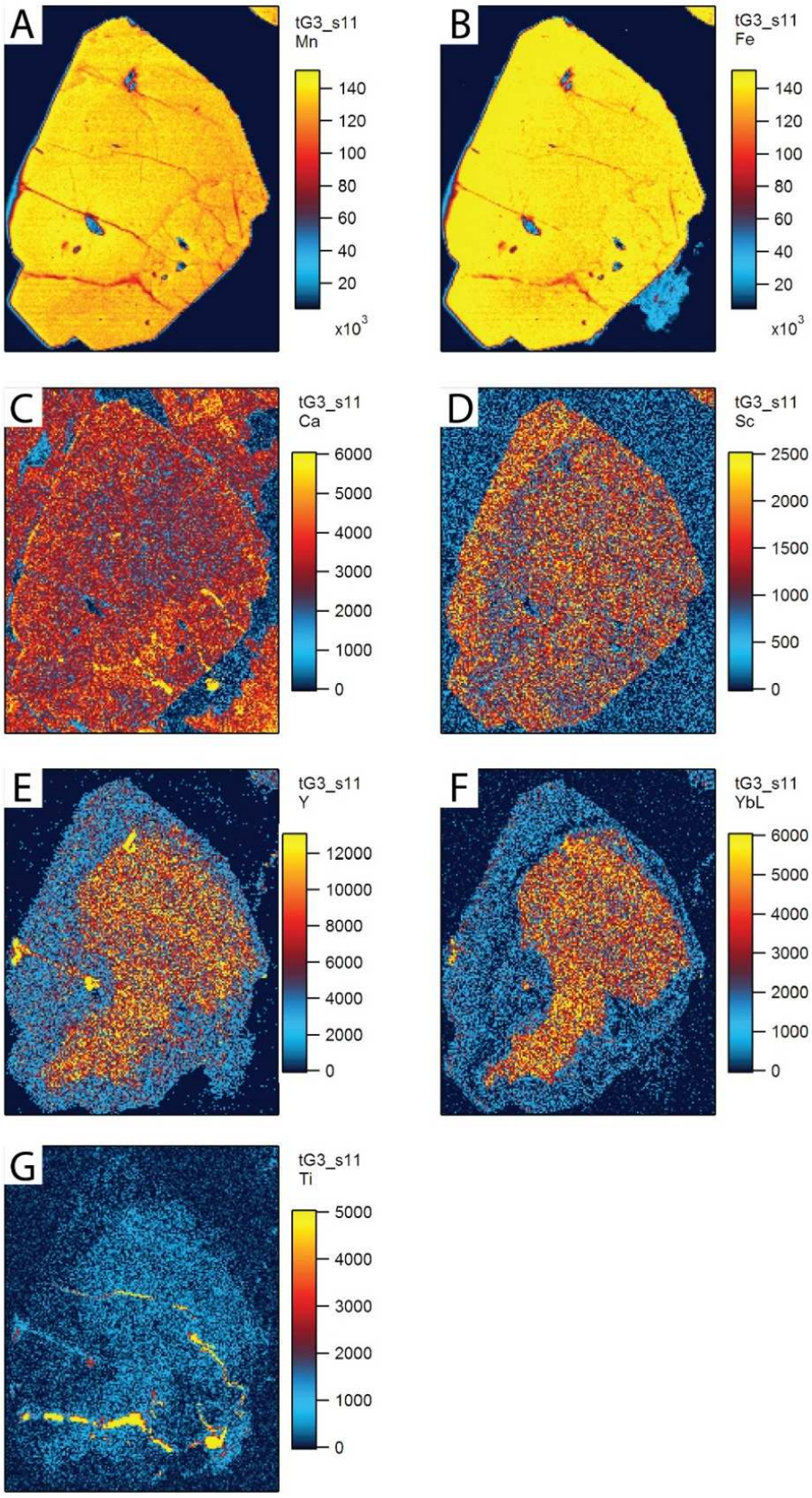

Figure 3.40: Ion beam microanalysis mapping of Heftetjern 2 (08061601), grain 3. A - Distribution (Mn), B – (Fe), C – (Ca), D – (Sc), E – (Y), F – (Yb), G – (Ti). Stripes seen in images A and B are instrument artifacts.

3.4 Petrography and chemistry of pegmatite host rocks

3.4.1 Optical microscopy

Thin sections of three different types of host rock, comprising amphibolites from the Kleppe quarry and Mjeltedalen locations and a granite from the Tørdal pluton, which were studied with the optical microscopy. Mineral identification criteria by (Nesse, 2013) were applied. Studied features of these rocks include mineral assemblage, crystal habit, size ranges, fabrics/texture and grain alteration.

Kleppe quarry and Mjeltedalen amphibolites:

The major mineral assemblage of the Kleppe quarry sample constituted amphibole (40 vol.%) and plagioclase (20 vol.%), with minor biotite (20 vol.%), quartz (15 vol.%) and opaque minerals (5 vol.%). In general, the amphiboles had a euhedral-anhedral habit, with sizes ranging from 0.1 to 0.7 mm in length. Euhedral crystals exhibited a typical diamond-shaped cross-section with perfect cleavages of approximately 60° and 120° or bladed and/or columnar longitudinal sections when cut parallel to the c-axis. Some of the larger amphibole crystals were poikiloblastic with inclusions of quartz and opaque minerals (Fig. 3.41 C-D). In addition, anhedral masses occurred (Fig. 3.41 A-B). Plagioclase exhibited the characteristic polysynthetic twinning, with a tabular subhedral-anhedral habit. The sizes of these crystals ranged from 0.1 mm to 1.0 mm. The biotite crystals appeared both as platy euhedral-subhedral shapes, and occasionally as anhedral masses. The sizes ranged from 0.1 to 0.7 mm. Both quartz (0.01 – 0.1 mm sizes) and the opaques (sizes of 0.01 – 0.6 mm) were interstitially situated in both samples. In addition, the opaque minerals were seen to be intergrown with both amphibole and biotite crystals. The Kleppe quarry amphibolite appeared weakly foliated due to the alignment of amphiboles and biotites.

The major minerals in the Mjeltedalen amphibolite were amphibole (50 vol.%) and quartz (20 vol.%), with minor plagioclase (10 vol.%), biotite (10 vol.%), and opaque minerals (10 vol.%). Sizes and habits of the minerals were more or less similar to that of the minerals of the Kleppe quarry sample; although amphibole crystals were commonly larger (the larger crystals are in the range of 1.3 to 2.2 mm). The Mjeltedalen amphibolite showed a more distinct foliation then the Kleppe quarry sample. Some of the larger amphibole crystals were poikiloblastic with inclusions of quartz and opaque minerals (Fig. 3.41 C-D). The opaque minerals were intergrown with both amphibole and biotite crystals. Some of the plagioclase crystals had been partly altered to sericite (Fig. 3.41 E-F).

Tørdal granite (Granite outcrop near Kleppe quarry)

Major minerals in the thin section of the Tørdal granite were quartz (35 vol.%), microcline (30 vol.%), and plagioclase (20 vol.%), while minor minerals are biotite (8 vol.%), opaque minerals (5 vol.%), and xenotime (2 vol.%) (Fig. 3.42 A-B). The minerals exhibited a phaneritic texture. The plagioclase crystals were euhedral-subhedral tabular shaped, with the characteristic polysynthetic twinning. Grain sizes ranged from 0.3 to 3.0 mm. In some of the plagioclase antiperthitic lamellae were observed (Fig. 3.42 C-D). Some larger plagioclase

crystals were poikiloblastic with inclusions of biotite, microcline, and quartz. Microcline formed euhedral crystals typically 0.4-2.7 mm in size and exhibited the characteristic “tartan” twinning. The microcline crystals occasionally appeared as perthite (Fig. 3.42 E-F), with exsolution lamellae of albite. Myrmekites occurred commonly at microcline-plagioclase contacts (Fig. 3.42 G-H). Some of the larger microclines were poikiloblastic with inclusions of plagioclase and quartz. Quartz occurred in larger anhedral masses (average size of 1.5 mm) or as small equal-sized crystals (average size of 0.2 mm). Both large and small crystals exhibited undulose extinction. Sericite formed as an alteration product of both microcline and plagioclase. The biotite crystals were platy euhedral-subhedral shaped, and typically 0.2 to 0.7 mm in size with strong pleochroism (green/pale yellow). The opaque minerals (0.05 – 0.6 mm) showed anhedral amoeboid or euhedral cubic shapes. The xenotime crystals were colorless or pale brown, showed weak pleochroism (colorless-pale brown), had a high positive relief, and high birefringence. Color zoning was seen in some crystals, where the core was darker than the rim. These crystals showed subhedral tetragonal elongate prisms, with sizes ranging from 0.1 to 0.4 mm. Some of the xenotime crystals were slightly altered, and overgrown and/or intergrown with opaque minerals.

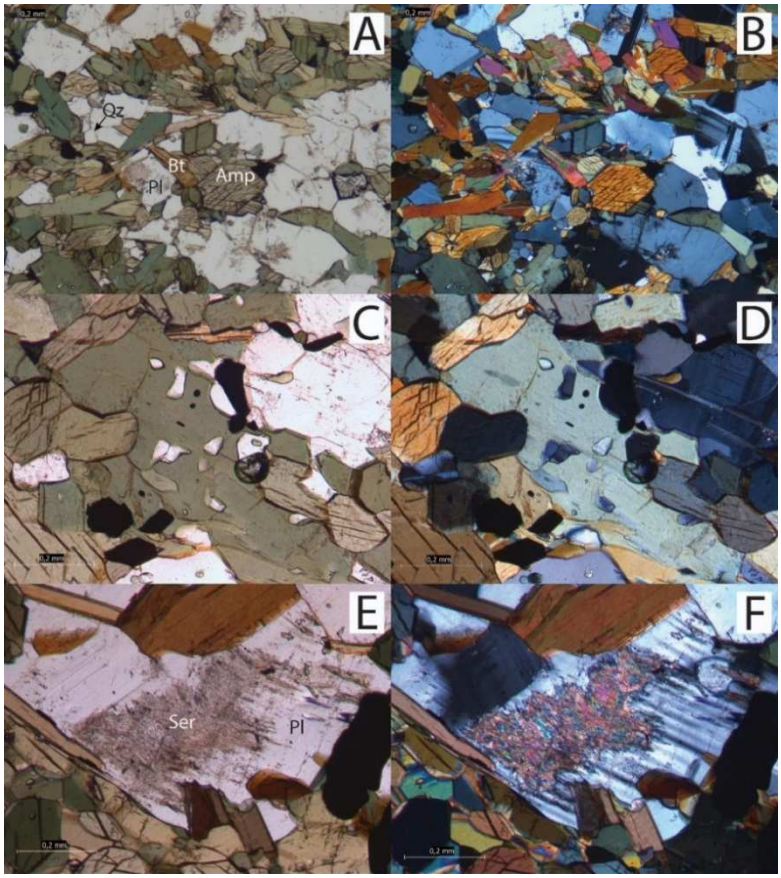

Figure 3.41: Images on the left side are in PPL with comparative images in XPL on the right. A-B – Representative images of the main mineral assemblage present in the Kleppe quarry and Mjeltedalen amphibolites. Amp = Amphibole, Bt = Biotite, Pl = Plagioclase, Qz = Quartz. C-D – Image displaying the instances of poikiloblastic amphibole crystals containing quartz and opaques. E-F – Partly altered plagioclase containing sericite.

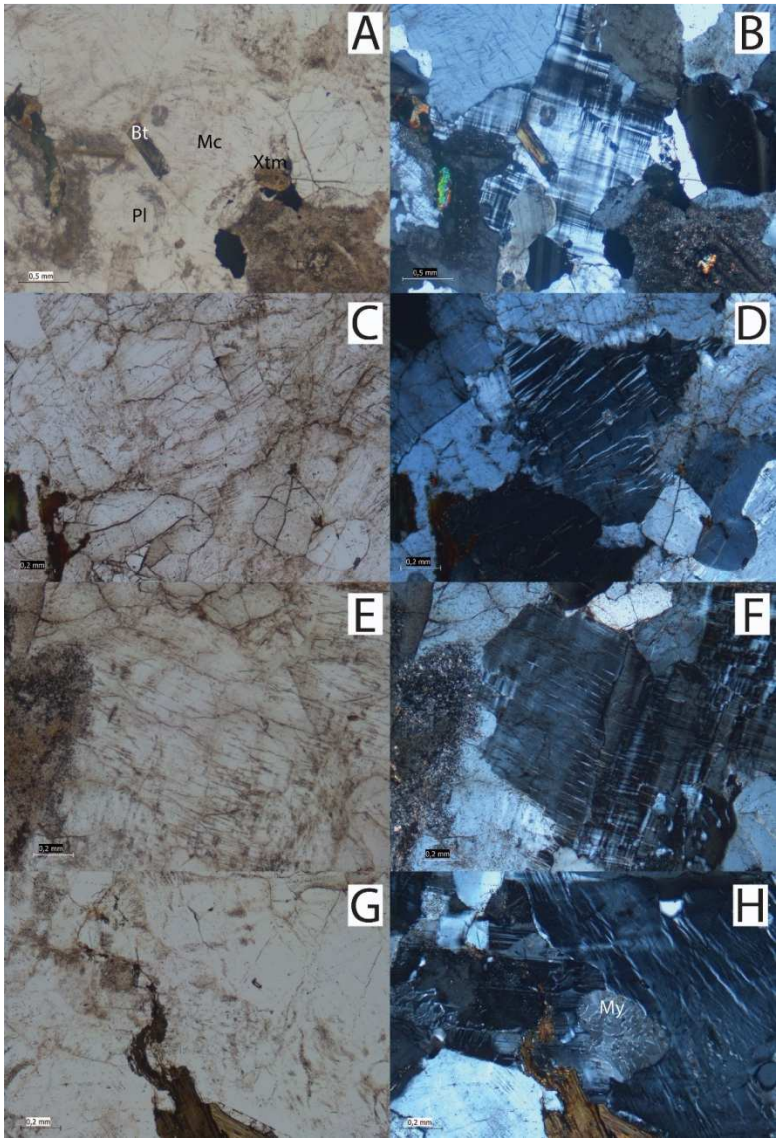

Figure 3.42: All Images are displayed in PPL on the left with corresponding XPL images on the right. A-B – Representable image of the main mineral assemblage in the granite. Pl = Plagioclase, Qz = Quartz, Mc = Microcline, Xtm = Xenotime. C-D – Antiperthitic plagioclase with exsolution lamellae of K-feldspar. E-F – Pertitic microcline exhibiting exsolution blebs of albite. G-H – Myrkmekite intergrowth typically situated at the contact between plagioclase and microcline.

3.4.2 Whole rock chemistry

Table 3.7 displays bulk rock chemistries of the three host rock samples acquired by solution ICP-MS at ACME Laboratories in Vancouver, Canada. In identifying potential sources of the amphibolitic host rocks, two plots were constructed, assuming that these rocks were mafic magmatic rocks prior to amphibolite facies metamorphism. The first plot, a Ti-V-plot, according to (Shervais, 1982) displays slight compositional differences for the two amphibolites. Even their compositions are relatively similar, the Mjeltedalen amphibolite (Ti/V-ratio = 20-50) plots in the MORB field and the other Kleppe quarry sample in the Alkalic field (Ti/V-ratio = 50-100) (Fig. 3.43 A). In the Th-Hf-Ta ternary diagram by (Wood, 1980) the two amphibolites are plotted in the same domain of primitive arc tholeiites (Fig. 3.43 B).

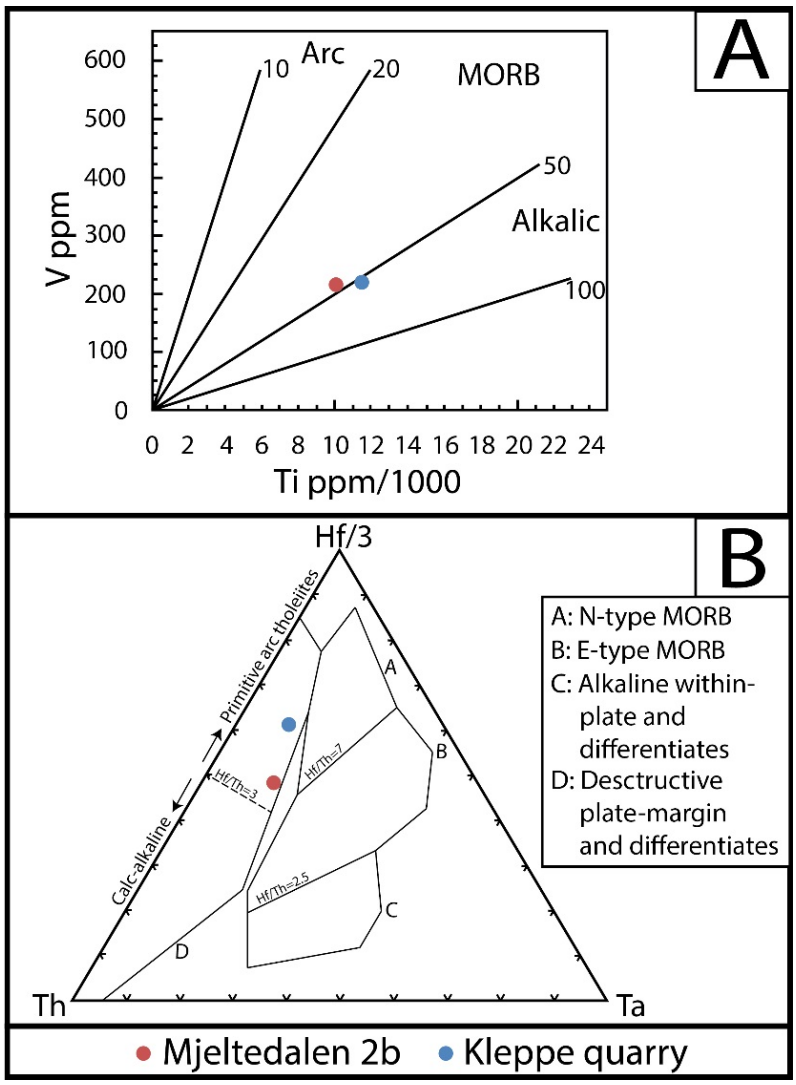

Figure 3.43: (A): Modified Ti-V-plot from (Shervais, 1982) *displaying acquired LA-ICP-MS data of titanium and vanadium ppm concentrations. (B): Modified Th-Hf-Ta ternary plot from* (Wood, 1980) *displaying relationship percentages of acquired LA-ICP-MS data of thorium, hafnium and tantalum ppm concentrations.*

The Tørdal granite is a felsic granite (SiO_2 > 74 wt. %) (Whalen et al., 1987) and plots as being peraluminous (see Fig. 3.44 A: Al_2O_3 / ($CaO+Na_2O+K_2O$) > 1.0, Al_2O_3 / Na_2O+K_2O > 1.0). The granite is identified as an A-type (Whalen et al., 1987) (Fig. 3.44 B), and Post-COLG (Post-collision granite) (Fig. 3.44 C) (Pearce et al., 1984). The abundance of Sc is significantly higher in both amphibolites (Kleppe quarry: 30 ppm, and Mjeltedalen: 29 ppm) in comparison with the Tørdal granite sample (2 ppm). Fluorine contents in the amphibolites are generally higher than in the Tørdal granite (0.16-0.08 and 0.01 wt.%, respectively). Concentrations of the HREEs show low levels for all host rock samples, while the LREEs are relatively more abundant in the Kleppe quarry amphibolite (maximum 106 ppm).

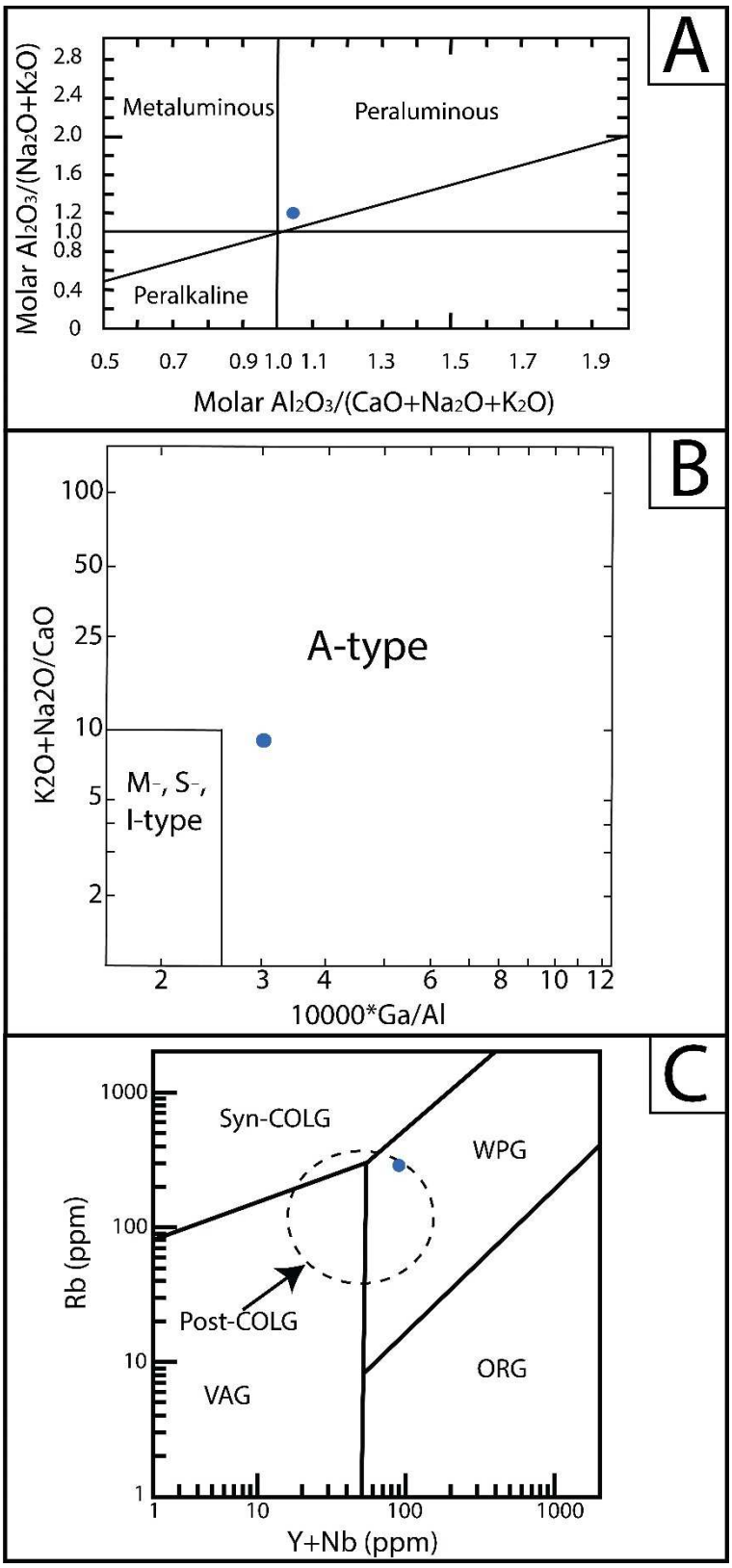

*Figure 3.44: A-C: Three modified plots of A/CNK versus A/NK from (Maniar and Piccoli, 1989), 10000*Ga/Al versus (K_2O+Na_2O)/CaO from (Whalen et al., 1987), and Rb versus Y+Nb (Pearce et al., 1984). All plots are displaying and discriminating the acquired LA-ICP-MS data of the analyzed Tørdal granite sample.*

Table 3.7 Whole rock chemistry of host rocks

Sample	MDL	GAS04071705	GAS06071716	GAS04071707
Rock type		Amphibolite	Amphibolite	Granite
Location		Kleppe quarry	Mjeltedalen	Kleppe
Wt.% oxides				
SiO_2	0.01	49.07	47.82	74.57
Al_2O_3	0.01	15.45	15.76	13.73
Fe_2O_3	0.04	12.16	12.09	1.42
MgO	0.01	6.71	8.05	0.14
CaO	0.01	9.20	9.03	0.96
Na_2O	0.01	3.13	2.94	3.67
K_2O	0.01	0.96	1.12	4.96
TiO_2	0.01	1.92	1.67	0.10
P_2O_5	0.01	0.40	0.27	0.01
MnO	0.01	0.19	0.18	0.03
Cr_2O_3	0.002	0.03	0.03	<0.002
Total		99.22	98.96	99.59
Trace elements, ppm				
Ba	1.00	188.00	174.00	207.00
Ni	0.10	37.00	0.80	60.00
Sc	1.00	30.00	29.00	2.00
Be	1.00	6.00	3.00	4.00
Co	0.20	40.10	46.40	1.00
Cs	0.10	10.80	11.30	1.30
Ga	0.50	19.30	19.40	22.00
Hf	0.10	5.60	4.20	4.00
Nb	0.10	6.00	6.20	25.80
Rb	0.10	135.20	86.00	291.00
Sn	1.00	4.00	2.00	<1.00
Sr	0.50	232.80	224.20	62.40
Ta	0.10	0.30	0.40	1.90
Th	0.20	0.90	1.10	27.70
U	0.10	0.70	2.20	15.20
V	8.00	217.00	214.00	13.00
Zr	0.10	234.90	160.90	91.60
Mo	0.10	5.70	0.20	0.30
Cu	0.10	45.70	2.70	35.80
Pb	0.10	2.30	18.30	1.40
Zn	1.00	50.00	43.00	37.00
Ti	0.10	0.90	0.20	0.70
Y	0.10	41.00	33.60	64.40
La	0.10	17.20	8.40	18.50
Ce	0.10	44.00	22.80	42.20
Pr	0.02	6.32	3.75	4.92
Nd	0.30	29.80	18.2	18.80
Sm	0.05	7.40	4.93	4.77
Eu	0.02	2.13	1.63	0.49
Gd	0.05	7.97	5.87	5.41
Tb	0.01	1.30	0.99	1.20
Dy	0.05	7.91	6.37	9.06
Ho	0.02	1.64	1.29	2.25
Er	0.03	4.61	3.85	7.75
Tm	0.01	0.64	0.54	1.25
Yb	0.05	4.03	3.43	8.60
Lu	0.01	0.63	0.57	1.35
∑LREE		106.58	59.71	89.68
∑HREE		28.73	22.91	36.87
Trace elements, wt.%				
Li	0.001	0.004	0.005	<0.001
S	0.01	0.07	0.09	<0.01
F	0.01	0.16	0.08	0.01

Table 3.7: Displayed whole rock chemistry of the host rocks. Elements excluded from the list are As, Cd, Sb, Bi, Ag, Au, Hg, Se, and W (below detection limits).MDL = mean detection limit.

4. Discussion

4.1 Regional distribution of scandium

The Tørdal area is geochemically distinct in comparison with other Sveconorwegian pegmatite fields of Southern Norway, because of the enrichment of Sn, Sc, Y, Be, and Li (Bergstøl and Juve, 1988). The Tørdal pegmatites belong generally to the petrogenetic family of NYF pegmatites. Some of these pegmatites, however, show in addition to the mineralogy and zoning typical for NYF pegmatites, "cleavelandite" replacements zones with LCT signature (e.g. Kristiansen, 1998). These pegmatites are classified as chemically evolved NYF pegmatites.

Average Sc concentrations (determined by EPMA and LA-ICP-MS) of garnets from all investigated locations are shown in the regional map of Tørdal (Fig. 3.35). Concentrations of 987 to 1895 ppm Sc are classified as high, 392 to 987 ppm as medium, and 14 to 392 ppm as low. In the studied area, Sc is concentrated in the Heftetjern-Høydalen area exhibited in the Sc content of garnets from the wall zones of the pegmatites (Sc ppm bulk averages of 1568 for the Heftetjern 1, 1895 for Heftetjern 2, and 1460 for Upper Høydalen 1 samples). Two of these pegmatites, the Upper and Lower Høydalen pegmatites, contain "cleavelandite" replacement zones and are the most evolved pegmatites of the Tørdal area. Garnets from the wall zone of the Upper Høydalen and Heftetjern pegmatites exhibit the highest Sc content (max. 2197 ppm for the Heftetjern locations, and max. 1538 ppm for Upper Høydalen location). The high Sc content of the Heftetjern pegmatite locations is especially reflected in the high abundance and diversity of Sc minerals, which include bazzite, cascandite, heftetjernite, kristiansenite, oftedalite, scandiobabingtonite, and thortveitite (Kristiansen, 2009). Notably, those minerals are a large proportion of the 15 known terrestrial Sc-minerals (Table 1.3). On the other hand, highly fractionated spessartines from the "cleavelandite" replacement zones of the Upper Høydalen and Lower Høydalen pegmatites exhibit very low levels of Sc (bulk averages of 15 and 52 ppm Sc, respectively). Northeastwards from the Heftetjern-Høydalen area, the average Sc content in garnet drops drastically to low Sc contents at the Bratterud and Sjauset (119 and 72 ppm, respectively) locations. In the opposite direction, southwestwards from Heftetjern-Høydalen area, Sc decreases to both medium and low Sc concentrations. Garnets with medium abundant Sc contents comprise the Svåheii 2, Butvatnet, Kleppe quarry, Lislegrønlia, and Storemyr 2 locations (bulk averages of 987, 392, 478, 646, and 529 ppm, respectively.), while the other Sc-poor garnets originate from the Storemyr 1, Storemyr 3, Mjeltedalen, Grønliheii, and Svåheii 3 locations (bulk averages of 338, 235, 295, 60, and 36 Sc ppm, respectively). Interestingly, garnets of the Svåheii 2 pegmatite in the outmost southwestern corner of the study area form a positive Sc anomaly surrounded by pegmatites with low Sc garnets. As observed through EDS analysis, only wall zone garnets from the Sc abundant areas in the NE (Upper Høydalen location) and SW areas (Svåheii 2 location) contain Sc-rich micro inclusions (thortveitite, as seen in Fig. 3.18 A-B).

Figure 3.34 A illustrates that Sc in most of the wall zone garnets increases with an increasing spessartine component (from 30 – 60 mol.%), which clearly reflects the general spatial increase of Sc in the garnets towards the NE-direction. However, the wall zone garnets from the most southwestern (Svåheii 2: ~47 mol.% spess) and northeastern locations (Bratterud: ~54 mol.% and Sjauset: ~76 mol.% spess), have very low Sc and do not follow the general NE trend. In addition, both "cleavelandite"-zone hosted garnets from the Høydalen pegmatites, exhibit the highest spessartine components (~81-93 mol.%), but virtually no Sc. In summary, Sc is generally correlated with an increasing spessartine component up to 60 mol.% and increases spatially towards the northeast. However, this general spatial distribution of Sc does not apply for the pegmatites in the most southwestern (intermediate spessartine components with high Sc) and northeastern corners in the area of this study (high spessartine components with low Sc). Notably, Sc also abruptly drops through internal melt fractionation, which is seen for the garnets related to the "cleavelandite" replacement zones of the most evolved NYF pegmatites from Høydalen.

Both Ca and Mg correlate with Sc in many of the investigated garnets (Fig. 3.34 B-C). The positive Sc-Ca correlation is observed to a Ca content up to 0.06 Ca *apfu*. Subsequently, at concentrations >0.06 Ca *apfu* the Sc-Ca correlation is negative. Interestingly, the garnets showing the negative Sc-Ca correlation (Svåheii 2, Kleppe quarry, Storemyr 3, Mjeltedalen 2a, and partly Storemyr 2) have a higher andradite component (up to 3.4 mol.%) than garnets comprising the positive Sc-Ca correlation. This indicates that an increased andradite component results in a decreased Sc content for these garnets. This is surprising as eringaite is the Sc analogue of andradite and the only known Sc-garnet (Galuskina *et al.*, 2010), thus implying the substitution of Sc for Fe in the B-site. Figure 3.34 C shows a weak negative Sc-Mg correlation from Sc-rich predominant spessartines (garnets from the Heftetjern-Høydalen area) to "pyrope-rich" garnets (up to 5.5 mol.%), which exhibit generally low Sc contents. Norman and Haskin (1968) suggested that Ca might be more favored by substitution together with Sc than e.g. Mg, which may explain the mentioned positive Sc-Ca correlation. However, this does not apply to the negative >0.06 Ca *apfu* Sc-Ca correlation. Despite the latter observations, the same author also confirmed that there is no direct link between Sc^{3+} and other ions, such as Ca and Mg, in igneous rocks in general. This makes it rather uncertain if any of mentioned garnet endmembers has a significant impact on the general Sc content in garnets.

4.2 Mineral-scale distribution of scandium

As mentioned by e.g. Shannon (1976) and Raade et al. (2002) Sc, Y, and REEs often occur together in various minerals (e.g. thortveitite). This is because they share chemical similarities, despite their differences in the ionic radii (0.745 Å for Sc^{3+} in 6-coordination compared to with 0.900 Å and 0.868 Å for Y^{3+} and Yb^{3+}, respectively) (Shannon, 1976; Raade et al., 2002). In spessartines, trivalent Y and Al can replace Mn and Si because of their akin radii (Reaction 1) (Jaffe, 1951). Similarly to Y^{3+}, the incorporation of Sc^{3+} in the B-site of spessartines occurs through two possible reactions, in which Sc either replaces Al and trivalent Fe (Reaction 2) or divalent Fe and Mn (Reaction 3) (Raade et al., 2002).

Reaction 1: $2(Y^{3+},Al^{3+}) \leftrightarrow Mn^{2+} + Si^{4+}$

Reaction 2: $Sc^{3+} \leftrightarrow (Al^{3+}, Fe^{3+})$

Reaction 3: $2Sc^{3+} \leftrightarrow 3(Fe^{2+}, Mn^{2+})$

Scandium-rich garnets, from the Heftetjern 1, Heftetjern 2, Upper Høydalen 1, and Svåheii 2 pegmatites all share a predominate spessartine with subordinate almandine component. Some of the mentioned garnets, exhibiting general high Mn/(Mn+Fe) ratios, exhibit a decrease of the Mn/(Mn+Fe) *apfu* values from the core to the rim of the crystals (e.g. Figure 3.36 AC-AD). This characteristic of Mn- and Fe^{2+}-rich garnets has been reported also from aplites and pegmatites of other regions (e.g. Baldwin and Van Knorring, 1983; Samadi et al., 2014). Similar to the MnO/(MnO+FeO) ratio, all Sc-rich garnets, found in the wall zone of the investigated pegmatites, show a general decrease of the Sc concentrations from the core to the rim (up to 688 ppm). Growth zoning visualized through BSE imaging classify these Sc-rich garnets into different textural groups, which comprise the groups A, F, and G defined in chapter 3.2.2: (1) group A – garnets with contrast-rich step zoning (40-290 µm wide) with sub-ordinate fine-scale oscillatory zoning (<20 µm µm wide) (Svåheii 2), (2) group F – garnets with bright but contrast-poor crystal cores (step zone 1) overgrown by a relative thin (up to 200 µm), darker margin (step zone 2) (Heftetjern 1 and Heftetjern 2), and (3) group G – garnets without zoning (Upper Høydalen 1). However, also some Sc-poor garnets share the same zoning patterns as the Sc-rich garnets, which comprise the Lislegrønlia and Svåheii 3 (group A), and Butvatnet (group F) garnets. No consistent core-rim variations for Sc are seen for the Lislegrønlia garnets, while the Svåheii 3 garnet show no variation at all. Yet, the garnets of the Butvatnet location exhibit a general decrease of Sc from the core to the rim. The Sc-rich garnets from Svåheii 2, Heftetjern 1, and Heftetjern 2 exhibit a bright core in the BSE-imaging. Core-rim compositions of Sc for these garnets (from group A and F) generally decrease from the core to the rim. Based on these observations, the textural groups A and F and their core-rim compositions indicate that the garnet forming melts must have been relatively Mn-, Y-, and HREE-rich during the early stages of crystallization. During these early stages, significant substitutions of Mn, Fe, Al, and Si by Sc, Y, and HREE must have taken place (according to reactions 1 - 3). This process is especially well illustrated in the group F garnets. These garnets generally exhibit two highly contrasting step zones: the bright inner and the darker outer step zones. This may imply two different scenarios during crystallization: **1)** either sudden changes in temperature, pressure and/or composition of the garnet forming melt occurred, or **2)** the Sc, Y, and HREE content was buffered/triggered by the crystallization/stop of other simultaneously crystallizing Sc-, Y- and HREE-bearing minerals. Based on observations from BSE-imaging and core-rim chemistry, many of the garnets (especially those that are Sc-rich) may follow Y and HREEs fluctuations during crystallization. However, IBMA-images (see Chapter 3.3.3), indicate that the Sc-rich garnets do not exhibit any consistent intracrystalline distribution of Sc. These images show no particular correlation between Y and HREE (Yb) and Sc, as occasionally seen when comparing BSE-images and core-rim chemistry. Yet, according to this method, Sc is enriched in the garnet cores, and may decrease in some of the crystals towards the margins. In addition,

a clear negative Sc-Ca correlation can be seen in the IBMA-analyzed grains: Sc generally is abundant in the core, while Ca is depleted in the core and enriched at the margin of the garnet crystals.

Both growth zoning and core-rim chemistry of the Sc-poor garnets of the groups B-E (generally predominantly wall zone almandines) are significantly different and variable, than those that of Sc-rich garnets. Both group B (Mjeltedalen and Storemyr 3 locations) and especially group C (Bratterud, Sjauset, Grønliheii, and Kleppe quarry locations) garnets show evidence of significant crystal resorption/dissolution events, which partially dissolved the relative older growth zones. These events, visualized as generally dark truncating resorption surfaces, can be consequences of abrupt changes in temperature, pressure, and/or chemistry of the pegmatite-forming melt. These disturbances may be responsible for the variable intracrystalline distribution of Sc in those Sc-poor garnets. The other Sc-poor garnets of group D (Storemyr 1 location) and group E (Storemyr 2 location) both evidently exhibit that Sc does not follow Y and HREEs fluctuations. As seen for the Storemyr 1 garnets, with decreasing brightness from the core to the rim, Sc actually increases from the core to the rim (in BSE-images). On the other hand, the Storemyr 2 garnets show the opposite trend, in which the brightness increases from the core to the rim, while Sc decreases in the same direction. Lastly, the Sc-poor "cleavelandite" zone garnets (group G: Upper Høydalen 12 and Lower Høydalen) exhibit generally low and stable intracrystalline Sc contents, which are to be expected since they presumably crystallized in the highly fractionated and Sc-poor "cleavelandite"-zone forming pegmatitic melts. These melts are interpreted as alkaline melt proportions, which was separated by melt-melt immiscibility from the major pegmatite melt during pegmatite solidification (Müller et al., 2018). Nevertheless, the intracrystalline Sc-distribution in most Tørdal garnets does not show any consistency, nor any clear correlation with the intracrystalline Y and HREE distribution. Yet, in the Sc-rich wall zone garnets (Heftetjern-Høydalen area and Svåheii 2 location) Sc is abundant in the core and decreases towards the rim.

4.3 Potential sources of the scandium enrichment

Three processes are suggested to be responsible for the Sc enrichment in the Tørdal pegmatites: **(1)** the enrichment is a consequence of continuous pegmatite melt fractionation (Černý, 1991b), **(2)** the enrichment is due to low-degree partial melting (anatexis) of the relative Sc-rich amphibolitic host rocks (Müller et al., 2017), and **(3)** the Sc is leached by the pegmatite melts when moving through the amphibolitic host rocks; a hypothesis suggested by Bergstøl and Juve (1988). Anyway, there is the general consensus (e.g. Bergstøl and Juve, 1988; Raade and Kristiansen, 2000; Kristiansen, 2009), that the main source of Sc of the Tørdal pegmatites is the mafic supracrustal rocks of the Nissedal outlier (amphibolitic host rocks of the Tørdal pegmatites). According to Bergstøl and Juve (1988), the enrichment of Sc happened while the pegmatite melts penetrated these relatively Sc-rich rocks (third process) (Fig. 4.46). Similar observations were made during fieldwork; numerous pegmatite bodies and smaller pegmatitic veins intruded the amphibolitic host rocks. Additionally, this

hypothesis was during the fieldwork verified by the presence of amphibolite xenoliths within the Tørdal granite.

According to Černý (1991b), pegmatites are in general genetically related to a relatively larger granite intrusion (pluton). Considering this model, pegmatites surrounding the pluton, evolve chemically with increasing distance away from the granite source. This is reflected in the regional chemical/mineralogical zoning of the pegmatite field (Figure 4.45). Assuming that the Sc content in garnets increases with increasing fractionation degree of the pegmatite melt (at least up to a spessartine component up to 0.6 MnO/(MnO+FeO)), then the most Sc-rich garnets should occur in the most distant pegmatites, while pegmatites with Sc-poor garnets should be closest to the Tørdal granite. That is true for both the Sc-poor and medium in the southwest area, and the Sc-rich garnets from the Heftetjern-Upper Høydalen area, which occur close and far away from the pluton (Tørdal granite), respectively. However as mentioned above, garnets from pegmatites in the most southwestern (close to the pluton: Svåheii 2 location) and northeastern corners of the study area (far away from the pluton: Bratterud and Sjauset locations) do not apply to this model of fractionation.

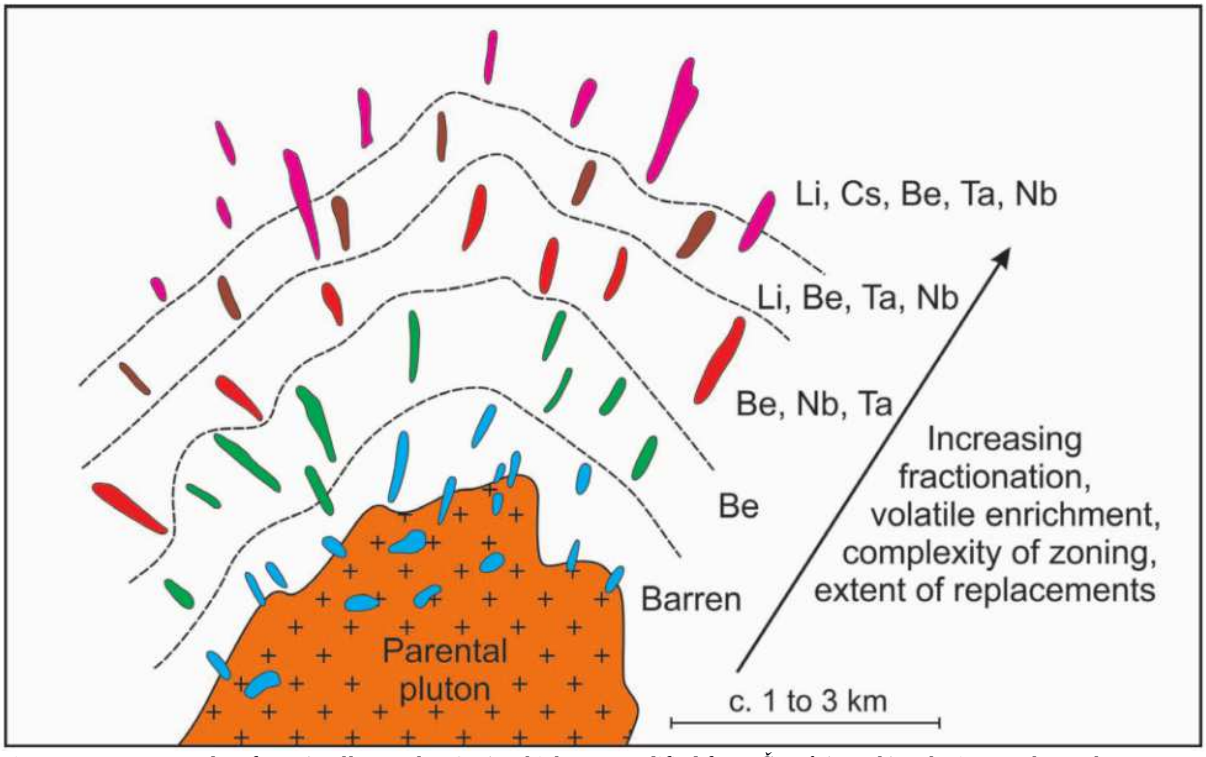

Figure 4.45: Image taken from (Müller et al., 2017), which was modified from Černý (1991b). The image shows the evolution of the geochemistry of an idealized fractionation trend from pluton source, barren and to evolved/complex pegmatites.

The regional distribution of Sc in the investigated Tørdal garnet-bearing pegmatites does generally apply to Černý's (1991b) model (systematic chemical zoning in pegmatite fields). However, some anomalies as seen for the Svåheii 2 (Sc-rich, close to the pluton), Bratterud and Sjauset locations (Sc-poor, farthest away from the pluton) occur. Wise et al. (1998) made similar findings, stating that the regional distribution of Sc-rich minerals (e.g. Sc-enriched columbite-group minerals) among pegmatites from various locations in North America is

highly unpredictable, and cannot be related to regional fractionation trends of pegmatite fields. As stated by Goldschmidt (1937), Sc does not follow the general partitioning rules of other elements. Due to its special incompatible character (e.g. Bergstøl and Juve, 1988; Wise et al., 1998; Raade and Segalstad, 2002; Pezzotta et al., 2005), the Sc distribution in granitic pegmatites is still not well understood. The overall Sc concentration in the Tørdal garnets both increases with increasing spessartine components (30 – 60 mol.%), and for pegmatites farther away from the pluton. However, some of the outmost SW and NE pegmatites do not follow this general regional fractionation trend of the Tørdal pegmatite field. Therefore, another or an additional source to the Tørdal granite must be investigated for the Sc enrichment observed in the study area.

The 10000*Ga/Al *versus* $(K_2O+Na_2O)/CaO$ plot in Fig. 3.44 B indicates that the Tørdal granite is anorogenic (A-type). This anorogenic origin is supported when plotting the data in the Y+Nb *versus* Rb diagram (Fig. 3.44 C). According to Whalen et al. (1987) the formation of A-type granites, which typically marks the latest magmatic stage of orogenic events, happens after the creation and abduction of earlier orogenic granites in the lower crust. The same authors state that the partially melted dry granulitic remnants, which are rich in e.g. F, generate these anorogenic granites. On the other hand, the much older and metamorphosed amphibolites of the Tørdal area originate from protoliths of primitive arc tholeiitic composition, according to both the Ti-V- and Th-Hf-Ta ternary plots (Fig. 3.43 A-B). Scandium in such rocks crystallized from mafic melts, acts as a compatible element, according to experimental evidence by Norman and Haskin (1968). Table 3.7 shows that both Sc and F are significantly more abundant in the amphibolites than in the Tørdal granite (Fig. 4.46). Based on this observation, it is evident that the source of Sc and F in the pegmatites are most likely from the amphibolites. However, the question remains; were Sc and F leached from the amphibolitic host rocks and absorbed by the pegmatite melt during anatexis, at the time of migration and emplacement in these host rocks?

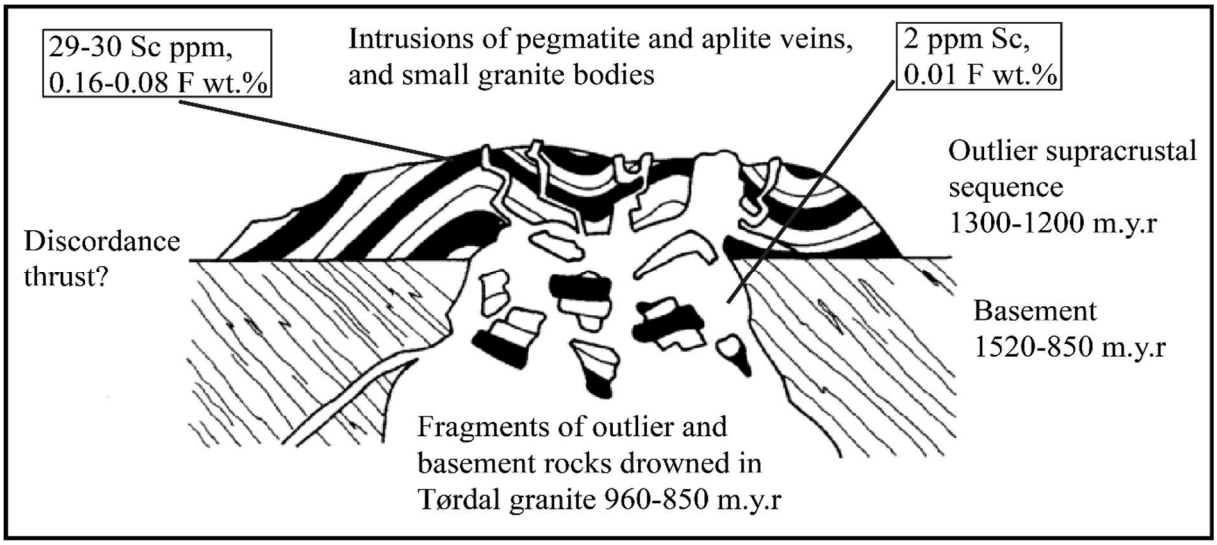

Figure 4.46: This image is modified from (Bergstøl and Juve, 1988), which displays the view by these authors for the Sc enrichment in the Tørdal pegmatites. The Tørdal granite, from which the Tørdal pegmatites derived, intruded both the basement and the Sc-enriched supracrustal rocks. Scandium concentrations in the two analyzed types of host rock are outlined in the image – amphibolitic host rock: 29-30 Sc ppm, and the Tørdal granite: 2 ppm.

According to Andersen et al. (2007), the Tørdal granite yielded a U-Pb zircon age of 918 ± 7 Ma, while the ages of the pegmatites were not known until recently. Recent studies by Rosing-Schow et al. (2018), using fergusonite from the Tørdal granite, disclosed a discordant U-Pb age of 946 ± 4 Ma. The same study revealed U-Pb columbite ages of 892 ± 8.8 Ma of the Skardsfjell pegmatite. This pegmatite shares the geochemistry and is in the proximity of the evolved NYF pegmatites of the Heftetjern-Høydalen area (Oftedal, 1942). This implies that the pegmatites may be up to ~40 Ma younger than the Tørdal granite. Consequently, the Tørdal granite is, therefore, an unlikely source for the pegmatites. Müller et al. (2017) support this hypothesis since they made similar findings for the neighboring Sveconorwegian pegmatite fields of Evje-Iveland and Froland. The same authors forward the supposition that the Tørdal pegmatites like other Sveconorwegian pegmatites (e.g. from the Evje-Iveland and Froland pegmatite fields) may be formed by direct anatexis of the amphibolitic host rocks. Evidence supporting the anatectic origin of the Tørdal pegmatites during this thesis' fieldwork were observed from e.g. the Kleppe quarry location. For instance, at this location, the amphibolites show clear textural evidence for local partial melting and the generation of pegmatite melt (Figures 3.7 E-F). In light of this, the Sc in the pegmatites was probably taken up by fractional partial melting (anatexis) of the amphibolites and through continuous melt fractionation. The pegmatite melt may therefore not have been generated as late hydrous fractionated melts from the Tørdal granite as previously believed.

Fluorine is known, as an effective fluxing agent, to assemble Sc and other rare metals in the latest magmatic fully fluid-saturated pegmatitic melts (e.g. Segalstad and Raade, 2003; Pezzotta et al., 2005), in the form of relatively stable Sc-F-complexes (Gramaccioli et al., 2000). This is evident especially for wall zone biotites in both the Heftetjern and Skardsfjell pegmatites, which exhibit both high F and Sc contents (up to 6.04 F and 0.43 Sc wt.%) (Rosing-Schow et al., 2018). Wall zone muscovites (same publication) from the Upper Høydalen pegmatites exhibit lower Sc and F contents (0.89 – 6.34 F and 0 – 0.08 Sc wt.%). Yet, wall zone muscovite from the Skardsfjell pegmatite actually exhibit higher F (7.12 wt.%), but no Sc contents. On the other hand, garnet naturally lacks F in its structure. Consequently, relatively few occurrences of F-rich micro inclusions are present in the wall zone garnets (up to 0.29 Sc_2O_3 wt.%) from all the investigated pegmatites (with the exception of "cleavelandite"-zone garnets). The Sc and F contents in micas and garnets, in particular from the wall zones of the evolved NYF pegmatites, can be explained in the following process: during anatexis of the amphibolitic host rocks (Sc- and F-rich) relatively stable ligands, such as ScF_3 were formed (Fig 4.47). This ligand acted as a transport medium for Sc and entered the pegmatite melt during its initial formation. During the crystallization of the different mineral phases of the first proportion of pegmatitic melt (e.g. wall zone), this ligand was dissociated. Scandium and F, therefore, went into different mineral phases based on the variable compatibility/incorporation of Sc and F (e.g. garnet, mica, K-feldspar, plagioclase). Fluorine in the wall zone is preferentially incorporated into micas (ideal formula: $AB_{2-3}(X,Si)_4O_{10}(O,F,OH)_2$). Most of the Sc-rich minerals in Tørdal are formed during the late hydrothermal stages of the pegmatite formation (e.g. Raade et al., 2002; Chukanov et al.,

2017). In particular, pegmatites of the Heftetjern area are type localities for the Sc minerals heftetjernite, kristiansenite, oftedalite – all of which are related to the late hydrothermal stages (Kristiansen, 2009). Due to the tiny crystal sizes (e.g. up to 2 mm for kristiansenite according to observations by Raade et al., 2002) and rare occurrence within the pegmatite bodies, a relatively small portion of Sc bulk content is incorporated into these minerals. Therefore, the major part of Sc, during the late hydrothermal wall zone crystallization, went into the other Sc-compatible minerals such as e.g. biotite and garnet (with occasional thortveitite micro inclusions according to EDS analysis), and minuscule amounts into K-feldspars and plagioclases (Table 4.8). Plausibly, a considerable portion of Sc in those minerals may have been re-mobilized from primary mica and/or garnet altered during these late-stage hydrothermal processes. Despite the mentioned suppositions, the partition of Sc into the different mineral phases remains an open question, which needs to be further investigated.

Table 4.8 Sc partition coefficients in rhyolite

Mineral	***Sc Kd***	***Authors***
Garnet	13.6 – 19.2	*(Irving & Frey, 1978)*
	63	*(Sisson & Bacon, 1992)*
Biotite	4.9 – 20	*(Nash & Crecraft, 1985)*
K-feldspar	0.029	*(Leeman & Phelps, 1981)*
	0.01 – 0.04	*(Nash & Crecraft, 1985)*
Plagioclase	0.01	*(Bacon & Druitt, 1988)*
	0.02 – 0.06	*(Nash & Crecraft, 1985)*

Table 4.8: Displayed partition coefficients for Sc in different mineral phases. Rhyolites shares similar geochemistry as granitic pegmatites, which may indicate the incorporation of Sc into different pegmatitic mineral phases. Data on the incorporation of Sc into muscovite and quartz appear inaccessible in literature, and is therefore not included.

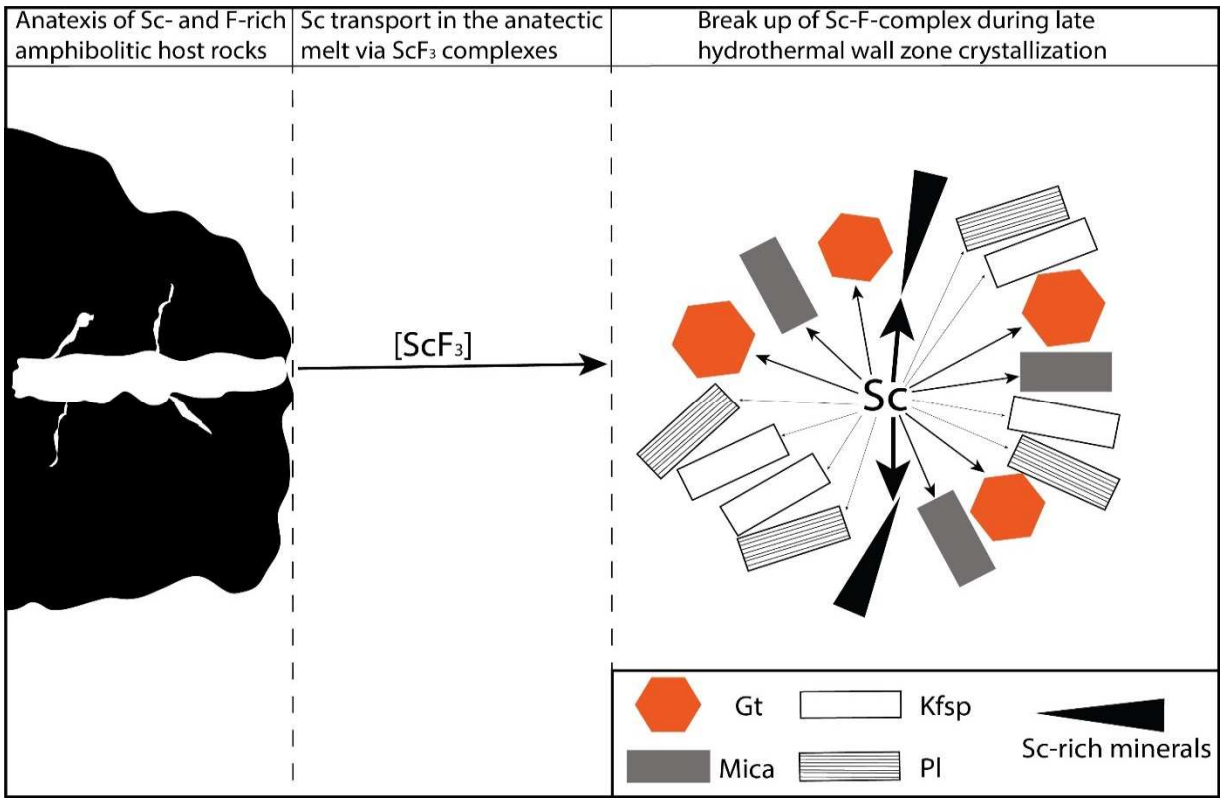

Figure 4.47: Schematic illustration of the origin (anatexis of amphibolites), transport via ScF_3 complexes in the anatectic pegmatite melt, and final incorporation of Sc into the different mineral phases in the wall zone of the NYF pegmatites. The

size of arrows indicate degree of Sc partition into the distinct pegmatite-forming mineral phases. Importantly, only a small portion of the bulk Sc contents in the pegmatites is incorporated into the tiny and rarely occurring Sc-minerals. Thus, most of the Sc is incorporated into the relatively bigger minerals such as micas and garnets. Mineral abbreviations: Gt = garnet, Kfsp = K-feldspar, Pl = plagioclase. The micas are mainly biotites, while accessory Sc-rich minerals include e.g. thortveitite.

The regional distribution of Sc in garnets shows generally a systematic zoning in Tørdal. Clearly, Sc becomes enriched from the Sc-poor garnets in the Butvatnet-Grønliheii area (SW) to the Sc-rich garnets of the Heftetjern-Høydalen area (NE). This may imply that the pegmatitic melts were probably generated by partial melting (anatexis) of the amphibolitic host rocks in the SW-area of this study (Sc-poor pegmatites residing in the pink K-feldspar zone). Considering this assumption, the pegmatitic melt would have moved in the NE-direction, being continuously fractionated, while lastly generating the Sc-rich "amazonite" pegmatites in the Heftetjern-Høydalen area (Fig. 4.48). However, this model does not apply for the pegmatites of the most SW (Sc-rich and pink K-feldspar dominated pegmatite of the Svåheii 2 location) and NE corners (both the Sc-poor and "amazonite" dominated pegmatites of the Bratterud and Sjauset locations). It is therefore suggested that at least some melt portions moved in the NE-direction from the Sc-poor to the Sc-rich pegmatites. This is indicated by the overall regional distribution of Sc in the Tørdal pegmatites as discussed above.

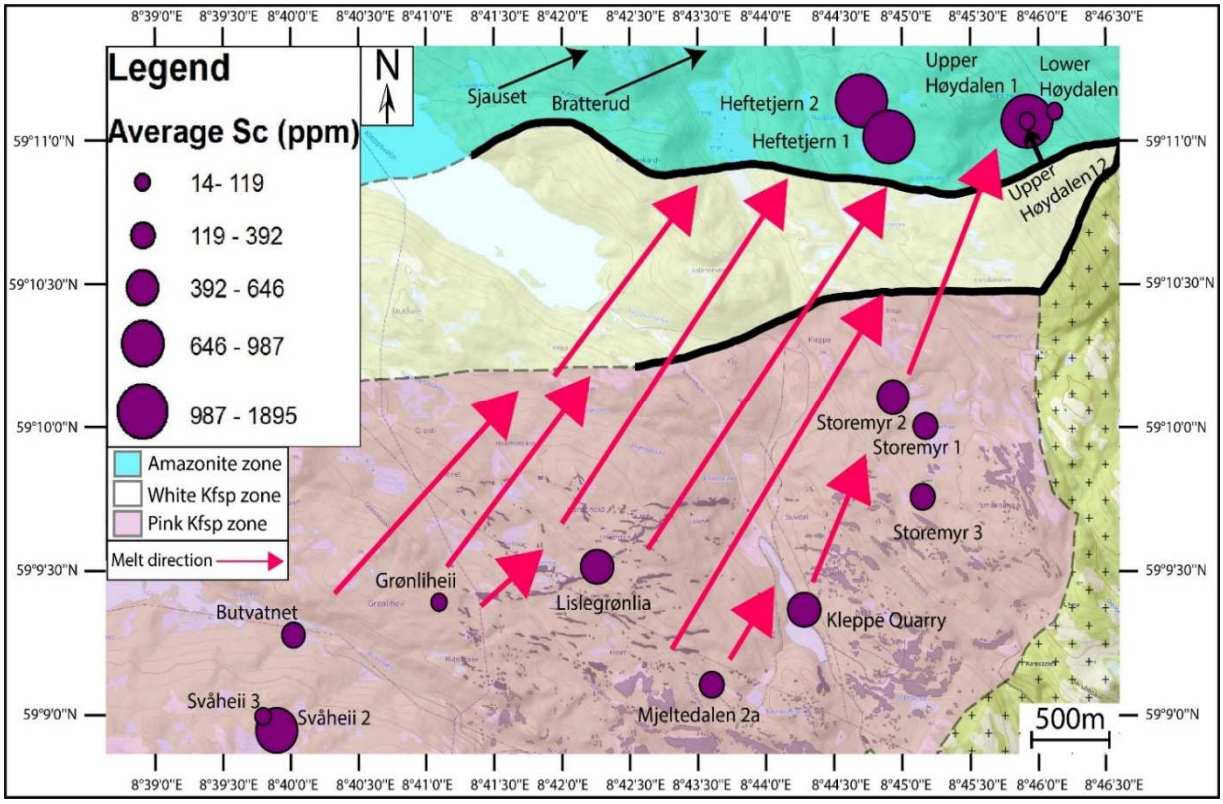

Figure 4.48: The displayed map shows the plausible relative pegmatitic melt direction in Tørdal. The pegmatitic melt was most probably continuously fractionated from the less evolved Sc-poor NYF pegmatites in the SW-area towards the more evolved NYF pegmatites in the Heftetjern-Høydalen area (northeast). Importantly, the pegmatitic melt most probably did not originate from the Tørdal granite. The more plausible source of this melt was generated through anatexis (partial melting) of the Sc-rich amphibolitic host rocks. Solid lines are based on the regional zoning of the Tørdal pegmatites suggested by Bergstøl and Juve's (1988) on the base of distribution of K-feldspar types (pink K-feldspar, white K-feldspar and "amazonite"). Stippled lines are highly uncertain zone borders, which need to be further investigated. Bratterud and Sjauset are outside the map area. The Tørdal granite (black crosses) is displayed at the eastern edge of the map. The granite contact is still uncertain in some parts due to limited outcrops and access challenges.

4.4 Economic implications of the scandium enrichment

According to the achieved results, Sc in garnets of the Tørdal pegmatites generally exhibits an overall systematic distribution pattern with increasing enrichment towards NE in the area of this study (Sc-poor in the SW-area to Sc-rich in the NE-area). Thus, from an economic perspective, the Heftetjern-Høydalen area yields the highest Sc concentrations and therefore has the highest economic potential. The Tørdal area has been in the past subjected to several exploration campaigns e.g. the Scandium International Mining Corporation. As a result of their 2011-2012 prospects of the Tørdal area (Scandium International Mining Corp., 2018b), the company reported promising potential exploitation of various rare metals (e.g. Sc and REEs) of relatively high concentrations from over 300 mapped and sampled pegmatites. According to Scandium International, the highest measured Sc concentrations of pegmatites was above 1.600 ppm (bulk rock analysis by XRF). The company stated further that notable mineralizations of Sc, as well as HREE, occur in the amphibolitic host rocks. These rocks are therefore considered as the source for both the Sc and HREE enrichment. In addition, the company announced the following distribution of Sc in the area based on XRF bulk rock measurements of the pegmatites (Fig. 4.49). The highest concentrations were detected in the Heftetjern area with an average of 1.000-1.500 Sc ppm (Area 1: Kleppe), and 500-1.500 Sc ppm in the Storemyr area (Area 2: Heftetjern). From these areas, Sc generally decreases in the SW direction towards Solli (Area 3) with 300-700 ppm Sc, South Kleppsvatn (Area 4) with 300-900 ppm Sc, and Butvatn (Area 5) with 300-1.000 ppm Sc. This study also shows that mica is more Sc-rich than garnet (moderate Sc). Importantly, the result by Scandium International, revealing the gradual NE-oriented enrichment of Sc, has been confirmed by this study.

Mica data by Rosing-Schow et al. (2018) from different pegmatites from Tørdal show variable Sc contents. The lepidolites from Lower and Upper Høydalen pegmatites have no Sc, whereas muscovite from the Upper Høydalen pegmatite has slightly higher Sc contents (0.1 – 0.8 Sc_2O_3 wt.%, 0.00 – 0.01 Sc *apfu*). Muscovite from the Skardsfjell pegmatite contains no Sc. However, biotites from the latter local show elevated Sc (0.14 – 0.23 Sc_2O_3 wt.%, 0.01 – 0.03 *apfu)*, and biotites from Heftetjern has even higher Sc contents (0.12 – 0.43 Sc_2O_3 wt.%, 0.01 – 0.05 *apfu*). Oftedal (1943) detected Sc contents in micas from pegmatites at Høydalen (0-0.07 Sc wt.% in muscovite and 0.005 Sc in lepidolite) and Skardsfjell (0.2 Sc wt.% in zinnwaldite and 0.04-0.05 Sc wt.% in muscovite). Consequently, these presented mica data indicate that biotites are most abundant in Sc compared to white micas, but exhibiting variable concentrations.

According to this study, the Tørdal garnets yield bulk average concentrations of ~ 0.08 Sc_2O_3 wt.% (EPMA) and ~ 876 Sc ppm (ICP-MS). The highest Sc concentrations in garnet were detected in samples from the Heftetjern area up to 0.29 wt.% Sc_2O_3 or 0.02 *apfu* Sc (EPMA), and 2197 ppm Sc (ICP-MS). For comparison, biotites in the Heftetjern area also exhibit the highest Sc concentrations (Rosing-Schow et al., 2018). These values correspond to other measurements of garnets from the Heftetjern area ~ 0.3 to ~ 0.5 wt.% Sc_2O_3 (Raade and Kristiansen 2000, 2003). Similarly, in other pegmatites fields of southern Norway, such as the

Evje-Iveland field, both biotite and garnet have high Sc contents (1,040 and 1,240 ppm, respectively) (Stokkeland, 2016). This study shows that garnets can indeed be used as pathfinder mineral for the Sc mineralization in granitic pegmatites. As discussed above, garnets exhibit relatively consistent Sc concentrations in one pegmatite body in comparison to e.g. micas, which can have much more variable Sc contents. However, it could also imply that various members of the garnet family occurring in one pegmatite will show different Sc-contents. In particular, almost pure spessartine from the "cleavelandite" zones of the Høydalen pegmatites have no Sc, whereas more almandine-rich spessartines from the wall zone of the same pegmatites are rich in Sc. Therefore, it is crucial to pay attention during sampling from which zone of the pegmatite the garnets originate, before making any conclusions on the overall Sc distribution and economic potential of an area.

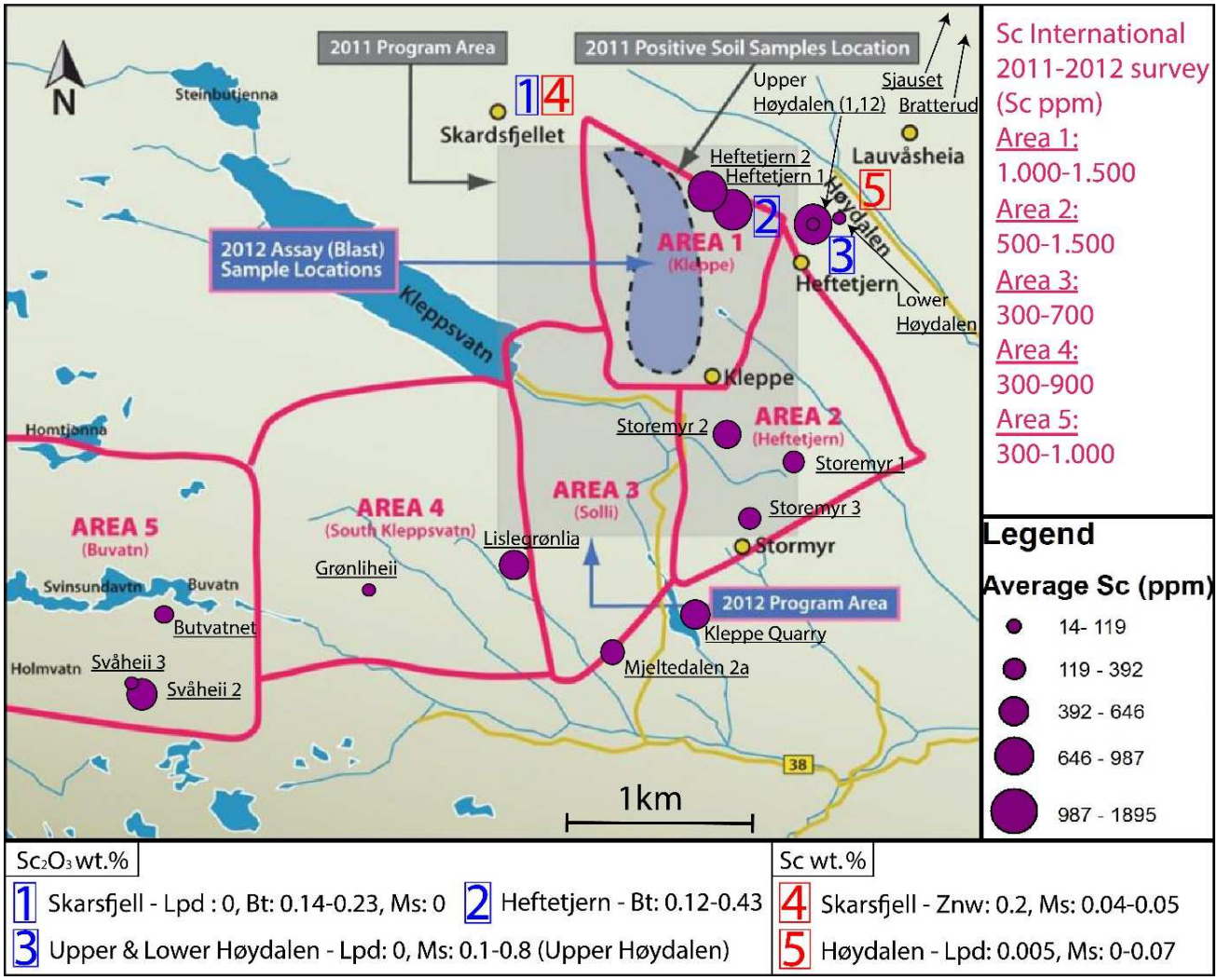

Figure 4.49: Modified image from Scandium International's 2011-2012 study of Sc concentrations in the pegmatites of the Tørdal area (Scandium International Mining Corp., 2018b). Upper right: Published Sc concentrations by Scandium International's 2011-2012 survey in the Tørdal area. Lower right: Measured average Sc concentrations done by this thesis through EPMA and ICP-MS. Bottom: Sc concentrations (blue number boxes) from mica data by Rosing-Schow et al. (2018), and mica data (red number boxes) from (Oftedal, 1943).

5. Summary and outlook

1) Regional distribution of Sc in the Tørdal garnets

Most of the investigated garnets of the Tørdal pegmatites show a distinct spatial increase of the Sc content from SW (Butvatnet-Grønliheii areas) to NE (Heftetjern-Høydalen area) of the study area. Evidently, Sc-rich micro inclusions are only present in the wall zone garnets from the Sc abundant NE-area (Upper Høydalen) and SW corner (Svåheii 2) of the study area. The spatial increase of Sc is correlated with the increase of the spessartine component from 30 to 60 mol.% (up to 0.29 Sc_2O_3 wt.% and 2197 ppm Sc). Regarding this general trend, Sc contents in garnet-bearing pegmatites increase with the degree of fractionation, commonly seen in other pegmatite fields. However, wall zone garnets from both the most SW (Sc-rich ~47 mol.% spessartines from the Svåheii 2 location) and NE (Sc-poor ~54 mol.% spessartines from the Bratterud and ~76 mol.% spessartines from the Sjauset locations) corners of the study area do not follow this general trend. In the chemically most evolved Tørdal NYF pegmatites of the Høydalen area, Sc in garnet drastically drops from the wall zone Sc- and almandine-rich spessartines (up to 1538 ppm Sc and ~50 mol.% spess) towards the "cleavelandite"-zone garnets. Evidently, these "cleavelandite"-zone garnets represent the most advanced stages (81-93 mol.% spessartine component) of fractionation, where Sc is nearly absent.

2) Mineral-scale distribution of Sc within the Tørdal garnets

Scandium in the Sc-rich garnets (Heftetjern 1-2, Upper Høydalen 1 and Svåheii 2) generally decrease from the core towards the crystal margin (up to 688 ppm Sc difference). This decrease of Sc, especially for the Heftetjern garnets is accompanied, by the decrease in Mn/(Mn+Fe) ratios and both Y and HREE contents. In addition, IBMA indicate that the investigated Sc-rich garnets (Heftetjern 1-2 and Svåheii 2 locations) exhibit Sc-abundant cores, where Sc might slightly decrease towards the rim. Other garnets with lower Sc abundances did not show any overall consistent distribution of intracrystalline Sc, nor any particular correlation with other major or trace elements (e.g. Y and HREEs).

3) Potential sources of Sc-enrichment in the Tørdal pegmatites

Similarly to other pegmatite fields, the Sc content in most of the garnet-bearing Tørdal pegmatites is accompanied by a systematic SW-NE-oriented increasing degree of fractionation. Initially, this implies that the pegmatite melts may have originated as fractionated melts from the Tørdal granite pluton south in the study area. As proposed by Bergstøl and Juve (1988) Sc was leached from the mafic supracrustals (amphibolites) into these fractionated pegmatite melts, as these melts passed through them. Geochemical whole rock analysis concurs with this theory and reveals significantly higher Sc (including F) contents in these amphibolitic host rocks (29-30 ppm Sc) than in the Tørdal granite (2 ppm Sc). However, fieldwork indicates evidence for local and direct anatexis of the amphibolitic host rocks. In addition, the most recent dating of the pegmatites and the spatially related Tørdal granite by Rosing-Schow et al. (2018) revealed that the Tørdal pegmatites are about 40

Ma younger than the Tørdal granite. Thus, the Tørdal pegmatite melts did not originate from the Tørdal granite but were rather formed by local and direct anatexis of the amphibolitic host rocks. As suggested, the anatectic pegmatite melts moved from the Sc-poor SW to the Sc-rich NE area of the study. During this melt migration through the amphibolitic host rocks, Sc in the pegmatite melts, both assembled and transported by ScF complexes, became increasingly fractionated and continuously Sc-enriched. Lastly, most of these highly fractionated and most Sc-enriched melts were emplaced in the NE part of the study area (the most Sc-rich Heftetjern-Høydalen area). In these evolved NYF pegmatites (especially the Heftetjern pegmatites), a large portion of Sc was incorporated into micas and garnets in the late hydrothermal wall zone. However, this incorporation of Sc into the different mineral phases of the late hydrothermal wall zone needs to be further investigated.

4) Economic implications of the Sc-enrichment in Tørdal.

The main outcome of this study demonstrates that the pegmatites of Heftetjern-Høydalen area are most abundant in Sc, and thus, yields the highest potential for future exploitation of this metal. In an individual pegmatite body, Sc contents are considerably more consistent in garnets compared to micas, as revealed by this study. Garnet is, therefore, a significantly more reliable pathfinder mineral for Sc mineralization related to granitic pegmatite fields. This study also shows that the different garnet endmembers within distinct evolved NYF pegmatite zones will have a great impact on the Sc content. Evidently, the Sc drops through internal fractionation from the Sc abundant almandine-rich spessartines of the wall zone to the almost pure spessartines from the “cleavelandite”-zone. These cleavelandite”-zone spessartines virtually have no Sc and should, therefore, be avoided during exploration. With this in mind, it is of great importance for future Sc exploration to consider from which zone of the evolved NYF pegmatite the garnets originated. Considering the findings of this study, the following aspects should be considered for future studies, in terms of the estimation of both distribution and economic potential of Sc mineralization in granitic pegmatite fields:

1) Further mapping of the pegmatites in the Tørdal area, in order to know the total size of this pegmatite field (The study area comprises only a part of the Tørdal pegmatite field).
2) Investigation of Sc distribution in the whole Tørdal pegmatite field, since the pegmatites of the SW- and NE-corners of the study area do not follow the main SW-NE-oriented spatial systematic Sc-enrichment trend, as seen for most of the other pegmatites.
3) Exploration on why the Sc content suddenly drops at a spessartine component >60 mol.%, and the impact of other elements such as e.g. Ca and Mg (reflected in other endmembers such as e.g. andradite and pyrope) on the Sc content in garnet.
4) Inspection on the potential late hydrothermal processes, which are involved in the incorporation of Sc into distinct mineral phases (such as garnet and micas as well as other minerals) of the wall zone in the evolved NYF pegmatites.

6. References

Allègre, C. J., Provost, A. and Jaupart, C. (1981) 'Oscillatory zoning: A pathological case of crystal growth', *Nature*, 294, pp. 223–228. doi: 10.1038/294223a0.

Anders, E. and Grevesse, N. (1989) 'Abundances of the elements: Meteoritic and solar', *Geochimica et Cosmochimica Acta*, **53**(1), pp. 197–214. doi: 10.1016/0016-7037(89)90286-X.

Andersen, T., Graham, S. and Sylvester, A. G. (2007) 'Timing and tectonic significance of Sveconorwegian A-type granitic magmatism in Telemark, southern Norway: New results from laser-ablation ICPMS U-Pb dating of zircon', *Norges Geologiske Undersøkelse Bulletin*, **447**, pp. 17–31.

Bacon, C.R. and Druitt, T.H. (1988) 'Compositional Evolution of the Zoned Calcalkaline Magma Chamber of Mount-Mazama, Crater Lake, Oregon', *Contributions to Mineralogy and Petrology*, **98**(2), pp. 224-256.

Baldwin, J. R. and Van Knorring, O. (1983) 'COMPOSITIONAL RANGE OF Mn-GARNET IN ZONED GRANITIC PEGMATITES', *Canadian Mineralogist*, **21**, pp. 683–688.

Bergstøl, S. and Juve, G. (1988) 'Scandian ixiolite, pyrochlore and bazzite in granite pegmatite in Tørdal, Telemark, Norway. A contribution to the mineralogy and geochemistry of scandium and tin', *Mineralogy and Petrology*, **38**(4), pp. 229–243. doi: 10.1007/BF01167090.

Bernhard, F., Walter, F., Ettinger, K., Taucher, J., Mereiter, K. (1998) 'Pretulite, $ScPO_4$, a new scandium mineral from the Styrian and Lower Austrian lazulite occurrences, Austria', *American Mineralogist*, **83**(5–6), pp. 625–630. doi: 10.2138/am-1998-5-622.

Bianchi, R., Pilati, T., Diella, V., Gramaccioli, C. M., Mannu G. (1988) 'A re-examination of thortveitite', **73**, pp. 601–607.

Bottinga, Y., Kudo, A. and Weill, D. (1966) 'Some observations on oscillatory zoning and crystallization of magmatic plagioclase', *American Mineralogist*, **51**, p. 792.

Černý, P. (1990) 'Distribution, affiliation and derivation of rare-element granitic pegmatites in the Canadian Shield', *Geol. Rundschau*, **79**, 183-226.

Černý, P. (1991a) 'Rare-element granitic pegmatites. Part I: Anatomy and Internal Evolution of Pegmatite deposits', *Geoscience Canada*, **18**(2), pp. 49–67.

Černý, P. (1991b) 'Rare-element granitic pegmatites. Part II: regional to global environments and petrogenesis', *Geoscience Canada*, **18**(2), pp. 68–81.

Černý, P. and Ercit, T. S. (2005) 'The classification of granitic pegmatites revisited', *Canadian Mineralogist*, **43**, pp. 2005–2026. doi: 10.2113/gscanmin.43.6.2005.

Černý, P., London, D., Novák, M. (2012) 'Granitic pegmatites as reflections of their sources', *Elements*, **8**(4), pp. 289–294. doi: 10.2113/gselements.8.4.289.

Chassé, M. Griffin, W.L., O'Reilly, S.Y., Calas, G. (2017) 'Scandium speciation in a world-class lateritic deposit', *Geochemical Perspectives Letters*, pp. 105–114. doi: 10.7185/geochemlet.1711.

Chukanov, N. V., Aksenov, Sergey M., Rastsvetaeva, R. K., Kristiansen, R., Pekov, I. V., Belakovskiy, D. I., Van, K. V., Bychkova, Y. V., Britvin, S. N. (2017) 'Crystal structure of the OH-dominant gadolinite-(Y) analogue $(Y,Ca)_2(Fe,\square)Be_2Si_2O_8(OH,O)_2$ from Heftetjern pegmatite, Norway', *Acta Crystallographica*, **2**(B73), pp. 899–906. doi: 10.1107/S2052520617006588.

Cooper, M. A., Hawthorne, F. C., Ball, N. A., Černý, P., Kristiansen, R. (2006) 'Oftedalite, $(Sc,Ca,Mn^{2+})_2K(Be,Al)_3Si_{12}O_{30}$, a new member of the milarite group from the Heftetjern pegmatite, Tordal, Norway: description and crystal structure.', *Canadian Mineralogist*, **44**(4), pp. 943–949. doi: 10.2113/gscanmin.44.4.943.

Das, H. A., Zonderhuis, J. and van der Marel, H. W. (1971) 'Scandium in rocks, minerals and sediments and its relations to iron and aluminium', *Contributions to Mineralogy and Petrology*, **32**(3), pp. 231–244. doi: 10.1007/BF00643336.

Demartin, F., Gramaccioli, C. M. and Pilati, T. (2000) 'Structure refinement of bazzite from pegmatitic and miarolitic occurrences', *Canadian Mineralogist*, **38**(6), pp. 1419–1424. doi: 10.2113/gscanmin.38.6.1419.

Fedorowich, J. S., Jain, J. C., Kerrich, R., Sopuck, V. (1995) 'TRACE-ELEMENT ANALYSIS OF GARNET BY LASER-ABLATION MICROPROBE ICP-MS', **33**, pp. 469–480.

Fersman, A. (1930) 'O geokhimicheskoi geneticheskoi klassifikatsii granitnykh pegmatitov (A geochemical genetic classification of pegmatites)', *Monograph Akademiia Nauk SSSR*. (in Russian)

Fersman, A. (1931) 'Über die geochemisch-genetische Klassifikation der Granitpegmatite', *Tschermaks Mineralogische und Petrogrpahische Mitteilungen (Zeitschrift für Kristallographie, Mineralogie und Petrographie)*, **41**, pp. 64-83. (in German)

Galuskina, I. O., Galuskin, E. V., Dzierzanowski, P., Armbruster, T., Kozanecki, M. (2005) 'A natural scandian garnet', *American Mineralogist*, **90**(10), pp. 1688–1692. doi: 10.2138/am.2005.1981.

Galuskina, I. O., Galuskin, E. V., Lazic, B., Armbruster, T., Dzierżanowski, P., Prusik, K., Wrzalik, R. (2010) 'Eringaite, $Ca_3Sc_2(SiO_4)_3$, a new mineral of the garnet group', *Mineralogical Magazine*, **74**(2), pp. 365–373. doi: 10.1180/minmag.2010.074.2.365.

GINSBURG, A.I., RODIONOV, G.G. (1960) 'On the depth of formation of granitic pegmatites', *Geol. Rudn. Mestorozhd.*, pp. 45-54 (in Russ.).

GINSBURG, A.I, TIMOFEYEV, I.N., FELDMAN, L.G. (1979) 'Principles of Geology of the Granitic Pegmatites', *Nedra, Moscow, USSR* (in Russ.)

Glover, A. S., Rogers, W. Z. and Barton, J. E. (2012) 'Granitic pegmatites: Storehouses of industrial minerals', *Elements*, **8**(4), pp. 269–273. doi: 10.2113/gselements.8.4.269.

Goldschmidt, V. M. (1937) ‘The Principles of Distribution of Chemical Elements in Minerals and Rocks’, *Journal of the Chemical Society*, pp. 655–673.

Gramaccioli, C. M., Diella, V. and Demartin, F. (2000) ‘The formation of scandium minerals as an example of the role of complexes in the geochemistry of rare earths and HFS elements’, *European Journal of Mineralogy*, **12**, pp. 765–808.

Hedrick, B. J. B. (2002) ‘Rare Earths’, *U.S. Geological Survey Yearbook*, pp. 61.1-16.

Higuchi, H. and Nagasawa, H. (1969) ‘Partition of trace elements between rock-forming minerals and the host volcanic rocks’, *Earth and Planetary Science Letters*, **7**(3), pp. 281–287. doi: 10.1016/0012-821X(69)90066-1.

Hålenius, U., Hatert, F., Pasero, M., Mills, S. J. (2017) ‘IMA Commission on New Minerals, Nomenclature and Classification (CNMNC) Newsletter 40’, *Mineralogical Magazine*, **81**(1), pp. 209–213. doi: 10.1127/ejm/2017/0029-2709.

Haase, C. S., Chadam, J., Feinn, D., Ortoleva, P. (1980) ‘Oscillatory Zoning in Plagioclase Feldspar’, *American Association for the Advancement of Science*, **209**(4453), pp. 272–274.

Ihlen, P. M. and Müller, A. (2009) *NGU Rapport 2009.024 Forekomster av høyren kvarts langs Hardangerfjorden*.

Irving, A.J. and Frey, F.A. (1978). Distribution of Trace-Elements between Garnet Megacrysts and Host Volcanic Liquids of Kimberlitic to Rhyolitic Composition. *Geochimica et Cosmochimica Acta*, **42**(NA6), pp. 771-787. doi: 10.1016/0016-7037(78)90092-3.

Jaffe, H. (1951) ‘THE ROLE OF YTTRIUM AND OTHER MINOR ELEMENTS IN THE GARNET GROUP’, *American Mineralogist*, **36**, pp. 133–155.

Jahns, R. H. (1953a) ‘The genesis of pegmatites. I. Occurrence and origin of giant crystals’, *American Mineralogist*, **38**, pp. 563-598.

Jahns, R. H., Burnham C. W. (1969) ‘Experimental studies of pegmatite genesis: I. A model for the derivation and crystallization of granitic pegmatites’, *Economic Geology*, **64**, pp. 843-864.

Jambor, J., Pertsev, N. and Roberts, A. (1998) ‘New Mineral Names’, *American Mineralogist*, **83**, pp. 907–910.

Jarosewich, E. and Boatner, L. A. (1991) ‘Rare-Earth Element reference for microprobe analysis’, *Geostandards Newsletter*, **15**(2), pp. 397–399.

Juve, G. and Bergstøl, S. (1997) ‘Granittpegmatitter i Tørdal , Telemark’, *Kongsberg Mineralsymposium Norsk Bergverksmuseum Skrift*. Norsk Bergverksmuseum Skrift, **12**, pp. 56–57.

Kartverket (2017) < www.norgeskart.no > Accessed 3 July 2017.

Kolitsch, U., Kristiansen, R., Raade, G., Tillmanns, E. (2010) ‘Heftetjernite, a new scandium mineral from the Heftetjern pegmatite, Tordal, Norway’, *Eur J Mineral*, **22**(2), pp. 309–316. doi: 10.1127/0935-1221/2010/0022-1987.

Kristiansen, R. (1998) 'Høydalen Li-pegmatitt, Tørdal, Telemark.', *Norsk Bergverksmuseum Skrift*, **14**, pp. 17–28.

Kristiansen, R. (2009) 'A unique assemblage of Scandium-bearing minerals from the Heftetjern-pegmatite, Tørdal, south Norway', *Norsk Bergverksmuseum Skrift*, **41**, pp. 75–104.

Leeman, W.P. and Phelps, D.W. (1981) 'Partitioning of rare earths and other trace elements between sanidine and coexisting volcanic glass', *Journal of Geophysical Research*, **86**: doi: 10.1029/JB080i011p10193. issn: 0148-0227.

Linnen, R. L., Van Lichtervelde, M., Černý, P. (2012) 'Granitic pegmatites as sources of strategic metals', *Elements*, **8**(4), pp. 275–280. doi: 10.2113/gselements.8.4.275.

Locock, A. J. (2008) 'An Excel spreadsheet to recast analyses of garnet into end-member components, and a synopsis of the crystal chemistry of natural silicate garnets', *Computers and Geosciences*, **34**(12), pp. 1769–1780. doi: 10.1016/j.cageo.2007.12.013.

London, D. (1996) 'Granitic pegmatites', *Special Paper 315: The Third Hutton Symposium on the Origin of Granites and Related Rocks*, **87**, pp. 305–319. doi: 10.1130/0-8137-2315-9.305.

London, D. (2008) 'Pegmatites', 10th edn. Québec: *Mineralogical Association of Canada*.

Loomis, T. P. (1982) 'Numerical Simulations of Crystallization Processes of Plagioclase in Complex Melts: the Origin of Major and Oscillatory Zoning in Plagioclase', *Contributions to Mineralogy and Petrology*, **81**, pp. 219–229. doi: 10.1007/BF00371299.

Ma, C., Tschauner, O., Beckett, J. R., Rossman, G. R., Liu, W. (2012) 'Panguite, $(Ti^{4+},Sc,Al,Mg,Zr,Ca)_{1.8}O_3$, a new ultra-refractory titania mineral from the Allende meteorite: Synchrotron micro-diffraction and EBSD', *American Mineralogist*, **97**, pp. 1219–1225.

Ma, C. Tschauner, O., Beckett, J. R., Rossman, G. R., Liu, W. (2013) 'Kangite, $(Sc,Ti,Al,Zr,Mg,Ca,\square)_2O_3$, a new ultra-refractory scandia mineral from the Allende meteorite : Synchrotron micro- Laue diffraction and electron backscatter diffraction', **98**, p. 4290. doi: 10.2138/am.2013.4290.

Ma, C. and Beckett, J. R. (2009) 'Allendeite and Hexamolybdenum: Two New Ultra-Refractory Minerals in Allende and Two Missing Links', *Lunar and Planetary Science Conference*, (40), pp. 1402–1402.

Ma, C. and Rossman, G. R. (2009) 'Davisite , $CaScAlSiO_6$, a new pyroxene from the Allende meteorite', *American Mineralogist*, **94**, pp. 845–848. doi: 10.2138/am.2009.3209.

Maniar, P. D. and Piccoli, P. M. (1989) 'Tectonic discrimination of granitoids', *Geological Society of America Bulletin*, **101**(5), pp. 635–643. doi: 10.1130/0016-7606(1989)101<0635:TDOG>2.3.CO.

Mellini, M., Merlino, S., Orlandi, P., Rinaldi, R. (1982) 'Cascandite and jervisite, two new scandium silicates from Baveno, Italy.', *American Mineralogist*, **67**(5–6), pp. 599–603.

Mellini, M. and Merlino, S. (1982) 'The crystal structure of cascandite, CaScSi30S(OH)', *American Mineralogist*, **67**, pp. 604–609.

Mindat.org (2017): Tørdal, Drangedal, Telemark, Norway < https://www.mindat.org/loc-23233.html> Accessed 10 May 2017.

Müller, A., van den Kerkhof, A. M., Behr, H. J., Kronz, A., Koch-Müller, M. (2010) 'The evolution of late - Hercynian granites and rhyolites documented by quartz – a review', *Earth and Environmental Science Transactions of the Royal Royal Society of Edinburgh*, **1000**, pp. 185–204. doi: 10.1017/S17556909016144.

Müller, A., Kearsley, A., Spratt, J., Seltmann, R. (2012) 'Petrogenetic implications of magmatic garnet in granitic pegmatites from Southern Norway', *Canadian Mineralogist*, **50**(4), pp. 1095–1115. doi: 10.3749/canmin.50.4.1095.

Müller, A., Romer, R. L., Pedersen, R. B. (2017) 'The sveconorwegian pegmatite province - thousands of pegmatites without parental granites', *Canadian Mineralogist*, **55**(2), pp. 283–315. doi: 10.3749/canmin.1600075.

Müller, A., Spratt, J., Thomas, R., Williamson, B.J., Seltmann, R. (2018). 'Alkali-F-rich albite zones in evolved NYF pegmatites - the product of melt-melt immiscibility', Canadian Mineralogist (in press)

Nash, W.P. and Crecraft, H.R. (1985). 'Partition coefficients for trace elements in silicic magmas', *Geochimica et Cosmochimica Acta,* **49**, pp. 2,309-2,322. doi: 10.1016/0016-7037(85)90231-5.

Nesse, W. D. (2013) *Introduction to optical mineralogy*. 4th edn. New York: Oxford Univ. Press.

Norman, J. C. and Haskin, L. A. (1968) 'The geochemistry of Sc: A comparison to the rare earths and Fe', *Geochimica et Cosmochimica Acta*, **32**(1), pp. 93–108. doi: 10.1016/0016-7037(68)90089-6.

Oftedal, I. (1942) 'LEPIDOLIT- OG TINNSTEINFØRENDE PEGMATITT I TØRDAL, TELEMARK', *Norsk Geologisk Tidsskrift*, **22**, pp. 1–14.

Oftedal, I. (1943) 'Scandium in Biotite as a Geologic Thermometer', *Norsk Geologisk Tidsskrift*, **23**, pp. 202–213.

Orlandi, P., Pasero, M. and Vezzalini, G. (1998) 'Scandiobabingtonite, a new mineral from the Baveno pegmatite, Piedmont, Italy', *American Mineralogist*, **83**, pp. 1330–1334.

Pearce T.H. (1993): A simple deterministic model of oscillatory zoning in magmatic plagioclase. Geol. Assoc. Can. – Mineral. Assoc. Can., Program Abstr. **18**, p. A-81.

Pearce, J. a, Harris, N. B. W., Tindle, A. G. (1984) 'Trace element distribution diagrams for the tectonic interpretation of granitic rocks', *Journal of Petrology*, **25**(4), pp. 956–983. doi: 10.1093/petrology/25.4.956.

Pezzotta, F., Diella, V., Guastoni, A. (2005) 'Scandium silicates from the Baveno and Cuasso al Monte NYF-granites, Southern Alps (Italy): Mineralogy and genetic inferences', *American Mineralogist*, **90**(8–9), pp. 1442–1452. doi: 10.2138/am.2005.1478.

Pouchou, J. L., Pichoir, F., (1984) 'A new model for quantitative X-ray microanalysis I. Application to the analysis of homogeneous samples', *Recherche Aérospatiale*, **3**, pp. 13-38.

Rosing-Schow, N., Müller, A., Romer, R., Corfu, F., Friis, H. (2018) 'New age constraints on the age of the Tørdal pegmatites, southern Norway', *Abstracts with Program, IMA2018 13th-17th August 2018*, Melbourne (in press)

Rudnick, R. L. and Gao, S. (2003) '3.01 - Composition of the Continental Crust', *Treatise on Geochemistry*, **1**(7), pp. 1–64. doi: http://dx.doi.org/10.1016/B0-08-043751-6/03016-4.

Raade, G., Ferraris, G., Gula, A., Ivaldi, G., Bernhard, F. (2002) 'Kristiansenite, a new calcium-scandium-tin sorosilicate from granite pegmatite in Tørdal, Telemark, Norway', *Mineralogy and Petrology*, **75**(1–2), pp. 89–99. doi: 10.1007/s007100200017.

Raade, G. and Brastad, K. (1993) 'Kamphaugite-(Y), a new hydrous Ca-(Y,REE)-carbonate', *European Journal of Mineralogy*, **5**, pp. 679–683.

Raade, G. and Kristiansen, R. (2000) 'Mineralogy and geochemistry of the Heftetjern granite pegmatite, Tørdal: a progress report', *Norsk Bergverksmuseum Skrift*, **17**, pp. 19–25.

Raade, G. and Kristiansen, R. (2003) 'Scandium as a trace element in the Heftetjern pegmatite minerals', *NGF Abstracts and Proceedings*, (2), pp. 36–37.

Raade, G. (2003): Scandium. *Chemical Engineering News* **81**, 68. http://pubs.acs.org/cen/80th/scandium.html. Accessed 20 April 2018. Accessed 20 March 2018

Raade, G. and Segalstad, T. V (2002) *Scandium 2003: an International Symposium on the Mineralogy and Geochemistry of Scandium : Oslo, Norway 16-22 August 2003*. 2nd edn, *NGF abstracts and proceedings*. 2nd edn. Edited by G. Raade and T. V Segalstad. Trondheim: Norsk geologisk forening.

Samadi, R. Miller, N. R., Mirnejad, H., Harris, C., Kawabata, H., Shirdashtzadeh, N. (2014) 'Origin of garnet in aplite and pegmatite from Khajeh Morad in northeastern Iran: A major, trace element, and oxygen isotope approach', *Lithos*. Elsevier B.V., **208**, pp. 378–392. doi: 10.1016/j.lithos.2014.08.023.

Scandium International Mining Corp. (2018a) 'Home page', <http://www.scandiummining.com/s/Home.asp> Accessed 13 March 2018

Scandium International Mining Corp. (2018b) 'Southern Norway Program Tørdal Property (100% SCY Control)', <http://www.scandiummining.com/s/explorationprojects.asp.> Accessed 28 April 2018.

Segalstad, T. V and Eggleston, T. L. (1993) 'Pegmatittene i Tørdal, Telemark.', *STEIN*, **20**, pp. 190–195.

Segalstad, T. V and Raade, G. (2003) 'Scandium mineralizations in southern Norway – geological background for the field trip', *NGF Abstracts and Proceedings*, (2), pp. 57–86.

Shannon, R. D. (1976) 'Revised effective ionic radii and systematic studies of interatomic distances in halides and chalcogenides', *Acta Crystallographica Section A*, **32**(5), pp. 751–

767. doi: 10.1107/S0567739476001551.

Shchekina, T. I. and Gramenitskii, E. N. (2008) 'Geochemistry of Sc in the magmatic process: Experimental evidence', *Geochemistry International*, **46**(4), pp. 351–366. doi: 10.1134/s0016702908040046.

Shervais, J. W. (1982) 'Ti-V plots and the petrogenesis of modern and ophiolitic lavas', *Earth and Planetary Science Letters*, **59**(1), pp. 101–118. doi: 10.1016/0012-821X(82)90120-0.

Shore, M. and Fowler, A. D. (1996) 'OSCILLATORY ZONING IN MINERALS: A COMMON PHENOMENON', *Canadian Mineralogist*, **34**, pp. 1111–1126.

Sibley, D. F., Vogel, T. A., Walker, B. M., Byerly, G. (1976) 'THE ORIGIN OF OSCILLATORY ZONING IN PLAGIOCLASE: A DIFFUSION AND GROWTH CONTROLLED MODEL', *American Journal of Science*. American Journal of Science, **276**, pp. 275–284.

Simakin A.G. (1984) 'A simple quantitive model of rhythmic zoning in crystals', *Geochem. Int.*, **21**, pp. 13-26.

Stokkeland, K. (2016) 'Formation of thortveitite and garnet chemistry in the Evje- Iveland pegmatite field Formation of thortveitite and garnet chemistry in the Evje- Iveland pegmatite field'.

Strategic Metal Investments Ltd. (2018): Scandium Price <http://strategic-metal.com/products/scandium/scandium-price/> Accessed 23 April 2018.

U.S. Geological Survey (2016) 'Mineral Commodity Summaries 2016', *Reston, USA: U.S. Geological Survey*, pp. 1-201. doi: 10.3133/70140094.

Voncken, J. H. L. (2016) 'The Rare Earth Elements, an Introduction', SpringerNature, Dordrecht. doi: 10.1007/978-3-319-26809-5.

Whalen, J. B., Currie, K. L. and Chappell, B. W. (1987) 'A-type granites: geochemical characteristics, discrimination and petrogenesis', *Contributions to Mineralogy and Petrology*, **95**(4), pp. 407–419. doi: 10.1007/BF00402202.

Whitney, D. L. and Evans, B. W. (2010) 'Abbreviations for names of rock-forming minerals', *American Mineralogist*, **95**(1), pp. 185–187. doi: 10.2138/am.2010.3371.

Williams, P. A., Hatert, F., Pasero, M., Millis, S. J. (2014) 'IMA Commission on New Minerals, Nomenclature and Classification (CNMNC) Newsletter 40', *European Journal of Mineralogy*, **78**(3), pp. 549–558. doi: 10.1127/ejm/2017/0029-2709.

Wise, M. A., Černý, P. and Falster, A. U. (1998) 'SCANDIUM SUBSTITUTION IN COLUMBITE-GROUP MINERALS AND IXIOLITE Department of Geological Sciences , University of Manitoba , Winnipeg , Manitoba R3T 2N2 Ercit et', *The Canadian Mineralogist*, **36**, pp. 673–680.

Wood, D. A. (1980) 'The application of a Th-Hf-Ta diagram to problems of tectonomagmatic classification and to establishing the nature of crustal contamination of basaltic lavas of the British Tertiary Volcanic Province', *Earth and Planetary Science Letters*, **50**(1), pp. 11–30. doi: 10.1016/0012-821X(80)90116-8.

Yang, H. *et al*. (2007) ‘Kolbeckite, $ScPO_4.2H_2O$, isomorphous with metavariscite’, *Acta Crystallographica Section C: Crystal Structure Communications*, **63**(10), pp. 2–4. doi: 10.1107/S0108270107038036.

7. Appendix

Appendix 7.1: Sample/thick & thin sections list							
Sample	**Location**	**Mineral/Rock**	**Pegmatite zone**	**UTM Zone**	**East**	**North**	**Thickness**
GAS09061603	Bratterud	Garnet/Pegmatite	Bratterud	32V	488817	6562727	300-µm
GAS05061618	Butvatnet	Garnet/Pegmatite	Butvatnet	32V	481700	6557482	300-µm
GAS06071703	Grønliheii	Garnet/Pegmatite	Grønliheii	32V	482611	6557673	300-µm
GAS20091508	Heftetjern 1	Garnet/Pegmatite	Heftetjern	32V	485407	6560383	300-µm
GAS08061601	Heftetjern 2	Garnet/Pegmatite	Heftetjern	32V	485238	6560598	300-µm
GAS07061611	Kleppe quarry	Garnet/Pegmatite	Kleppe	32V	484884	6557627	300-µm
GAS04071705	Kleppe quarry	Amphibolite	Kleppe	32V	484892	6557629	30-µm
GAS04071707	Kleppe quarry, granite outcrop	Granite	Kleppe	32V	485303	6556713	30-µm
GAS06071710	Lislegrønlia	Garnet/Pegmatite	Lislegrønlia	32V	483592	6557878	300-µm
GAS23091545	Lower Høydalen	"Cleavelandite" garnet	Høydalen	32V	0486445	6560532	300-µm
GAS06071715	Mjeltedalen 2a	Garnet/Pegmatite	Mjeltedalen	32V	484311	6557191	300-µm
GAS06071716	Mjeltedalen 2b	Amphibolite	Mjeltedalen	32V	484311	6557191	30-µm
GAS05071708	Sjauset	Garnet/Pegmatite	Sjauset	32V	486505	6562085	300-µm
GAS06061609	Storemyr 1	Garnet/Pegmatite	Storemyr	32V	485640	6558697	300-µm
GAS06061604	Storemyr 2	Garnet/Pegmatite	Storemyr	32V	485441	6558866	300-µm
GAS07071703	Storemyr 3	Garnet/Pegmatite	Storemyr	32V	485627	6558286	300-µm
GAS05061609	Svåheii 2	Garnet/Pegmatite	Svåheii	32V	481596	6556927	300-µm
GAS05061613	Svåheii 3	Garnet/Pegmatite	Svåheii	32V	481515	6557011	300-µm
GAS08061612	Upper Høydalen	Garnet/Pegmatite	Høydalen	32V	486274	6560473	300-µm
GAS03071715	Upper Høydalen	"Cleavelandite" garnet	Høydalen	32V	486274	6560473	300-µm

Appendix 7.2: Thick samples descriptions			
Samples	**Garnet occurrence within pegmatite**	**Crystal sizes (minimum-maximum) and habit**	**Garnet color (PPL) and zonation**
Bratterud GAS09061603	Wall zone	0.2-4mm. Subhedral to anhedral	Brown-orangish. Slight color zonation, commonly resembling pale rims around dark cores.
Butvatnet GAS05061618	Wall zone	0.3-2.6mm. Euhedral-subhedral crystals	Brown-orangish color. Thin pale color zones around dark cores are common.
Grønliheii GAS06071703	Wall zone	0.2-1.5mm. Euhedral to subhedral.	Brown-orangish. Some crystals exhibit slight color zonation resembling pale rims around dark cores, while others show no apparent color zonation.
Heftetjern 1 GAS20091508	Wall zone	0.1-6mm. Euhedral (smallest garnets) to subhedral-anhedral (larger garnets)	Brown-orangish. Slightl color zonation, commonly resembling pale rims around dark cores.
Heftetjern 2 GAS08061601	Wall zone	0.2-7mm. Subhedral-anhedral.	Brown-orangish. Slightl color zonation, commonly resembling pale rims around dark cores.
Kleppe quarry GAS07061611	Wall zone	0.2-1.5. Euhedral-subhedral. with some dendritic overgrowth.	Brown-orangish. Slightly color zonation, commonly resembling pale rims around dark cores.
Lislegrønlia GAS06071710	Wall zone	0.3-1.2mm. Euhedral to subhedral.	Brown-orangish. Color zonation, commonly resembling dark rims, pale cores, and several intermediate zones both dark and pale.
Lower Høydalen GAS23091545	Cleavelandite replacement zone	1.2cm. Fragment of larger crystal	Light brownish/reddish. No apparent color zonation.
Mjeltedalen 2a GAS06071715	Wall zone	0.6-3mm. Subhedral to anhedral. Often resembling skeletal/amoeboid shapes.	Brown-orangish. Color zonation, commonly resembling pale rims, relative paler intermediate zones, and dark cores.
Sjauset GAS05071708	Wall zone	0.1-1.5mm. Euhedral to subhedral.	Dark/light grey to pale orangish color. Some crystals exhibit no apparent color zonation, while others exhibit slight color zonation, resembling pale orangish rim around light grey cores.
Storemyr 1 GAS06061609	Wall zone	2-4mm. Euhedral-subhedral.	Brown-orangish color. Pale rims around dark cores are common.
Storemyr 2 GAS06061604	Wall zone	0.2-1mm. Euhedral-subhedral. with some dendritic overgrowth.	Brown-orangish color. Commonly dark rims around pale cores.
Storemyr 3 GAS07071703	Wall zone	0.2-2mm. Anhedral. resembling skeletal/amoeboid shapes	Dark brown-orangish. Slight color zonation, commonly resembling pale rims around dark cores.
Svåheii 2 GAS05061609	Wall zone	0.7 – 2 mm. Euhedral	Brown-orangish color. Commonly multiple color zoning, resembling both dark rims and cores with intermediate pale color zones.
Svåheii 3 GAS05061613	Wall zone	2 cm. Crystal fragment	Brown-orangish color. No apparent color zoning.
Upper Høydalen 1 GAS08061612	Wall zone	1.5cm. Subhedral fragment	Brown-orangish. No apparent color zonation.
Upper Høydalen 12 GAS03071715	Cleavelandite replacement zone	2cm. Subhedral/anhedral fragment. Garnet fragments in alterated	Yellow alterated mica with white anhedral fragments: 0,1-2mm. Surrounded by purple mica (lepidolite).

Appendix 7.3: Thick sections images, garnet

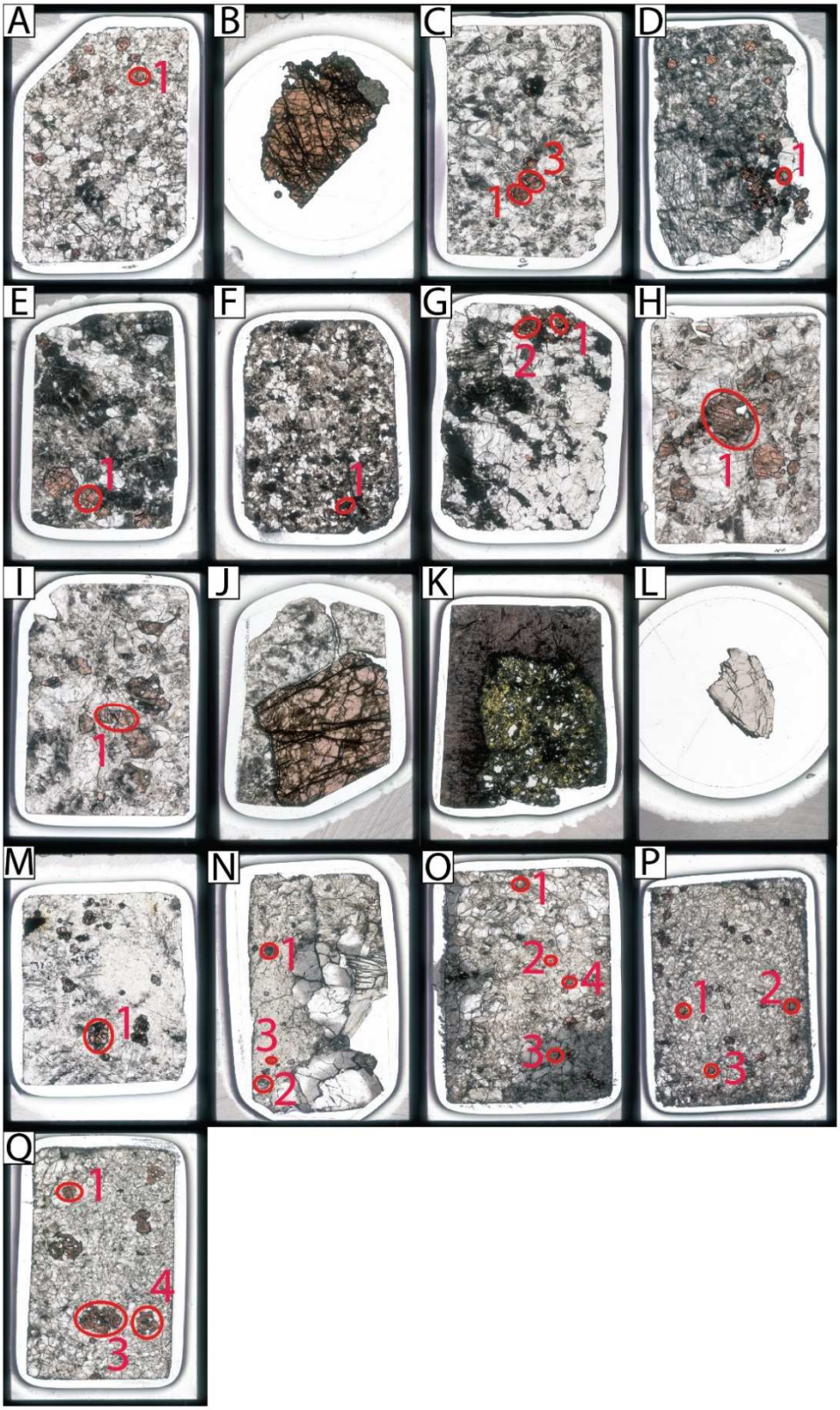

Appendix 7.3: Displayed images of the all the 17 thick sections of the sampled garnet-bearing pegmatites in Tørdal. A: Svåheii 2, B: Svåheii 3, C: Butvatnet, D: Storemyr 2, E: Storemyr 1, F:Storemyr 3 (grain cluster 1), G: Kleppe quarry, H: Heftetjern 2, I: Heftetjern 1, J: Upper Høydalen 1, K: Upper Høydalen 12, L: Lower Høydalen, M: Bratterud, N: Sjauset, O: Grønliheii, P: Lislegrønlia, Q: Mjeltedalen 2a. The red circles indicate the garnet grains (with grain numbers), which were imaged both in PPL and in BSE.

Appendix 7.4: Thin sections images, side rocks

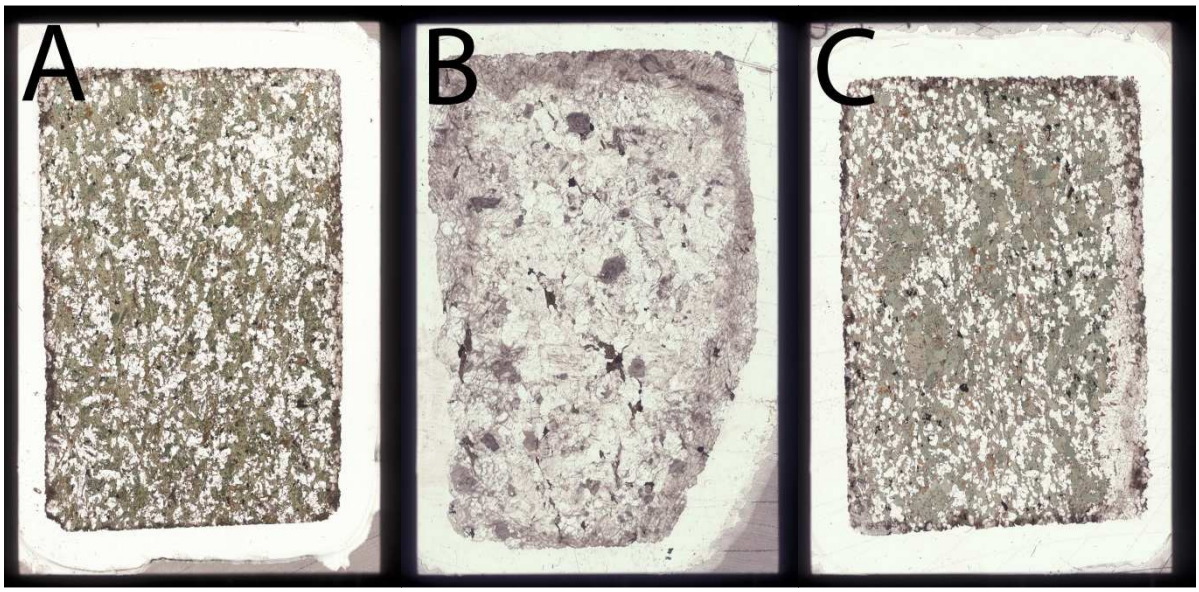

Appendix 7.4: A: Kleppe quarry amphibolite, B: Tørdal granite near Kleppe quarry, C: Mjeltedalen (2b) amphibolite.

Appendix 7.5 Original garnet BSE-images

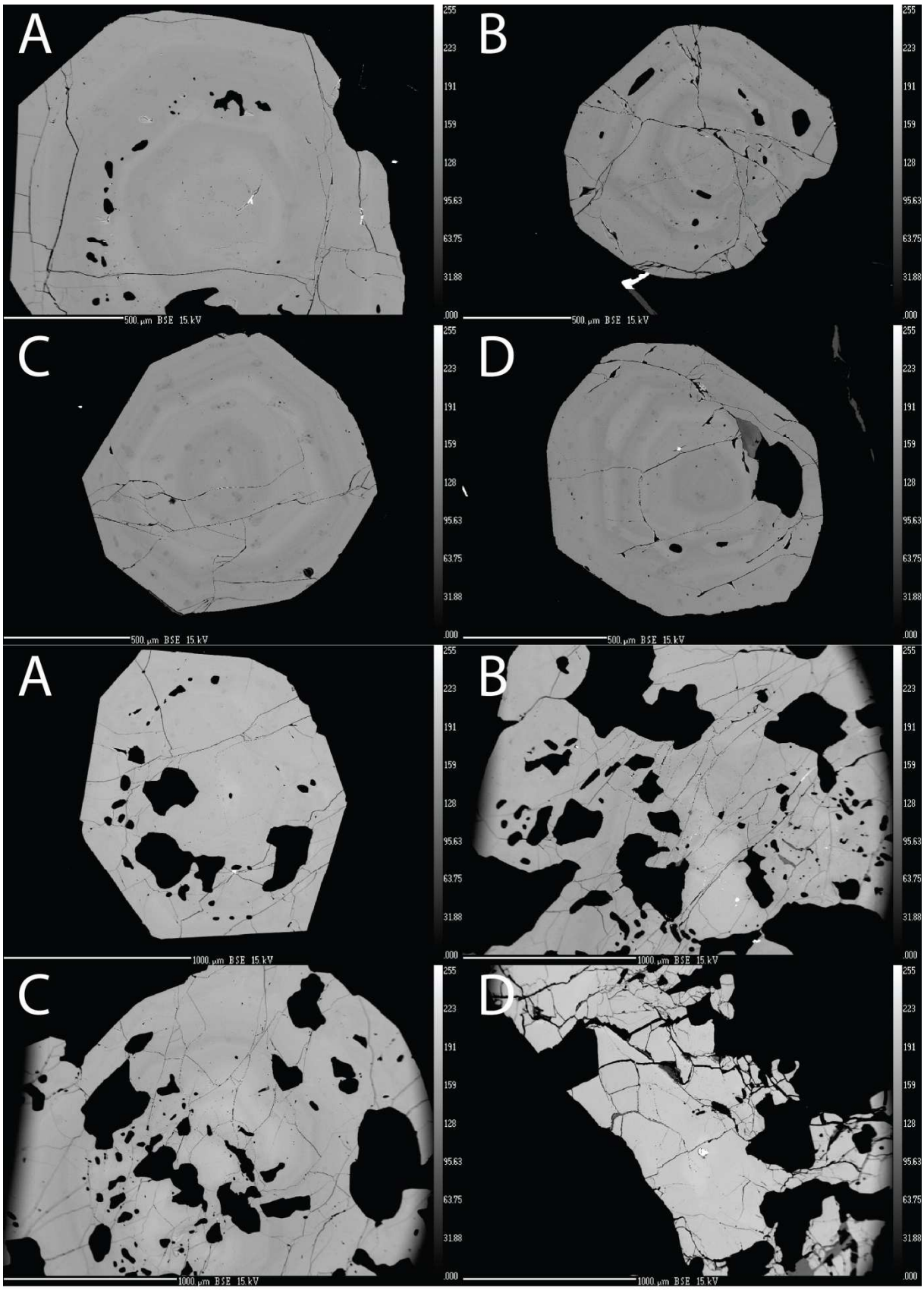

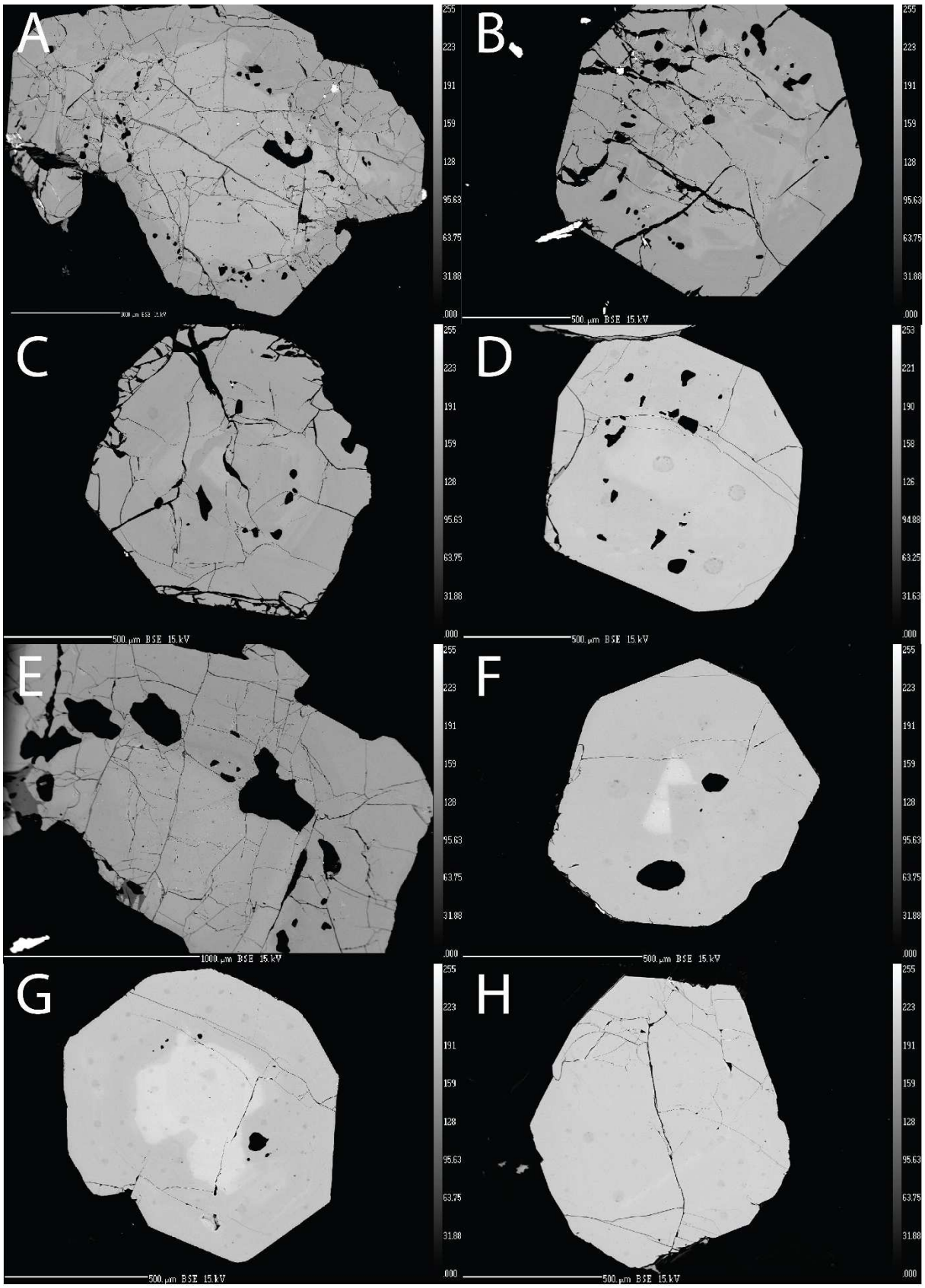
A
B
C
D
E
F
G
H
500 µm BSE 15 kV
1000 µm BSE 15 kV

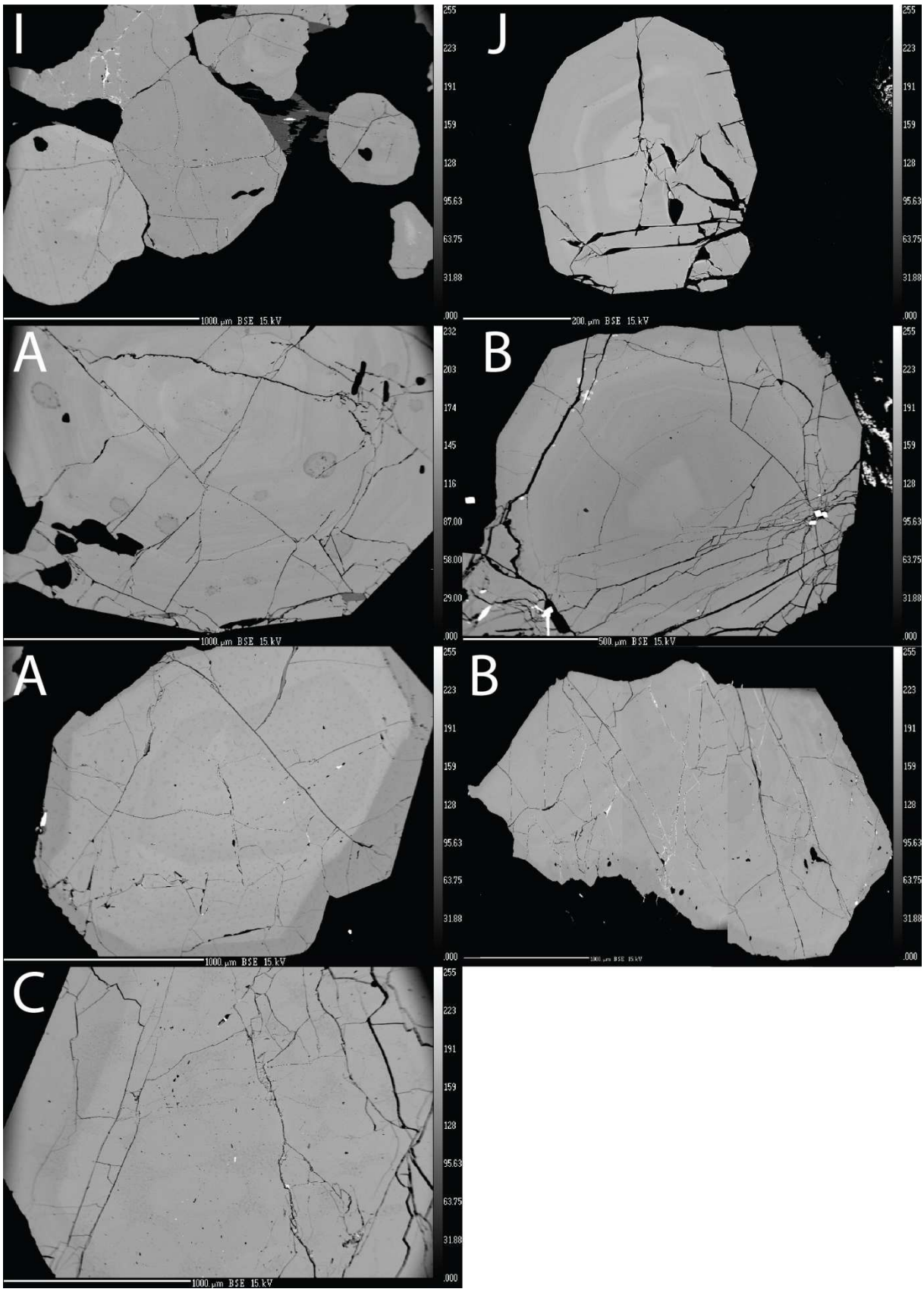

Appendix 7.5: Original BSE-images of the displaying the studied garnets: group A (A-D), group B (A-D), group C (A-J), group D(A), group E(B), group F (A-C). Group G is not included due to their lack of zoning and relatively large sizes.

Appendix 7.6-8 are all attached as excel spreadsheets. Appendix 7.6: EPMA-acquired data of chemical core-rim compositions in 33 analyzed Tørdal garnets. Some of the grains' cores and rims (Storemyr 1 and 3) in some analyses were not defined, but were however considered for regional bulk concentration data. Appendix 7.7: ICP-MS data of average core-rim compositions from 18 Tørdal garnets, and chondrite normalized core-rim compositions of those garnets. Seven (96-7=88) laser ablation points are not included since these points either exhibited "untrue" concentrations or the zone (core/rim) of the crystals was not defined. Appendix 7.8: ICP-MS data of bulk rock geochemistry concentrations of the three investigated host rocks from the Kleppe quarry and Mjeltedalen locations in Tørdal.

Appendix 7.9: Overview of minerals in the Tørdal

Mineral	**Formula**	
Actinolite	$Ca_2(Mg_{4.5\text{-}2.5}Fe_{0.5\text{-}2.5}{}^{2+})_{\Sigma=5}Si_8O_{22}(OH)_2$	
Agakhanovite-(Y) (TL)	$YCa\square_2KBe_3Si_{12}O_{30}$	
Albite	$NaAlSi_3O_8$	
var: Cleavelandite	$NaAlSi_3O_8$	
var: Oligoclase-Albite	$NaAlSi_3O_8$	
Allanite-(Ce)	$CaCeAl_2Fe^{2+}(Si_2O_7)(SiO_4)O(OH)$	
'Apatite'	$Ca_5(PO_4)_3X$	
'Axinite Group'	Axinite-(Fe)	$Ca_2Fe^{2+}Al_2BSi_4O_{15}OH$
	Axinite-(Mg)	$Ca_2MgAl_2BSi_4O_{15}OH$
	Axinite-(Mn)	$Ca_2Mn^{2+}Al_2BSi_4O_{15}(OH)$
	Tinzenite	$Ca_2Mn_4{}^{2+}Al_4[B_2Si_8O_{30}](OH)_2$
Bastnäsite-(Ce)	$CeCO_3F$	
Bavenite	$Ca_4Be_{2+x}Al_{2-x}Si_9O_{26-x}(OH)_{2+x}$, (x=0-1)	
Bazzite	$Be_3(Sc,Fe^{3+},Mg)_2Si_6O_{18} \cdot Na_{0.32} \cdot nH_2O$	
Bertrandite	$Be_4Si_2O_7(OH)_2$	
Beryl	$Be_3Al_2Si_6O_{18}$	
Beusite	$Mn^{2+}Fe_2{}^{2+}(PO_4)_2$	
'Biotite'	$K(Mg, Fe^{2+})_3AlSi_3O_{10}(OH,F)_2$	
Bismoclite	$BiOCl$	
Bismuth	Bi	
Bismutite	$Bi_2O_2(CO_3)$	
Bohseite	$Ca_4Be_{3+x}Al_{1-x}Si_9O_{25-x}(OH)_{3+x}$, (x = 0-1)	
Brookite	TiO_2	
Calcite	$CaCO_3$	
Cascandite	$CaScSi_3O_8(OH)$	

Cassiterite	SnO_2
Cerianite-(Ce)	CeO_2
Cerussite	$PbCO_3$
Clinochlore	$Mg_5Al(AlSi_3O_{10})(OH)_8$
Clinozoisite	$Ca_2Al_3(Si_2O_7)(SiO_4)O(OH)$
Epidote	$Ca_2Fe^{3+}Al_2(Si_2O_7)(SiO_4)O(OH)$
Euxenite-(Y)	$(Y,Ca,Ce,U,Th)(Nb,Ta,Ti)_2O_6$
Fergusonite-(Y)	$YNbO_4$
Fluocerite-(Ce)	CeF_3
Fluorite	CaF_2
var: Yttrofluorite	$(Ca_{1-x}Y_x)F_{2+x}$, $(0{,}05 < x < 0{,}3)$
Fluor-schorl	$NaFe_3^{2+}Al_6(Si_6O_{18})(BO_3)_3(OH)_3F$
Gadolinite-(Y)	$Fe^{2+}Be_2Y_2(SiO_4)_2O_2$
Gahnite	$ZnAl_2O_4$
Galena	PbS
Goethite	FeO(OH)
Heftetjernite (TL)	$ScTaO_4$
Hellandite-(Y)	$(Ca,REE)_4Y_2Al(Be,Li)_{2-x}B_4Si_4O_{22}(OH)_2$
Helvine	$Be_3Mn_4^{2+}(SiO_4)_3S$
'Hingganite-(Y)'	$(Y,REE,Ca)_2(\square,Fe^{2+})Be_2[SiO_4]_2(OH)_2$
Ilmenite	$Fe^{2+}Ti^{4+}O_3$
var: Manganoan Ilmenite	$Fe^{2+}TiO_3$
Ixiolite	$(Ta,Mn,Nb)O_2$
var: Scandian Ixiolite (of Bergstøl & Juve	$(Ta,Sc,Nb,Sn,Fe,Ti)_4O_8$
Kainosite-(Y)	$Ca_2Y_2(SiO_3)_4(CO_3) \cdot H_2O$
Kamphaugite-(Y)	$Ca_2Y_2(CO_3)_4(OH)_2 \cdot 3H_2O$
Kristiansenite (TL)	$Ca_2ScSn(Si_2O_7)(Si_2O_6OH)$
Kuliokite-(Y)	$Y_4Al(SiO_4)_2(OH)_2F_5$
Laumontite	$Ca(Si_4Al_2)O_{12} \cdot 4H_2O$
Lepidocrocite	$Fe^{3+}O(OH)$
'Lepidolite'	$K(Li,Al)_3(Si,Al)_4O_{10}(F,OH)_2$
'Limonite'	(Fe,O,OH,H_2O)
Magnetite	$Fe^{2+}Fe_2^{3+}O_4$
Microcline	$KAlSi_3O_8$
var: Amazonite	$KAlSi_3O_8$
Microlite Group	$(Ca,Na)_2Ta_2(O,OH,F)_7$
var: Scandium Microlite (of Bergstøl & Juve)	Incompletely described Sc-microlite group mineral.
Milarite	$KCa_2(Be_2AlSi_{12}O_{30}) \cdot xH_2O$
Molybdenite	MoS_2
Monazite-(Ce)	$CePO_4$
'Morganite'	$Be_3Al_2(Si_6O_{18})$
Muscovite	$KAl_2(Si_3Al)O_{10}(OH)_2$
'Muscovite-2M1'	“Muscovite-polytype”
Nontronite	$Na_{0,3}Fe_2^{3+}(Si,Al)_4O_{10}(OH)_2 * nH_2O$
Oftedalite (TL)	$KSc_2(Be_3AlSi_{11})O_{30}$
Opal	$SiO_2 \cdot nH_2O$

Phenakite	Be_2SiO_4
Plattnerite	PbO_2
'Plumbomicrolite (of Hogarth 1977)'	Pb-rich microlite, Plumboan member of the microlite-pyrochlore family.
Polycrase-(Y)	$Y(Ti,Nb)_2(O,OH)_6$
Pyrite	FeS_2
Pyrochlore Group	$A_2Nb_2(O,OH)_6Z$, (A = Na,Ca,Sn^{2+},Sr,Sb^{3+},Y,U^{4+},H_2O or □) (Z = OH,F,O,H_2O or □)
var: Yttropyrochlore (of Hogarth 1977)	$A_2Nb_2(O,OH)_6Z$, (A = Na,Ca,Sn^{2+},Sr,Sb^{3+},Y,U^{4+},H_2O or □) (Z = OH,F,O,H_2O or □)
Pyrochlore Supergroup	$A_{2-m}B_2X_{6-w}Y_{1-n}$ (A = Na,Ca,Sn^{2+},Sr,Sb^{3+},Y,U^{4+},H_2O or □, rarer Ag,Mn,Ba,Fe^{2+},Bi^{3+},Ce (including other REE), Sc or Th) (B = Ta,Nb,Ti,Sb^{5+},W,V^{5+},Sn^{4+},Zr,Hf,Fe^{3+},Mg,Al,Si) (X = O, also with OH and F) (Y = Anion, vacancy, H_2O, or large cation of OH,F,O, □,H_2O,K,Cs,Rb)
var: Yttrobetafite (of Hogarth 1977)	$A_{2-m}B_2X_{6-w}Y_{1-n}$ (A = Na,Ca,Sn^{2+},Sr,Sb^{3+},Y,U^{4+},H_2O or □, rarer Ag,Mn,Ba,Fe^{2+},Bi^{3+},Ce (including other REE), Sc or Th) (B = Ta,Nb,Ti,Sb^{5+},W,V^{5+},Sn^{4+},Zr,Hf,Fe^{3+},Mg,Al,Si) (X = O, also with OH and F) (Y = Anion, vacancy, H_2O, or large cation of OH,F,O, □,H_2O,K,Cs,Rb)
Quartz	SiO_2
Rutile	TiO_2
var: Ilmenorutile	$Fe_x(Nb,Ta)_{2x} \cdot 4Ti_{1-x}O_2$
var: Strüverite	$(Ti,Ta,Fe)O_2$
Rynersonite	$CaTa_2O_6$
Scandiobabingtonite	$(Ca,Na)_2(Fe^{2+},Mn)(Sc,Fe^{3+})Si_5O_{14}(OH)$
Schorl	$NaFe_3^{2+}Al_6(Si_6O_{18})(BO_3)_3(OH)_3OH$
Spessartine	$Mn_3^{2+}Al_2(SiO_4)_3$
Sphalerite	ZnS
Stilpnomelane	$(K,Ca,Na)(Fe,Mg,Al)_8(Si,Al)_{12}(O,OH)_{36} * nH_2O$
Synchysite-(Y)	$CaY(CO_3)_2F$
'Tantalite'	$(Mn,Fe)(Ta,Nb)_2O_6$
Tantalite-(Fe)	$Fe^{2+}Ta_2O_6$
Tengerite-(Y)	$Y_2(CO_3)_3 \cdot 2\text{-}3H_2O$
Thorite	$ThSiO_4$
Thortveitite	$Sc_2Si_2O_7$
Titanite	$CaTiSiO_5$
var: Triclinic Titanite	Both Ta- and Al-bearing titanite from Heftejern pegmatite
Topaz	$Al_2SiO_4F_2$
'Tourmaline'	$A(D_3)G_6(T_6O_{18})(BO_3)_3X_3Z$, (A = Ca,Na,K or vacant (large cations)) (D = Al, Fe^{2+},Fe^{3+}, Li,Mg^{2+},Mn^{2+}) (G = Al, Cr^{3+}, Fe^{3+},V^{3+}) (T = Si, occasionally minor Al

	and B^{3+}) (X = O and/or OH) (Y = F,O and/or OH)
Tveitite-(Y) (TL)	$(Y,Na)_6(Ca,Na,REE)_{12}(Ca,Na)F_{42}$
Uedaite-(Ce)	$Mn^{2+}CeAl_2Fe^{2+}(Si_2O_7)(SiO_4)O(OH)$
Xenotime-(Y)	YPO_4
Yttrotantalite-(Y)	$(Y,U,Fe^{2+})(Ta,Nb)_2(O,OH)_4$
'Zinnwaldite'	$KLiFe^{2+}Al(AlSi_3O_{10})(F,OH)_2$
Zircon	$ZrSiO_4$
var: Alvite	$Zr(SiO_4)$, commonly referred to as a metamict hafnium-rich zircon

Appendix 7.9 : Mineral overview of reported minerals from the Tørdal area taken from https://www.mindat.org/loc-23233.html